Tropical Cyclone Cloud and Intensity Relationships

by
Charles P. Arnold

Department of Atmospheric Science
Colorado State University
Fort Collins, Colorado

Colorado
State
University

Department of
Atmospheric Science

Paper No. 277

TROPICAL CYCLONE CLOUD AND INTENSITY RELATIONSHIPS

by

Charles P. Arnold

Department of Atmospheric Science

Colorado State University

Fort Collins, Colorado

November, 1977

ABSTRACT

This paper describes an observational study of tropical cyclones
based on high resolution visual and infrared Defense Meteorological
Satellite Program (DMSP) pictures of western North Pacific storms. It
also utilizes composited rawinsonde data about storms in the same geo-
graphical region. It discusses the physical characteristics, cloud
characteristics and wind and thermodynamic characteristics associated
with each of four stages of tropical cyclone development (developing
cluster, tropical depression, tropical storm, and typhoons). Among
the physical characteristics discussed are typical storm sizes, types
of banding most often observed, location and type of circulation center,
intensification rates, and eye dimensions. Cloud characteristics in-
clude the percent of storm area covered by cirrus and convective cloud
types and the distribution and characteristics of the basic convective
element found in DMSP data. Among the wind and thermodynamic parameters
investigated were vertical motion, vorticity, tangential wind, moisture
and temperature.

Results of this study reveal a substantial variability exists in
the cloudiness of tropical cyclones. This variability exists within
a given storm, between similar stages of different storms, and even
diurnally. As a corollary to this variability, only a weak relationship
was found between vorticity and cloudiness. While the average or com-
posited storm cloudiness changes little with storm stage, vorticity
increases dramatically. There are obvious implications in this regard
to cloudiness-storm intensity models.

Incipient pre-storm circulation centers appear to be located in
the clear region surrounding a cluster or as a suppressed cloud region
within the boundary of the cluster. These incipient circulation centers
are hypothesized as being formed by dynamically forced subsidence. It
appears that merging outflows of favorably positioned convective elements
produce the necessary upper level warming required to drop the surface
pressure and initially form the tropical cyclone. The implications of
this indirect method of cumulus warming with regard to cumulus para-
meterization are discussed.

This study has also revealed that deep convection in the tropical
cyclone typically is found in multi-cellular complexes. These meso-
convective elements have been termed basic convective elements. An exam-
ination of wind and thermodynamic characteristics support the findings
from the satellite analysis. Mean storm stage vertical motions near the
outflow level conform to the observed statistical trend in cloudiness.
Relative humidities indicate a progressive moistening of the inner core
with increasing storm intensity. Temperature anomalies near 250 mb are
highly correlated with lower tropospheric height values suggesting that
a satellite or aircraft analysis of the storm's upper level temperature
field may provide an alternate means of estimating storm intensity. Other
tropical cyclone features are discussed.

TABLE OF CONTENTS

TABLE OF CONTENTS (cont'd)

1. INTRODUCTION

The study of the basic physical processes involved with tropical
cyclone formation and structure is a challenging subject. It has been
suggested that had man never observed tropical storms he would never
have thought their existence possible in that their formation seems so
unlikely in the weak wind and barotropically stratified summer atmos-
phere of the tropics. Understanding has been hampered by the limited
amount of meteorological information available over tropical oceans.
In an attempt to perform quantitative studies, some researchers have
recently turned to composite data analysis. These studies have typical-
ly been limited to conventional rawinsonde data. With the advent of
high resolution, polar orbiting Defense Meteorological Satellite
Program (DMSP) satellites another very important data source became
available for tropical cyclone studies in the western Pacific (WESTPAC).
This research was undertaken with the purpose of increasing our know-
ledge of tropical cyclones, particularly our knowledge of the cyclone's
cirrus shields and of deep convective cells which penetrate the cirrus
shield. Several general areas of interest studied in this paper
include the relationship between storm cloudiness and storm intensity,
the degree of variability in cloudiness associated with tropical
cyclones, and the manner in which upper level warming can be concen-
trated in order to trigger cyclone development.

1.1 Previous studies

Only a few limited studies of tropical cyclones have been made
from satellite data. Among these studies are Fritz, 1962; Frank, 1963;
Fett, 1964; Bandeen et al., 1964; Fujita and Arnold, 1964; Merritt,

1964; Timchalk et al., 1965; Allison et al., 1966; Yanai, 1968; Lopez, 1968; Dvorak, 1968, 1973, 1975; Williams and Gray, 1973; Balogun, 1973; Zehr, 1976; Erickson, 1977.

Fett (1964) was perhaps the first to devise an intensity-cloud-iness model for the formative stages of tropical cyclones. Essentially the model was based on the amount and organization of satellite observed cloudiness. Four stages were identified by Fett as representing the developing cloud cluster (Fig. 1).

Following the work of Fett, Timchalk et al. (1965) and Fritz et al. (1966) developed an empirical technique by which maximum wind speeds in tropical depressions through typhoons could be estimated from satellite data based on two parameters:

1) size of the cirrus canopy - also called the overcast circle or DIA and

2) a ranking based on the degree of spiral band organization. Picture data based on these parameters were plotted against the Maximum Wind Speed (MWS) taken from aircraft reconnaissance logs of the 1962 typhoon season.

They concluded that cirrus canopy size and degree of spiral band organization are empirically related to the maximum wind speed. They did note, however, that the high degree of correlation (0.79 linear coefficient) between DIA and MWS existed only because the DIA was defined so that it represented the cloud shield directly associated with a known storm circulation. They noted that many bright tropical cloud masses are as large as hurricane cloud shields but that there is in such cases no correlation in general between DIA and MWS.

The physical model which they used to explain the relationship be-tween canopy size and intensity and which has served as the physical

A. THE TROPICAL DISTURBANCE
(NO CLOSED SURFACE ISOBARS)

CLOUD MASS ELONGATED
ALONG WAVE AXIS

B. THE TROPICAL DEPRESSION I
MAX. CENTRAL ISOTACH
LESS THAN 20 KTS

THE 'COMMA CONFIGURATION'
CENTER ILL-DEFINED

C. THE TROPICAL DEPRESSION II
MAX. CENTRAL ISOTACH 20-30 KTS

THE
'COMMA CONFIGURATION'
CENTER WELL-DEFINED

INITIAL OBSCURATION OF
CENTER, SOME EVIDENCE
OF OUTFLOW ALOFT

D. THE TROPICAL DEPRESSION III -
TROPICAL STORM I
MAX. CENTRAL ISOTACH 31-40 KTS
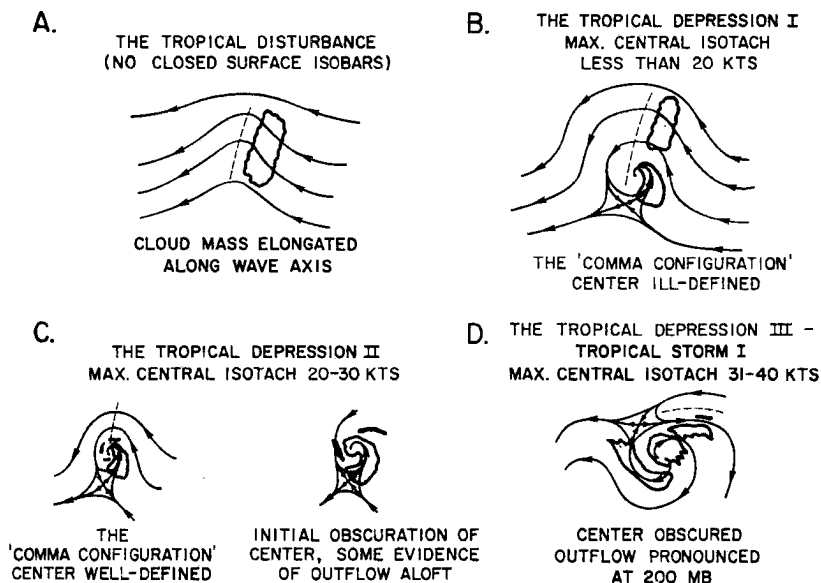
CENTER OBSCURED
OUTFLOW PRONOUNCED
AT 200 MB

Fig. 1. Schematic model of the formative stage of tropical cyclone development (from Fett, 1968).

basis for subsequent models was as follows. Low level inflow into the storm is equal to upper level outflow based on a simple continuity argument. Low level inflow is related to maximum wind speed, the weakest link in the argument. Upper level outflow is related to the size of the DIA. Therefore, DIA is related to MWS.

Working with this hypothesis several investigators have attempted to derive useful relationships from upper level cloud vectors using geostationary satellite data (C. Erickson, 1974). Erickson calculated divergence, vorticity and other wind derived parameters over a number of tropical cyclones using cirrus-level cloud vectors obtained from ATS-3 data. While some statistical significance was found between certain of these parameters and cyclone intensity, the scatter of individual results was quite large.

Hoping to find a more precise relationship between storm cloudiness and intensity Dvorak introduced an analog or storm fingerprint

technique which later was developed into a picture-pair technique
(Dvorak, 1968, 1973, 1975). Initially he investigated some 200 once-
per-day visual satellite pictures of the life spans of 47 typhoons and
tropical storms in the western north Pacific. These cyclones were
arranged in three groups based on aircraft reconnaissance MWS inter-
polated to satellite data time. These three groups were pre-storm,
33 knots or less; tropical storm, 34-63 knots; and typhoon, 64 knots or
greater. The groups were further divided into weak and strong subdivi-
sions resulting in a total of seven developmental classes labeled
D-1 through D-7. Each class was examined for similar visual characteris-
tics that distinguished it from the others. The basic assumption of
this analog technique was that given a system displaying a visual
signature characteristic of one of the seven classes one could infer
the maximum wind speed of the system. However, storms whose cloudiness
looked alike were too often found to have much different intensities.

Concluding that the direct cloud-intensity analog approach was
not the most satisfactory one, he then set about developing a picture
pair method which incorporates both current and past cloudiness and
relies on a cyclone developmental model. This technique describes
cyclone development and dissipation as a day to day progression
through recognizable combinations of cloud characteristics, or classes,
referred to as T numbers. Similar to the earlier models of Timchalk
et al. (1965) the cloud characteristics that define each class are
described as either central features or banding features (Fig. 2).
Examples of storms representative of the various classes are shown
in Fig. 3. The central feature portion of the intensity estimate
depends on the size, shape, and definition of the central features

CF

PRELIMINARY T = CF + BF
CF = CENTRAL FEATURES
BF = OUTER BANDING FEATURES

IS THERE A CDO? — NO →

CLOUD LINE OR BAND FEATURES DEFINE THE CSC

| BANDING TYPE EYE*? DENSE ⊕ BAND WIDTH: ≳1¼° ~ ¾° ~ ¼° | → NO → | TIGHT CURVATURE AT EDGE OF ≥3° DENSE ⊕ ? WITH DIAM. OF CURVATURE: <1° ~1¼° | → NO → | LOW CLD CSC NEAR DENSE OR CB LINE CSC (CONV ⊕ ≥ 3°) DIAM. OF CURVE ~1¾° ~ 2½° |

YES CF5   YES CF4   YES CF3   YES CF3   YES CF25   YES CF2   YES CFI   NO CFO

YES ↓

IS THERE AN EYE WITHIN THE CDO? — NO →

CDO FEATURES DEFINE THE CSC

| IS CDO WELL DEFINED? SHAPE: ROUND, OVAL, ANGULAR. SURFACE TEXTURE: SMOOTH. SIZE (USE SMALLEST WIDTH) ≳2½° ~ 1¾° ~ 1¼° ~ ¾° | → NO → | SHAPE: IRREGULAR RAGGED EDGE. SIZE: ≳1½° >1°>1½° |

YES CF5   YES CF4   YES CF3   YES CF2   YES CF3   YES CF2

YES ↓

| IS THERE A ROUND DISTINCT EYE*? IMBEDDED BY: ≳1¼° ~1° ~¾° ~½° ~¼° |

YES CF7   YES CF6   YES CF5   YES CF4   YES CF3

***EYE QUALIFICATIONS:**

1. EYE IS DEFINED ONLY AFTER T2 OR GREATER OBSERVATION WAS MADE PREVIOUSLY

2. RAGGED EYE: ≤ CF4.5, SUBTRACT 1/2 NUMBER: FOR ≥ CF5, SUBTRACT 1 NUMBER.

3. INDISTINCT OR CLOUD COVERED EYE, SAME AS 2 OR USE CDO WIDTH VALUE.

4. LARGE EYE, (≳3/4° DIAM.): LIMIT MAX T-NUMBER TO T6 FOR ROUND DISTINCT EYE, T5 FOR ALL OTHERS.

BF = OUTER BANDING FEATURES

A NUMBER RELATED TO THE AMOUNT OF DENSE OVERCAST IN BAND FORM THAT CURVES EVENLY AROUND THE CENTRAL FEATURES.

BF = 0 WHEN LITTLE OR NO OUTER BANDING IS APPARENT

BF = 1 WHEN A BAND ~ 1/2° TO 3/4° WIDE COMPLETELY ENCIRCLES THE CF ONCE, OR WHEN A BAND > 1° WIDE ENCIRCLES MORE THAN ONE HALF OF THE CF.

BF = 2 WHEN A BAND ~ 1/2° TO 3/4° WIDE ENCIRCLES THE CF TWICE, OR WHEN A BAND > 1° WIDE ENCIRCLES THE CF ONCE.

VALUES OF 1/2, 1 1/2, OR 2 1/2 MAY BE USED.

Fig. 2. The diagram used for determining the preliminary T-number from cloud feature measurements (from V. Dvorak, 1975).
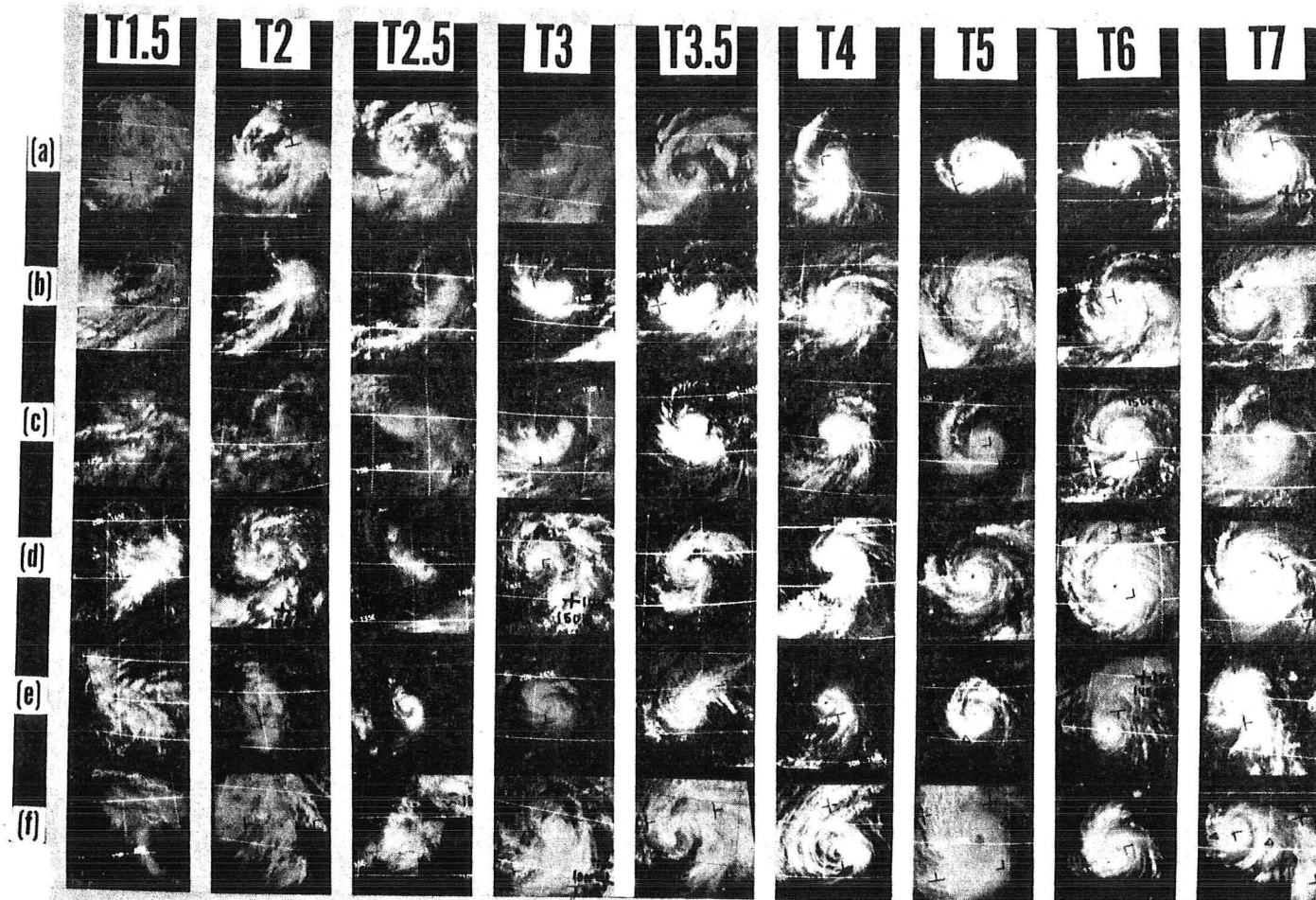
EXAMPLES OF PRELIMINARY T-NUMBER PATTERNS

Fig. 3. Examples of preliminary T-number patterns (provided by V. Dvorak, 1975).

as well as the amount of dense overcast associated with them (Dvorak,

1975). This system is currently used operationally at forecast centers

in Miami, Guam, Honolulu, San Francisco and elsewhere around the globe.

Several investigators have observed a general tendency in the

early stages of tropical cyclone formation for a concentration of deep

convection near the incipient storm center (Yanai, 1968; Balogun,

1973; Dvorak, 1975). Yanai (1968) observed that in a developing cluster

the precipitation area or general area of cloudiness approaches the

surface circulation center as the cyclone intensifies. More recently

Dvorak (1975) noted that "as the cyclone intensifies, the comma

configuration is usually observed to become more circular with its

central core clouds increasing in amount and density." Most investiga-

tions concerning the concentration of convection during early storm

development have been case studies and there has been little documen-

tation in a statistical sense to show a general tendency among

developing clusters to concentrate their convection. Neither have

there been any satisfactory explanations given for the physical pro-

cesses attending such convective cloud concentration. Balogun (1973)

used a form of the vorticity equation to qualitatively relate the

concentration of convection to the dynamics of the incipient cyclone.

His explanation failed, however, to explain subsequent changes in

convection beyond the tropical depression stage.

The visible existence of well-defined circulation centers within

or outside a cluster[1] has long been recognized (Fett, 1964, 1966, 1967;

Yanai, 1968; Oliver and Anderson, 1969; Arnold, 1972, 1974, 1975;

Lopez, 1973; Dvorak, 1975; Erickson, 1977). Fett (1964) was perhaps

the first investigator of satellite photos of tropical cyclones who

observed and discussed the presence of a low level circulation center

outside the main body of cloudiness associated with the developing

cloud cluster.

Yanai (1961) divided the process of cyclogenesis into three stages:

1) the wave stage in which there is a low level cold core
   disturbance associated with an upper level anticyclone to
   the east,

2) the warming stage in which the disturbance is transformed
   into a warm core, and

3) the developing stage in which the warm core is established
   throughout the troposphere.

He further noted that the upper level anticyclone became located over

the low level vortex as the upper level outflow intensified. In a

later paper Yanai (1968) performed a detailed case study of the cold

to warm core transformation of a developing cluster in the Caribbean.

From this study Yanai found a "small area devoid of clouds at the

storm center which may indicate the early formative stages of the eye".

He also observed that the precipitation area east of the disturbance

axis moved closer to the low level cyclone in time and that the "warm

---

[1]Visible in the sense that (1) a wind center is apparent from the
curved bands of shallow cumulus clouds in the otherwise clear area be-
yond the periphery of the cloud cluster (outside) or (2) a wind center
is apparent from the curved bands of shallow cumulus clouds in a pre-
dominantly cloud free region within the periphery of the cloud cluster
(within). Well-defined in the sense that there exists a high probabil-
ity that such features coincide with the storm's developing circulation
center.

air in the upper troposphere became located over the precipitation area". These observations correspond to the well-defined circulation center outside the cluster (in this case to the west of the cluster). Finally, he noted that in time the clouds surrounding the cyclone became more symmetrical.

Arnold (1974) was one of the first satellite analysts to observe and document the presence of one or more circulation centers within the developing clusters. These he referred to as multiple circulation centers. Earlier, in a then classified USAF letter, he introduced the possibility that these multiple centers may be a result of localized subsidence from surrounding embedded convection cells (Arnold, 1972). He later modeled the location of the low level circulation center based on the arrangement of penetrative cells in the cirrus canopy of a developing cluster. These cells were often observed to form semi-circular arcs about an area of depressed convection and/or cirrus (Fig. 4)[2]. Additional examples are shown in his 1974 report. Based on these results Dvorak (1972) modified his original intensity estimation technique to include the so called "eye without a Central Dense Overcast (CDO)".

As a comparison study to the work being done by this author, Erickson (1977) has shown that non-developing clusters often exhibit similar regions of depressed cloudiness at or near apparent circulation centers. The implication is that such features are common to all clusters and that while being necessary, are not sufficient for storm genesis.

---

[2]The Date, time, latitude and longitude of storm center, storm number as reported in the annual typhoon reports, and the scale used for all DMSP figures in the text are listed in Appendix C.
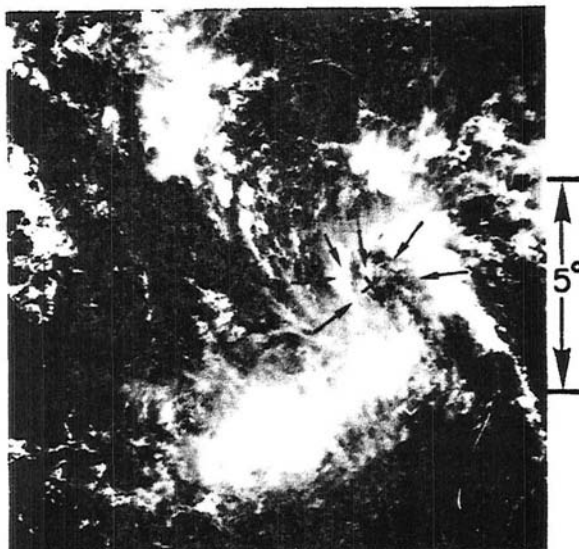
Fig. 4. Example of low level circulation center(indicated by the X)
with an area of depressed cloudiness. Convective elements
in an arc about the circulation center are indicated by the
arrows, 1 in = 484 km.

On satellite data of high resolution such as the DMSP these areas

can be clearly seen as regions of depressed convection and cirrus.

Low level cumulus lines and bands are often visible. Multiple centers

were often confirmed by aircraft reconnaissance as weak wind centers at

low levels. It was an accepted practice at the DMSP site on Guam for

satellite analysts to track such multiple centers until one became

dominant. No investigator to this author's knowledge, however, has

tied such features to a physical framework of early storm genesis.

It is the opinion of this author that such features are a significant

element in the genesis of tropical cyclones and that a study of them

could lead to an improved understanding and forecasting of storm

development.

1.2 Problems with previous studies

Although we have seen several tropical cyclone intensity estimation methods introduced since the advent of the meteorological satellite, all have experienced problems and demonstrated various degrees of accuracy.

Fett (1967) has documented several excellent cases which he felt had deviated considerably from the "normal pattern of development" dictated by his model. One storm was noted to have a visible low level circulation center on the edge of the cirrus canopy. It was classified according to the model as a stage C+ "comma configuration" (maximum winds of about 30 knots). However, maximum wind speed reported by reconnaissance within one hour of the satellite picture was 70 knots, a value noted to be "not at all in keeping with the storm's apparent formative structure."

On the 5th of July 1967, Fett flew a reconnaissance mission into what was considered to be a formative tropical cyclone. ESSA II pictures of the storm revealed a circulation center on the north side of overcast cloudiness. The storm had the appearance of a stage C, "comma configuration" with anticipated maximum winds of about 30 knots. As the aircraft approached the center, wind speeds of 70 to 80 knots were suddenly encountered. Fett further noticed that the circulation center corresponded to an area of flattened cumulus and stratocumulus with cloud tops at only four thousand feet. No higher cloudiness and no eyewall in the conventional sense existed.

Dvorak (1975) has observed that caution should be exercised in drawing conclusions from cloud patterns observed early in the morning since "signs of both intensification and intensity often appear weaker

than expected at that time of day". He went on to say that his analysis is accomplished most easily and reliably when "a comparison is made between pairs of pictures taken at the same time each day which would negate the problems resulting from diurnal variations in cloud characteristics".

In 1971 all National Environmental Satellite Service (NESS) bulletins received at the Joint Typhoon Warning Center (JTWC) at Guam were compared to the JTWC best track maximum winds. NESS bulletins were based on Dvorak's earlier (1968) intensity estimation scheme and the Hubert and Timchalk (1969) method. Best track winds are determined after a careful post analysis of each storm and are considered accurate if winds are within ± 10% of the actual maximum wind. Winds within 20% are considered adequate and wind estimate errors greater than 20% of the best track are considered inadequate. In this 1971 analysis, JTWC found 28% to be accurate, 53% adequate, and 47% inadequate (Annual Typhoon Report (ATR), 1971). There was no way to tell how much the warning bulletins issued by the JTWC may have influenced the NESS wind estimates.

A particularly glaring example of a bad estimate was based on an ESSA-9 view of typhoon Rose which at the time, was within hours of striking Hong Kong. Aircraft reconnaissance of the storm was impossible. The NESS estimate of Rose's intensity was 75-80 knots. Post analysis using ship data close to the eye indicated maximum sustained winds of 115-120 knots, a 50% error in the satellite estimate (ATR, 1971). Such results and others based on the experiences of this author while commanding the Guam DMSP site have made him leery of satellite intensity estimates (Arnold, 1975).

The Dvorak scheme (Dvorak, 1975) has shown the most skill and as pointed out in the previous section has been used extensively on an operational basis for the past 6 or 7 years. The initial success with the technique was so impressive that the U.S. Air Force implemented the Selective Reconnaissance Program (SRP) in the Western Pacific (Arnold, 1975). The SRP allows for selective substitution of satellite "fixes" in place of aircraft reconnaissance. Sheets and Grieman (1975), however, have pointed out that those individuals directly responsible for forecasts and warnings, especially in the Atlantic, do not feel that adequate data regarding the accuracy of the Dvorak technique is available for making decisions as to when and where satellite substitutions should be made for aircraft. Their evaluation of the Dvorak technique indicated that it works best for weak and "average" strength storms and worst for very strong or extremely fast developing storms (Sheets and Grieman, 1975). Hence, even though the system may work reasonably well as much as 80% of the time, it is the other 20% or so of the cases, like Typhoon Rose, which can cause larger problems.

1.3 Current Study

Malkus et al., 1960; Malkus and Riehl, 1964; Holle, 1968; and Lopez, 1976 have all reported on tropical cloud populations obtained from either photographic or radar data or a combination of the two. Photographic data are limited to daylight hours and are also restricted in range and resolution. Radar data are similarly restricted particularly within regions of highly attenuating clouds. High resolution satellite data (such as the DMSP) are not as limited in either range or resolution when dealing with penetrative convection or Ci and

provide a basis for composite study while simultaneously permitting case by case studies, a particularly unique feature of satellite data. Those studies previously cited based solely on satellite data, however, have generally lacked other supporting conventional data and were therefore unable to combine observational and dynamic features.

The current study was designed to eliminate many of the problems discussed thus far by using what is considered to be the finest satellite and rawinsonde data sets available. It includes the largest available set of independent satellite pictures and data composites built from the individual pictures from which a whole storm "radar" type depiction of cirrus and deep convection can be made, and the largest available rawinsonde data sets. Details of both data sets are described in the next chapter.

The initial expectations were that:

1) the composited satellite data of storms having the same intensity would reveal significantly different cloud signatures than the composite of storms of another intensity, thereby documenting and correcting the deficiencies of the earlier studies,

2) that composited satellite and rawinsonde data would yield better parameters with which intensity could be measured or estimated, and

3) that an analysis of both individual and composite satellite data would provide new insights regarding the physics of storm genesis.

The first expectation, however, did not prove to be true for several related reasons. First tropical cyclone cloudiness was found to be highly variable. Also vorticity and cloudiness were not found to be well related. Significant changes in cloudiness do not necessarily result in significant changes in vorticity. Likewise, significant changes in vorticity do not result necessarily in important changes

in cloudiness. Vorticity and cloudiness essentially were not found to
be well correlated.

1.4 The variability of tropical cyclone cloudiness

During the course of this research it became evident that storm
convection and cirrus were highly variable. Composited satellite data,
as will be shown, reveal only a weak statistical relationship between
intensity and cloudiness. The analysis of individual cases revealed
that a large and very significant variability exists between storms of
the same intensity, between stages of the same storm, and even diurnally
(over 3-4 hour periods). It soon became obvious that the problems
encountered by Fett and others were not a result of improper selection
of cloud parameters but were rather a result of the highly variable
nature of the tropical cyclone's cloudiness. Therefore, no technique
for estimating storm intensity based solely on cloudiness amount can,
with confidence, specify tropical cyclone intensity at individual
time periods.

While not dealt with in the general context of storm intensity,
there have been several papers which have pointed to different aspects
of a tropical cyclone's variable nature (Malkus et al., 1960; Dvorak,
1968; Chang, 1970; Anthes, 1974; Gray and Shea, 1973; Gray and Shea,
1976; Browner, 1976; Browner et al., 1977; Frank, 1976). Chang
(1970) has observed that the amount of cloudiness in westward propagat-
ing clusters varies from day to day. Sometimes the clusters are well
defined and at other times they may almost vanish. Anthes (1974)
noted that while the average radius of the tropical typhoon is 1000 km,
the size of individual storms may vary within a factor of 2 of this
figure. Malkus et al. (1960) speculated that each type or species of

tropical cyclone (cluster, depression, etc.) has a characteristic
arrangement of cloud forms which identifies it as a member of that
species. They observed, however, that each storm shows a relatively
persistent or slowly evolving character of its own which distinguishes
it from other members of the same species. Browner et al. (1977)
has analyzed 16 days of eight Atlantic storms and has identified a
large diurnal oscillation in tropical cyclone cirrus. This oscillation
shows a maximum at approximately 1700 local time and a minimum area at
0300 local time. The average ratio of maximum to minimum was ∿2.4.
Dvorak[3] has also observed a 2:1 variation in the amount of cirrus
associated with developed tropical cyclones from morning to afternoon.
Shea and Gray (1973) have documented a substantial variability in the
inner core of tropical cyclones. They found a very large variability
in the maximum wind speeds and central pressures (Fig. 5). The rela-
tionship between high maximum wind speed, small eye wall radius, and
low central pressure is only statistical. A very wide range exists
between individual cases. Figure 6 shows the large variability in
maximum winds for various central pressures. Central pressure alone
gives only a rough approximation of storm intensity. Figure 7 illus-
trates some of the radial variations of tangential wind profiles.

1.5 Purpose

The purpose for this research will be to document a number of
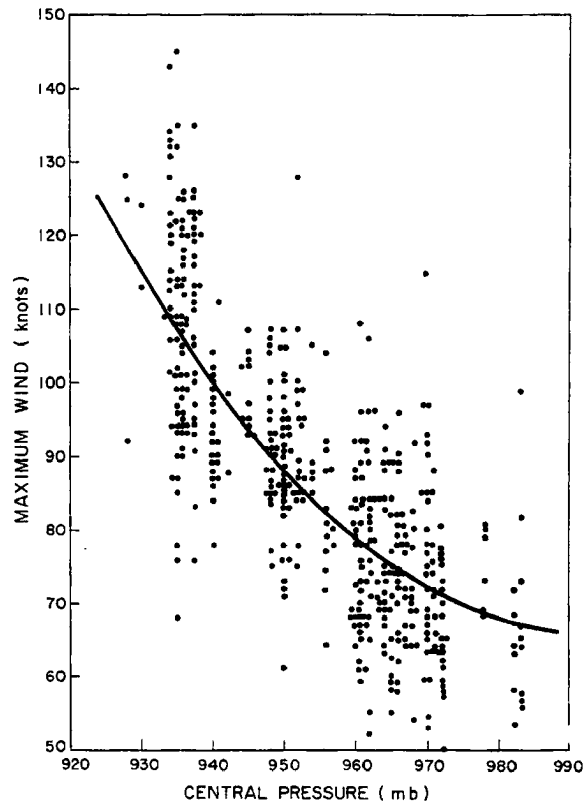findings:

---

[3]Personal communication.

Fig. 5. Variation of the maximum wind with central pressure. The best fit curve is indicated by the heavy line (from Shea and Gray, 1973)
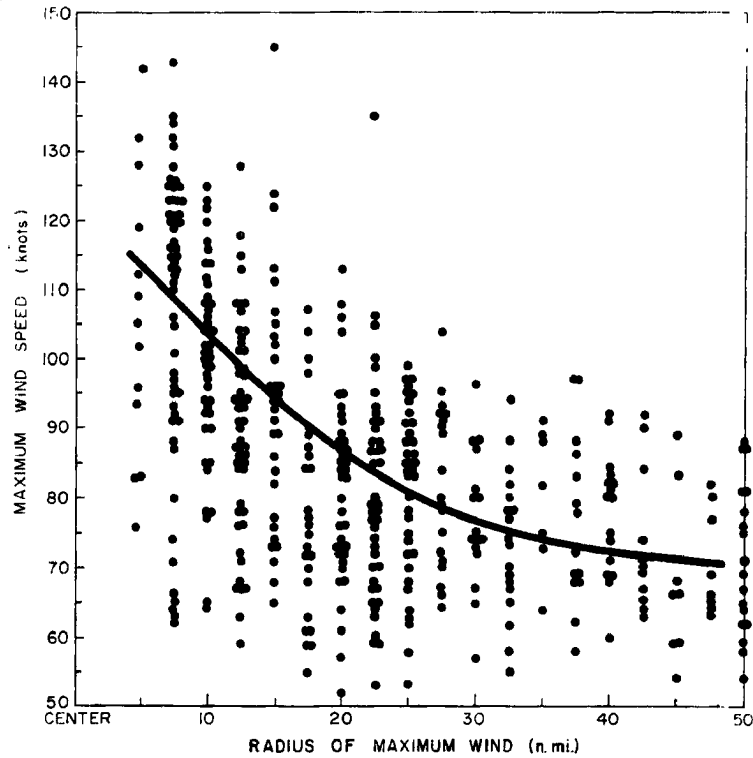

Fig. 6. Variation of the maximum wind with radius of maximum wind. The best fit curve is indicated by the heavy line (from Shea and Gray, 1973).
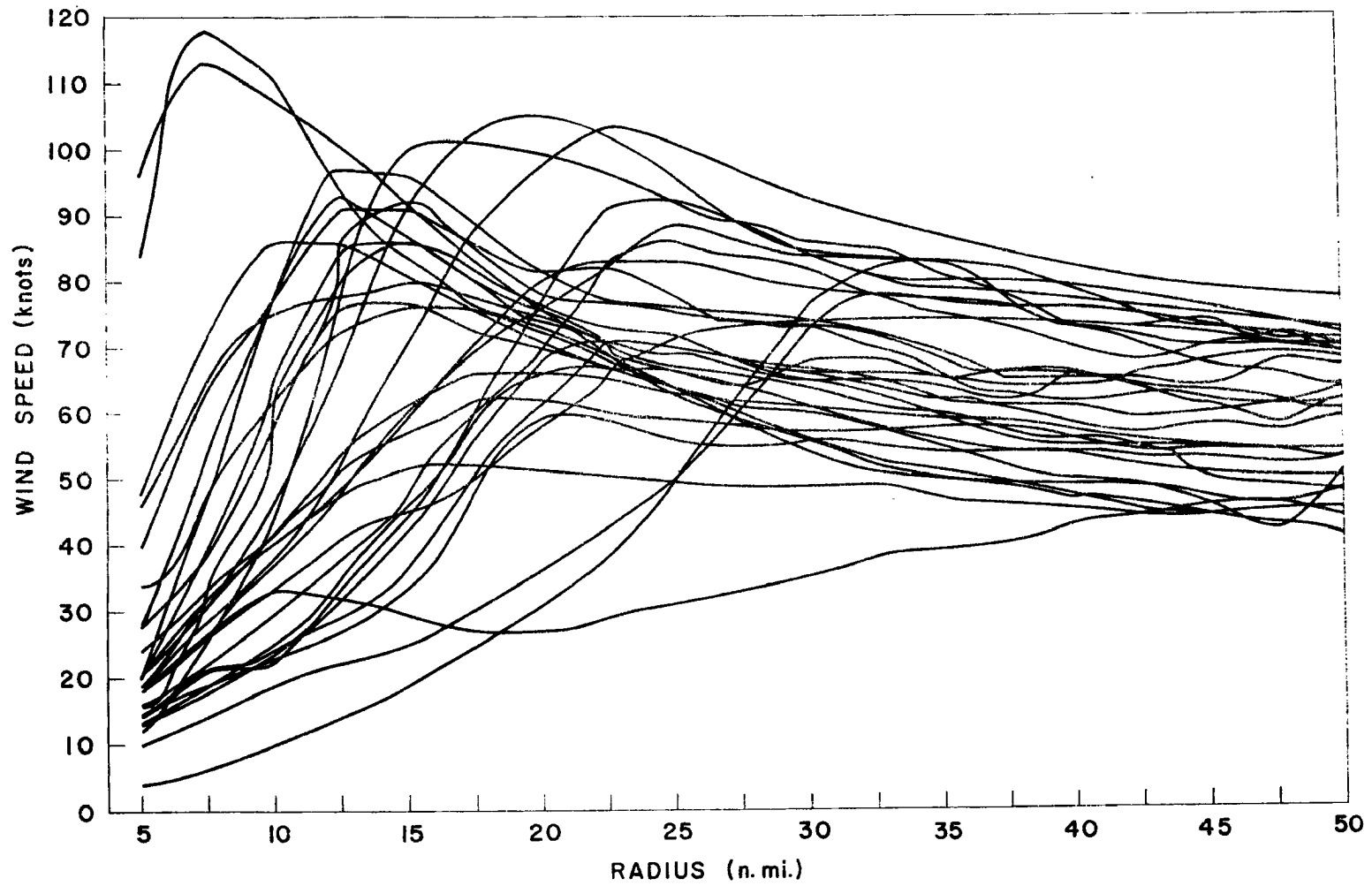
Fig. 7. Examples of observed tangential wind profiles (from Shea and Gray, 1973).

1) The physical characteristics of the intensifying tropical cyclone as revealed in satellite data.

2) The statistical trends observed in the composited satellite pictures of tropical cyclone convection and cirrus.

3) A 'basic convective element' will be defined and shown to be the elemental convective form in tropical cyclones.

4) The existence of cloud free regions associated with the incipient circulation center of the developing cyclone which are likely produced by a dynamically forced subsidence mechanism. It is suggested that this genesis mechanism operates in many developing and non-developing clusters.

5) The variability of convection and cirrus within various tropical cyclone classes.

6) Those influences on a storm which account for the observed cloudiness and wind variability.

7) The weak relationship between tropical cyclone cloudiness and vorticity.

8) Those parameters other than cloud features, such as thermodynamic parameters measurable by a satellite, which might be used to more reliably infer a storm's intensity.

9) The implications of this study with regard to cumulus parameterization.

10) The implications of this study with regard to satellite applications in tropical cyclone analysis.

2. DESCRIPTION OF THE DATA SETS

2.1 Satellite data sets

Satellite data used in this study was positive transparency DMSP photos obtained from the USAF DMSP site located on the island of Guam in the western North Pacific (WESTPAC), via the U. of Wisconsin DMSP data archive. Data was obtained for the period May 1971 through 1975 and included as much of the life cycle of each tropical cyclone as could be obtained by the Guam site. This normally included approximately 4 days of developing cluster data.

For the period indicated above there were normally two, and at times three, DMSP polar orbiting sun-synchronous satellites in 450 nautical mile orbits. They had daytime ascending nodes (AN) which were at approximately 0800 local sun time (LST) and approximately 1200 LST. With two such satellites the Guam site would normally obtain two daylight and two night passes from each satellite for a total of eight day/night passes. Because the satellite's tracks were seldom coincident on any given day, and because the total area of Guam's coverage extended from the South China Sea to near 170 E and from the equator to 35 N, there were not many tropical cyclones missed by the Guam site. Furthermore, with the distribution of DMSP satellites in space and time there were typically four looks at a tropical cyclone on any given day. For the time period 1971 to 1975 approximately 150 storms (30 storms per year) were observed by the Guam site.

During this period of time there were basically two types of DMSP imagery available:[4]

---

[4] Stored readout DMSP visual data is also available but has only 2 n mi resolution at subpoint and has far poorer visual resolution than the direct readout data used in this study.

1) daytime visual or VHR with a spatial resolution at subpoint
   of 1/3 n mi, and spectral band width 0.4-1.2 μ m, and

2) day/night infrared or IR with a thermal resolution as good
   as 1.6 K per gray shade, a spatial resolution of 2 n mi
   at subpoint and spectral bandwidth 8-13 μ m. The temperature
   range of IR is 210 K to 310 K with 16 shades of gray linearly
   distributed through this temperature range. The normal
   temperature resolution is 6.25 K per gray shade.

Each piece of data in normal mode is 1:15 million in scale and

covers a cross track path of 1600 n mi. DMSP imagery has almost con-

stant spatial resolution (1/3 n mi) from satellite subpoint to data

edges, in contrast to sensors on other meteorological satellites which

have much poorer resolution and which suffer degradation in resolution

towards the edges of the data scan. A more complete description of

the various DMSP data types is given in Meyer (1973) and the DMSP

User's Guide (1974) by Dickinson et al. The DMSP VHR and IR

imagery represent a unique data set from the standpoint of overall

quality, resolution, and number of tropical cyclones observed over a

relatively long and continuous period by the same type of satellite

sensor. No other satellite data available can provide the research-

er with these features.

As mentioned above, all available storm data has been used. Each

storm was classified into one of four stages according to its current

intensity. In a post analysis of each storm all available information

is carefully analyzed by the Joint Typhoon Warning Center (JTWC) in

an attempt to determine the storm's location, intensity (maximum

sustained surface wind and central pressure) and speed of movement.

This data provides the basis for the JTWC best track. Storm positions

used on the gridded satellite data were the best track locations

interpolated to satellite observation times or satellite positions when

no best track positions were available. During the majority of the period under study, and particularly for the 1971 and 1972 data, aircraft reconnaissance was the primary input to the best track.

During 1971 aircraft reconnaissance was performed by the Air Force's 54th Weather Reconnaissance Squadron operating WC-130 aircraft and by the Navy's Fleet Air Reconnaissance Squadron One operating WC-121 aircraft. The Navy flew standard low-level (500-1500 feet) investigative flights while the Air Force flew standard 700 mb flights. Investigative flights into disturbances were designed such that the aircraft would fly north from a pre-determined investigative point until the circulation was "closed off", (ATR, 1971). A circulation center could thereby be established. Aircrews would also look for curved cloud lines and bands which would indicate a low-level circulation center. During 1970 the Joint Typhoon Warning Center (JTWC) conducted a study to establish an optimum altitude for the reconnaissance of developing clusters. An exceptionally well documented case is presented in the 1970 Annual Typhoon Report in which no surface circulation could be detected after an extensive low-level investigative flight was made. A well defined 700 mb vortex was found, however. Additional investigative flights at 700 mb were made during the 1970 and 1971 seasons. Based in part on the results of these flights, low-level Navy reconnaissance was discontinued at the end of the 1971 season, and from 1972 on, all investigative and routine reconnaissance flights were made by the Air Force at 700 mb. It was the author's experience while associated with the JTWC that the disturbance circulation centers were typically best defined near 700 mb. This implies a low-level cold core structure in developing clusters and such

observations are supported by the recent findings of Zehr (1976). Air
Force aircrews also make it a practice to look for cloud bands which
spiral towards a circulation center. Developing cluster positions
used in this study were based essentially on aircraft investigative
flights and are considered very reliable.

Satellite positions were used only for the very early Stage I
(maximum wind speed 20 knots or less) storms when no aircraft recon-
naissance was available.[5] During 1971 and 1972 there were approximately
55 investigative flights flown into each developing cluster (Arnold,
1975). Maximum sustained surface winds given in the best track as
mentioned in the introduction are considered accurate to within 10%,
although this figure is likely to be too optimistic. These are based
on aircraft, ship reports, and island observations.

Each piece of data was tagged with the following information:

1) Year, month, day, hour, minute

2) Latitude and Longitude of storm center

3) Intensity in knots interpolated from best track

4) Stage (I, less than 20 knots; II, 20 to 33 knots inclusive;
   III, 34 to 63 knots inclusive; IV, 64 knots or greater[6])

5) Central pressure

6) Pressure tendency

7) Eye diameter from aircraft fix logs if within one hour of
   satellite AN, otherwise a satellite measurement was used

8) Storm direction of movement from best track

---

[5]See Appendix A for discussion and definition of storm stages used
in this paper.

[6]See Appendix A for discussion and definition of storm stages used
in this paper.

9) Type of storm development - equatorial trough, trade wind, or otherwise

10) Circulation center - eye, exposed low level center outside cluster, embedded center within cluster which may or may not be well defined (Fig. 8).

11) Banding features - six types of banding were observed (Fig. 9):

   a. comma shaped cyclone
   b. spiral shaped cyclone
   c. cyclone with quasi-circular cloud bands
   d. cyclone in the shape of a cradle, circulation center normally visible within the cradle
   e. no apparent banding and no peripheral convection outside the cluster
   f. no apparent banding and peripheral convection outside the cluster

12) Radial extent of cloudiness in the four cardinal directions.

From the above described data three data sets were created using the CSU Atmospheric Science Department's Optical Data Digitizer and Display (or OD^3). The OD^3 provides the capability for digitizing positive transparencies. As many as 256 separate brightness levels can be distinguished with the system. A digitized picture is an array of numbers each representing the brightness relative to a specified density range. A black and white vidicon type television camera scans 480 lines. Each line consists of 512 picture elements (pixels). Thus, the output of the scanner portion of the OD^3 is an analog signal representing the density or brightness of each pixel as a function of position.

The first data set (A) was based on a pattern recognition technique developed by the author which permitted a computer analysis of the digitized VHR data. The purpose of the analysis was to locate deep penetrative convective cells or meso-convective scale elements by analyzing albedo variations along the data scan. Initially this was to be the primary data set. The research showed this approach to be
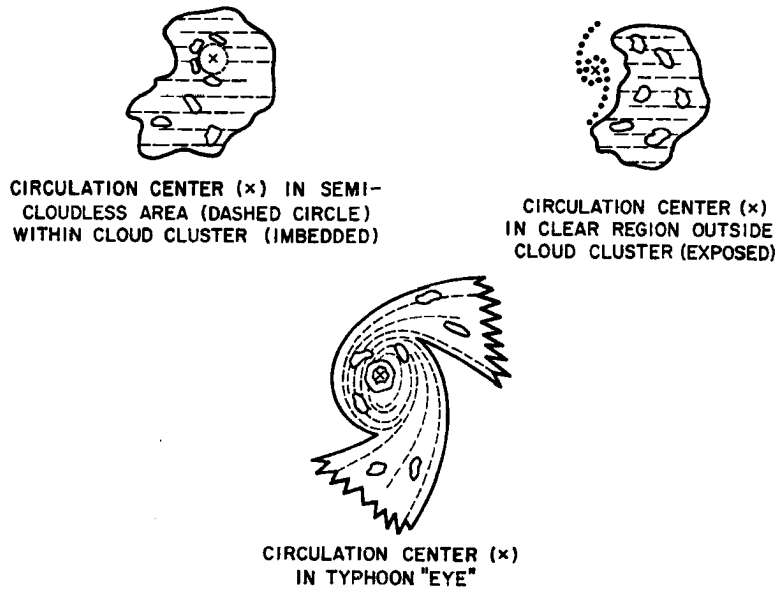
CIRCULATION CENTER (×) IN SEMI-
CLOUDLESS AREA (DASHED CIRCLE)
WITHIN CLOUD CLUSTER (IMBEDDED)

CIRCULATION CENTER (×)
IN CLEAR REGION OUTSIDE
CLOUD CLUSTER (EXPOSED)

CIRCULATION CENTER (×)
IN TYPHOON "EYE"

Fig. 8.   Illustration of the three basic circulation center types
associated with tropical cyclones.

COMMA   SPIRAL   QUASI CIRCULAR

CRADLE   NO BANDING   NO BANDING, SMALLER CONVECTIVE
              LITTLE CONVECTION   ELEMENTS OUTSIDE CLUSTER
              OUTSIDE CLUSTER
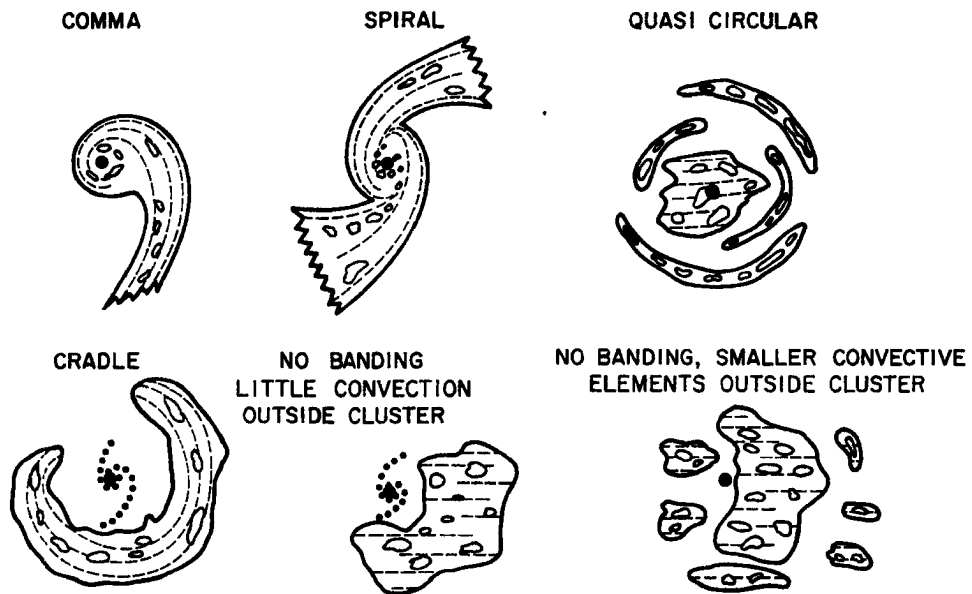
Fig. 9.   Illustration of the six banding feature types associated with
tropical cyclones. Large dot shows typical location of cir-
culation center.

quite inadequate for an individual case. The base-line energy level differences between individual pictures were too large. Although composite values were found to be quite agreeable with the other data sets, individual case studies could not be used with reliability.

A second data set (B) was then created from the VHR (1/3 n mi visual) data based on a partially subjective analysis of meso-convective elements[7] and an objective measurement of these elements using the OD^3 with a desk top CDC 2100 computer programmed to provide fractional percent area covered by a given cloud type. The subjective analysis was done by exploiting the wide dynamic range (brightness range or contrast) of DMSP VHR data in combination with IR data. With high contrast positive transparency film meso-convective elements (groups of deep convective cells) can easily be distinguished from other cirrus and lower level cloud types. Texture, shading and shadows all were used to locate these relatively small areas of deep convection. Infrared was used to confirm selected meso-convective elements. These elements were first outlined with pencil on the film and later traced onto tracing paper. With essentially two gray shades on the tracing paper (black for cloud, white for no cloud) it was an easy task for the computer to determine fractional coverage.

The third data set (C) utilized the digitizing procedure used for data set (A). Calibrating each piece of IR data with a 16 step gray

---

[7]Areas of penetrative convection and cirrus, referred to in the literature of meso-convective elements (GARP technical report, 1970; Sikdar and Suomi, 1971). These individual convective elements are made up of numerous cells and form the basic convective element observed in tropical cyclones. In this paper these features alternatively may be called meso-convective elements, basic convective elements (BCE) or simply convective elements. A more complete description of these elements will follow in a later chapter.

wedge the percent area of the top three shades of gray representing

temperatures in the range of less than or equal to 210 K to less than

222.5 K, i.e., approximately -50 C to -63 C, were measured. This temper-

ature range effectively measured most cirrus clouds assuming a maximum

sensor error reading of 5 C too cold (DMSP User's Guide). Sample sizes

for all three data sets for all four stages are given in Table 1. Table

2 breaks out the data given in Table 1 by year. The results reported

in this paper were based on data sets B and C unless otherwise noted.

Data set A did provide substantial qualitative agreement with the com-

posited data results of data sets B and C. An example which shows the

meso-convective elements obtained from the tracing procedure outlined

above is shown in Fig. 10. The Visual (VHR) picture used for this case

is shown in Fig. 13. The corresponding IR data enhanced with a color

densitometer and then photographed in black and white to emphasize

selected IR temperature ranges, is shown in Fig. 11 (total cirrus) and

Fig. 12 (coldest shade of cirrus).

An overlay grid (Fig. 14) centered on the storm and aligned north-

south was used with each system. The overall grid size and the size of

an individual grid box were determined by the typical storm size and

by the data resolution. In order that a 480 x 512 pixel representation

from the OD^3 gives a geometric resolution equivalent to that of the VHR

data (1/3 n mi), the size of an individual grid box had to be approxi-

mately a 160 x 170 n mi rectangle. It was found that 25 such boxes

centered on the storm were always able to cover the storm's major cloud

features. For data set A a normalization scheme was devised to account

for those grid boxes which did not appear on the data. This was not

necessary for either data set B or C as only those storms which were

TABLE 1

Sample Sizes for the Three Satellite Data Sets

Storm Stage	I(<20kts)	II(20-33kts)	III(34-63kts)	IV(>64kts)	TOTAL
Data Set:					
A (Digitized set)	302	157	243	274	976
B (Tracing set)	54	48	39	88	229
C (IR set)	68	48	41	92	249

TABLE 2

Sample Sizes by Year for Each of Four Storm
Stages and Three Data Sets

Storm Stage	I			II			III			IV		
Data Set:	A	B	C	A	B	C	A	B	C	A	B	C
YEAR												
1971	24	13	7	25	15	13	36	5	5	60	18	19
1972	98	23	30	63	28	32	96	28	27	161	58	58
1973	11	0	0	3	0	0	1	0	0	0	0	0
1974	130	18	9	43	5	3	76	6	2	35	12	9
1975	39	0	22	23	0	0	34	0	7	18	0	6
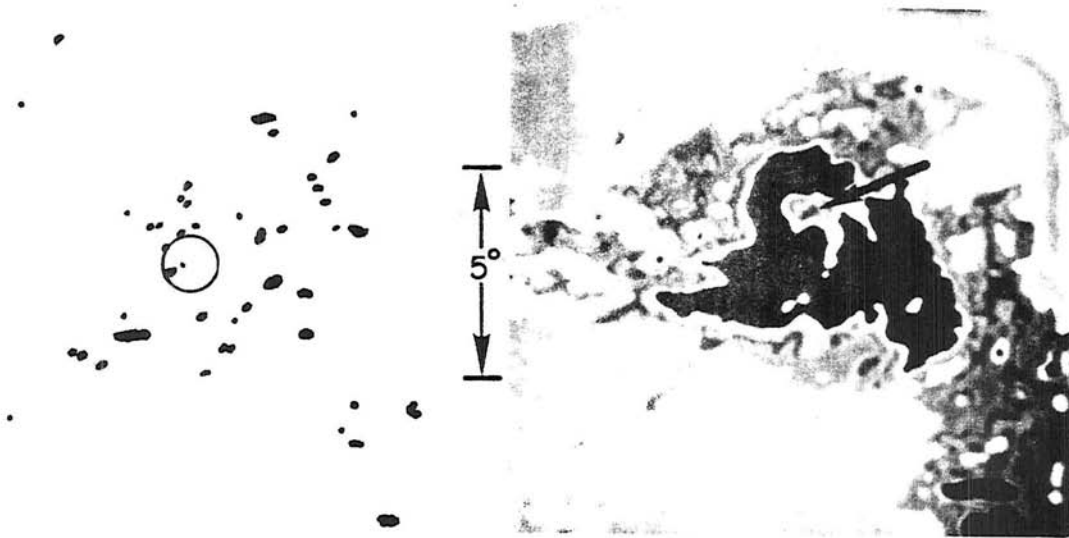
Fig. 10. Meso-convective elements of a developing cluster (Stage I) obtained from the tracing data set B. Storm's circulation center is within the circle. 1" = 484 km.

Fig. 11. Total cirrus (darkest shade) obtained from the infrared data set C for the cluster in Fig. 10. Arrow points to storm's circulation center. 1" = 484 km.
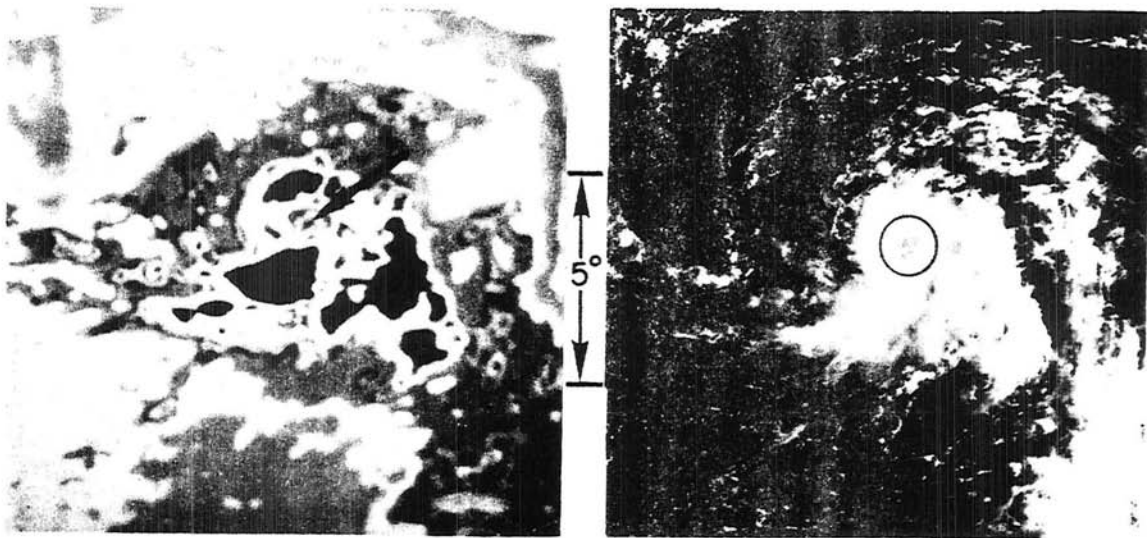
Fig. 12. Coldest shade (darkest shade) of cirrus (T< 210K) obtained from the infrared data set C for the cluster in Fig. 10. Arrow points to storm's circulation center. 1" ~ 484 km.

Fig. 13. The visual satellite picture used for Fig. 10. A developing cluster (Stage I of future Typhoon Nancy), 15 October 1972, 0109Z. Storm's circulation center is within the circle, 1" = 484 km.
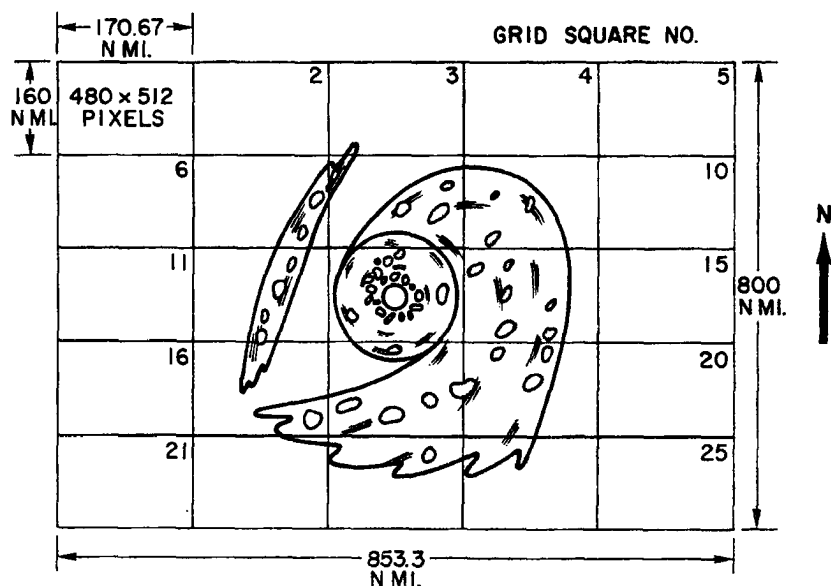
Fig. 14. Overlay grid centered on storm's circulation center and
oriented north-south used to create visual and infrared data
sets.

totally visible on the data were used. Fractional areas of convection
and cirrus (σ) were determined for the center box, 1x1 ($r \sim 0-1.4^{o}$);
the inner 9 boxes, 3x3 ($r \sim 0-4.2^{o}$); and the total 25 boxes, 5x5 ($r \sim$
$0-7.1^{o}$). From this data the σ values could be determined for the 3x3
excluding the 1x1, called the outer 8 ($r \sim 1.4-4.2^{o}$) as well as the 5x5
excluding the 3x3, called the outer 16 ($r \sim 4.2-7.1^{o}$) using the follow-
ing equations (see Fig. 15):

$$\sigma \text{ (outer 8)} = \frac{9 \times \sigma(3\times3) - \sigma(1\times1)}{8}$$

$$\sigma \text{ (outer 16)} = \frac{25 \times \sigma(5\times5) - 9 \times \sigma(3\times3)}{16}$$

2.2 Rawinsonde data sets

Rawinsonde data used in this study was obtained from two sources:
Zehr (1976) and Frank (1976). Both studies were based on ten years

N
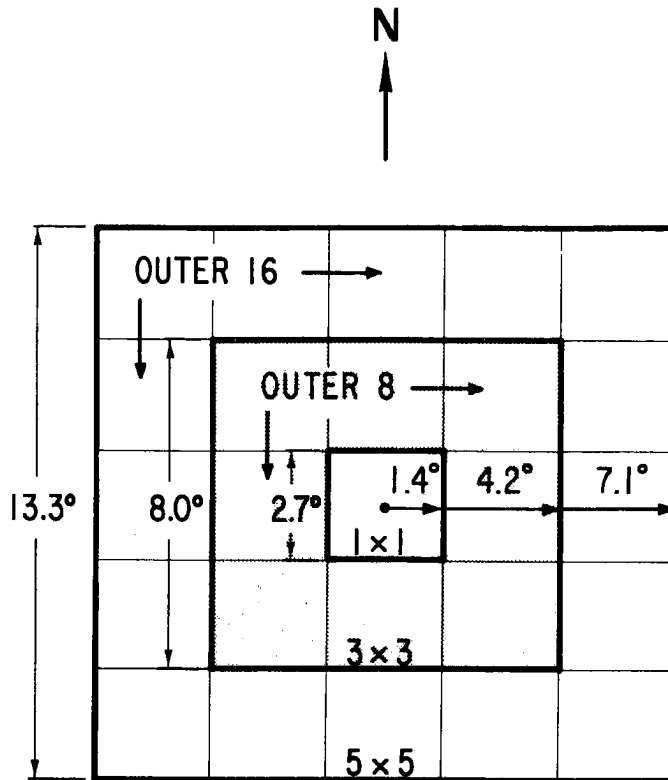
Fig. 15.   Same as Fig. 14.   Shows approximate radial equivalents of 1x1, 3x3 and 5x5 regions.

(1961-1970) of N.W. Pacific rawinsonde data.   Approximately 18,000

soundings from the 30 stations shown in Fig. 16 were used for their

studies.   A more detailed description of these data sets is given in

Frank (1976).   Rawinsonde data were used primarily to support any ob-

served statistical trends in the satellite data regarding storm inten-

sity or structure.   Zehr's pre-typhoon stage (Stage 2 in his paper)

corresponds very well with the Stage I classification in this paper.

Frank's tropical-depression stage was based on reported central pressure

greater than or equal to 1000 mb.   His tropical-storm stage was simi-

larly defined by having a central pressure given by 980 mb $\leq$ p < 1000

mb.   The typhoon stage was defined by 950 mb $\leq$ p < 980 mb and the super

typhoon class was defined by p < 950 mb.   In the remainder of this paper
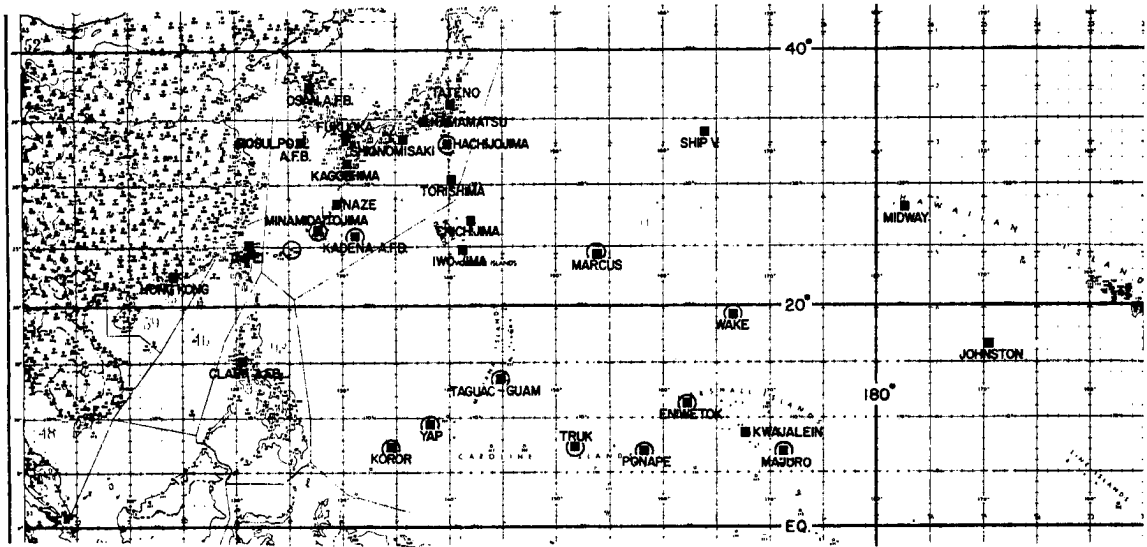
Fig. 16. Data network used in rawinsonde composites.

Zehr's stage 2 and Frank's tropical depression stage, tropical storm stage, and typhoon stage will be used interchangeably with stages I, II, III and IV, respectively, as defined earlier and discussed in Appendix A. Occasionally Frank's super-typhoon stage is used interchangeably with a subset of stage IV called STY also defined as having a central pressure < 950 mb. Well over 90% of the Stage I, II, III and IV storms based on maximum sustained surface winds have best track central pressure values which agree with Zehr's and Frank's storm stratifications.

Table 3 lists the mean characteristics of each of these stages. These compare favorably in all respects with similar storm characteristics observed from satellite data discussed in the next chapter. Table 4 lists the dynamic and thermodynamic parameters observed and calculated from the composited rawinsonde data sets that were used in this study. All rawinsonde data were used with a stationary north-pointing grid. The grid contains 8 octants and extends to 15° (Fig. 17). The $0-1^{o}$ radial band corresponds approximately to the 1x1 box

TABLE 3

Composite Stage Characteristics of Rawinsonde Data Sets

Rawinsonde Stages	Corresponding Stages used in this Paper	Estimate of Central Pressure (mb)	Estimate of Maximum Sustained Surface Winds	Total Number of Rawinsonde Observations	Number of Individual Storms	Mean Lat.	Mean Long.	Direction of Movement	Speed of Movement (m/s^{-1})
Developing Cluster (Stage 2 of Zehr, 1976)	I	1005	15	2404	130	10	153	287	5.5
Tropical Depression (Frank, 1976)	II	1002	25	2325	∿126	17	139	308	5.2
Tropical Storm (Frank, 1976)	III	990	50	5658	∿200	19	136	319	4.9
Typhoon (Frank, 1976)	IV	965	80	4573	∿175	22	136	326	5.0
Super-Typhoon (Frank, 1976)	STY	935	115	2854	85	21	137	329	5.2

33

TABLE 4

Parameters Derived From Composite Rawinsonde Sets

<u>Dynamic</u>

V_R = Radial wind

V_θ = Tangential wind

DIV = Divergence

ξ = Relative vorticity

<u>Thermodynamic</u>

T = Temperature

Z = Geopotantial height of standard pressure surfaces

RH = Relative humidity

q = Specific humidity
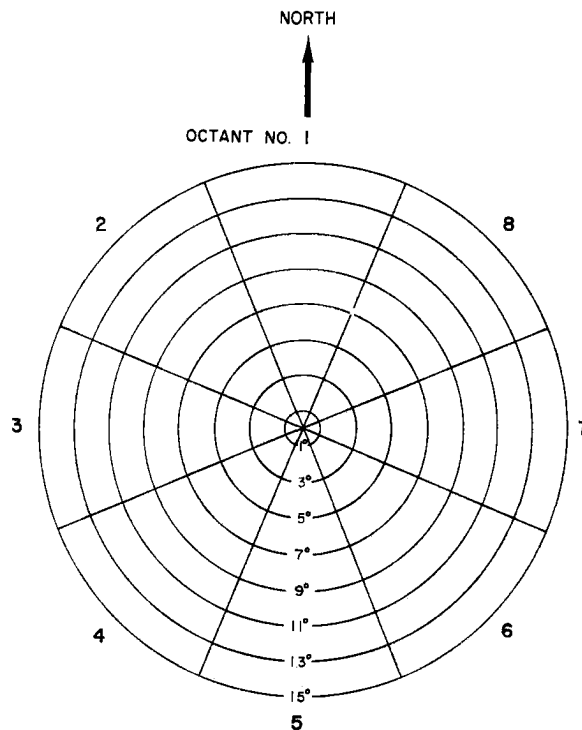
Fig. 17. Compositing grid used by Zehr (1976) and Frank (1976) with rawinsonde data sets.

of the overlay grid used with the satellite data. The 0-4° band corresponds approximately to the 3x3 and the 0-6° band corresponds approximately to the 5x5.

3. PHYSICAL CHARACTERISTICS OF THE TROPICAL CYCLONE DERIVED FROM SATELLITE DATA

Table 5 provides various mean values for the four-wind specified storm stages which can be compared to the mean values given in the previous chapter for the storm stages used by Zehr (1976) and Frank (1976). The following sections will describe such physical characteristics of tropical cyclones as their size, banding features, types of circulation center, and eye diameters.

3.1 The developing cluster (Stage I)

The radial extent of total cloudiness, mentioned as one of the 12 stratification parameters in the previous chapter and measured in the four cardinal directions is given in Table 6. Since virtually all these clusters developed along the equatorial trough, the distinction in size between them and the more northerly trade wind clusters should be noted. The average diameter of the latter is typically assumed to be 4° (Hayden, 1969, 1970). The average diameter of the former was found to be 10°. The standard deviations, however, reveal a substantial variability in overall cloudiness. Too, it must be remembered that this mean radius may enclose large cloud free regions.

Earlier satellite data with poor spatial resolution and less contrast (particularly in digitized reproduction of photographic prints) often made it difficult to distinguish between meso-convective elements and their associated cirrus clouds which were sufficiently close to one another. Convective elements such as A, B, and C in Fig. 18 led to the definition of the typical 4° diameter cluster. Convective elements D, E, and F occur in a region which previously

36

TABLE 5

Mean Storm Position and Track Characteristics

Stage	Latitude	Latitude Range	Longitude	Direction of Movement	Central Pressure
I	12	5-26	142	291	∿1005
II	14	7-29	140	295	998
III	19	9-39	140	311	988
IV	22	11-35	139	318	959

TABLE 6

Radial Extent of Total Storm Associated Cloudiness

Stage	I Ave.	I SD	II Ave.	II SD	III Ave.	III SD	IV Ave.	IV SD
Direction:								
North	4.6	2.1	3.9	1.5	6.1	2.0	5.3	2.2
East	5.6	2.7	5.2	2.1	5.9	2.7	5.7	2.5
South	5.1	2.8	4.7	2.9	6.5	3.1	5.8	2.5
West	5.0	2.6	3.5	1.8	5.2	2.3	4.9	1.8
$\bar{R}$	5.0	2.6	4.3	2.2	6.0	2.6	5.5	2.3

Average (Ave.) and Standard Deviation (SD) values given in °Lat.
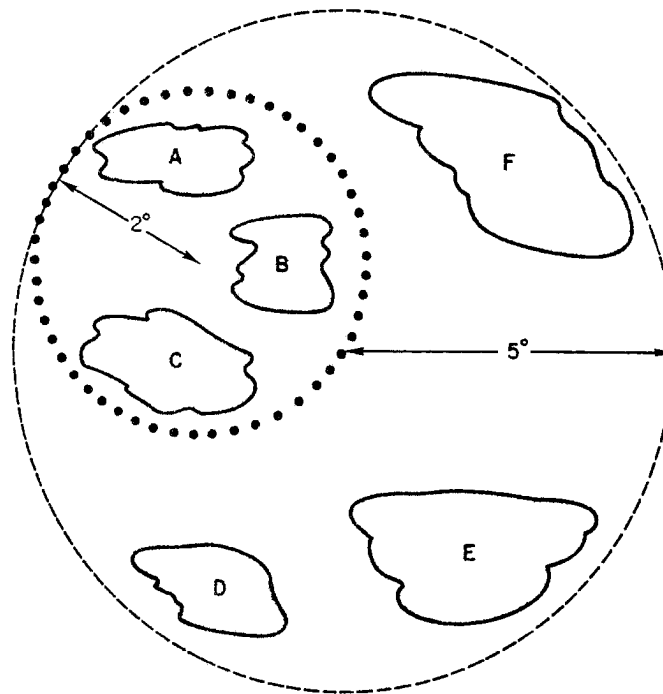
Fig. 18. Illustration of cluster definition. With poor resolution and contrast convective elements A, B, and C appear to merge and form a 4° cluster. With improved resolution and contrast convective elements A-F are separable and form a 10° cluster.

might have been defined as the variable cloud region (Gray, 1973).

With higher resolution and a wider dynamic range, convective elements

D, E, and F are considered in this study to be an integral part of

the typical overall cluster disturbance.

S. Erickson (1977) has recently shown that the areal extent of

non-developing clusters in the equatorial trough are smaller than

developing clusters by 30% or so. It is this author's opinion that

cluster size (as here defined) may be an important element in storm

genesis. Zehr (1976) suggested that while accumulation of upper

level enthalpy is necessary for development, there appears to be

little difference in the wind blow-through or ventilation of tempera-

ture at upper levels between developing and non-developing clusters.

Zehr (1976) found non-developing clusters had greater ventilation
at lower levels (below 600 mb) than developing clusters. If one
assumes equal low level ventilation for both systems, it is reason-
able to expect that ventilation of smaller clusters would have greater
drying effect than in larger clusters. If this drying were to be
compensated by evaporation of cloud particles and falling rain, a
net cooling in these layers would result, and there would be a ten-
dency to establish or maintain a cold core. The larger clusters would
not feel the drying effect as greatly due to the larger moist environ-
ment through which the blow-through would take place.

Cyclone intensification was computed for the two periods Jan.-June
and July-Dec. From the initial detection of a developing cluster to
the tropical depression stage, a shorter time period is required for
development during the latter months of the year. For the period
Jan.-June approximately 4.5 days were required before a cluster
reached the depression stage. For the period July-Dec. this intensifi-
cation stage required only 2.5 days on the average. It is well known
that the intensity of low level vorticity field in the vicinity of
the equatorial trough is greater during the second half of the year
and that storm genesis is directly tied to the relative vorticity field
(Gray, 1975). Apparently, if the vorticity field in which the cluster
is embedded is enhanced, a greater moisture convergence and flow
spin-up can occur towards the incipient storm center. Convection
can be triggered more easily, and development may occur more readily.
Vorticity, however, should not be considered as the primary difference.
Other equally important factors to be considered are sea temperatures
and mid-level moisture values, both of which are greater during the

second half of the year in the western Pacific and, as shown by Gray (1975), are important in seasonal storm statistics.

Clusters (Stage I) were found to have no notable banding features (excluding an upper level anticyclone), i.e. curved bands or spiral arms, in over 75% of the cases (Table 7). When significant banding was observed, 50% of those cases were associated with a cradle appearance. Circulation centers revealed that 25% were visible as low level exposed centers outside or along the periphery of the developing cluster (Stage I), the remaining 75% being embedded within the cluster. As will be discussed (Chapter 4) 50% of the latter were identified as being well-defined (Table 8). An upper anticyclone is an obvious feature with nearly 80% of all developing clusters regardless of the visible presence of banding features. It becomes more visible as the cluster nears the depression stage (Stage II). S. Erickson (1977) has pointed out that non-developing clusters apparently do not exhibit this feature nearly as often. It appears as if this may serve as a good indicator of intensification potential (C. Erickson, 1974).

3.2 The tropical depression (Stage II)

The average tropical depression (Stage II) is smaller than the cluster (Stage I) (Table 6). There is still a considerable variability in storm size, however. Practically every tropical depression (Stage II) exhibited a rather pronounced upper level anticyclone. While only 24% of the previous Stage I exhibited any banding features, 47% of all tropical depressions showed some degree of banding (Table 7). With intensification fewer circulation centers are observed outside the cluster (Table 8). This does reveal a tendency for an increase in convection and cirrus near the center at this stage. This

TABLE 7

Observed Banding Types as a Percent of Total Cases

Stage/Banding	Comma	Spiral	Quasi-Circular	Cradle	No Banding and no Outer Convection	No Banding but some Outer Convection
I	2	3	6	12	10	67
II	11	9	15	12	13	40
III	15	17	18	11	4	35
IV	17	22	30	4	3	24

Note: See Fig. 9 for description of banding types.

TABLE 8

Observed Circulation Center Type as a Percent
Of Total Cases

Circulation Center	<u>1</u>	<u>2</u>	<u>3</u>
Storm Stage:			
I	75	25	0
II	77	23	0
III	83	12	5
IV	49	3	48

1 = Embedded circulation center
2 = Exposed circulation center
3 = Eye
Note: See Fig. 8 for description of circulation center types.

---

concentration of inner convection will be discussed later. A sample

of storms in this stage suggests that the tropical depression is

generally short lived. The tropical cyclone progresses through

Stage II in something like 24-36 hours. Hurricane models generally

assume a system with an intensity associated with Stage II and often

require 3 to 5 days to reach typhoon intensity. The storm appears

to have a significant deepening period, although normally not rapid

deepening, which slows during the tropical storm stage. It may be

that with the development of outer spiral bands in the tropical storm

stage some center inflow is inhibited, and the deepening process,

although still going on through much of the cyclone, is still dampened

somewhat near the center.

3.3 The tropical storm (Stage III)

Stage III is characterized by not only an increase in overall

banding (65% of the cases) but particularly in an increase in spiral

banding which typically occurs at outer radii (Table 7). We also see

a substantial reduction in circulation centers outside the cyclone's

periphery. Nearly 88% of the circulation centers are within the

storm's central cloud mass. Approximately 5% of these centers are

visible eyes with well defined eye walls (Table 8). Based on the data

in Table 6 and statistics discussed in the next chapter, there is a

noticeable increase in overall cloudiness during Stage III. This occurs

primarily as a result of increased banding in the outer 8 boxes (r ∿ 1.4-

4.2°).

3.4 The typhoon (Stage IV)

Table 6 indicates that the total cloudiness associated with the

typhoon stage again decreases from the tropical storm stage. Banding

features are now observed in 75% of the cases (Table 7), and with

virtually all circulation centers embedded within the cyclone's central

cloud mass, nearly 50% of these are visible eyes. Eye diameter

ranges from 6 to 60 n mi with the average being 23 n mi. This agrees

very favorably with the average inner radar eye diameter of 26 n mi

calculated from W. Atlantic data by Gray and Shea (1976). Based on

satellite data alone, there were approximately 2.3 individual eye

observations per typhoon. Since each typhoon was observed twice each

day on the average, this implies that a storm will, on the average,

display an eye for approximately a one day period on satellite data.

3.5 Variability in size, banding, eye diameter

The statistics given in Table 6 reveal that storm size is a

highly variable characteristic and as such provides a very poor

physical parameter for categorizing a given storm. The degree of

banding shows significant increases with storm stage. This helps
explain why Dvorak's intensity estimation scheme has been generally
successful in data void regions. A good many storms, however, may
progress through their entire life cycle exhibiting little or no
significant changes in banding. This variability in size and banding
implies that any intensity estimation technique based solely on these
features will often incorrectly estimate intensity. As seen in Fig.
19, eye diameter is related only weakly to central pressure. The
same conclusion could be reached from Fig. 6.
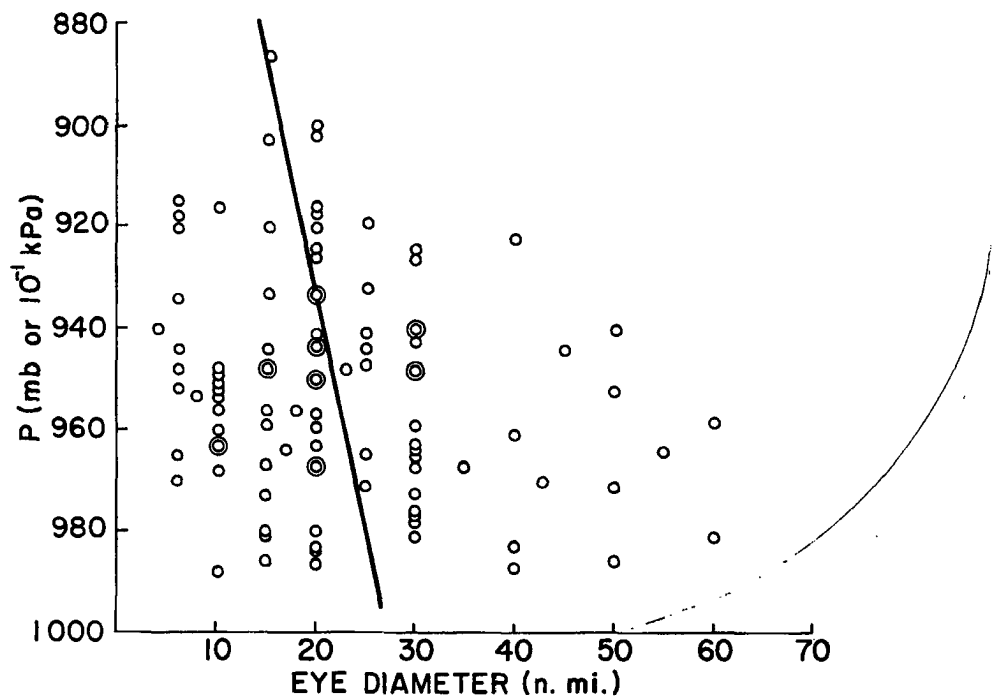
Fig. 19. Variation of eye diameter with central pressure. The best
fit line is indicated by the heavy line.

4. CLOUD CHARACTERISTICS OF THE TROPICAL CYCLONE AS REVEALED IN SATELLITE DATA

4.1 Cirrus and deep convection

As a developing cluster (Stage I) intensifies into a tropical depression (Stage II) there is apparently a concentrating of deep convection about the circulation center (Table 9). There is, correspondingly, a small but significant decrease in convection at outer radii (outer 8 and outer 16). The concentration of deep convection within the center box 1x1 is seen most clearly in the top shade of cirrus and in the total cirrus. The apparent contradiction resulting from the observed decrease in deep convection from the tracing data (Data set B) can be explained as a result of the increasing difficulty in identifying penetrative convection in a region experiencing a large percentage increase in cirrus. At outer radii the decrease in observed convection from Stage I to Stage II is reflected in a decrease in both the top shade of cirrus and in overall cirrus production.

Figures 20a, 20b, 21a, and 21b are of two cases which demonstrate the Stage I to Stage II mean condition changes quite well. In both cases there is a reduction in convection and cirrus at outer radii and the presence of a weak anticyclone over both storms (indicated by the arrows representing the direction of cirrus blowoff).

As the cyclone continues to intensify from the tropical depression (Stage II) to the super typhoon stage, deep convection, as revealed in both the tracing data and the top shade of IR, appears to increase gradually at all radii. However, σ values for the BCE area within the outer 16 region of Stages II, III and IV are not significantly

45

TABLE 9

Percent of Area Covered by Convective and Cirrus Clouds

Storm Region		I N	I σ̄	I SD	II N	II σ̄	II SD	III N	III σ̄	III SD	IV N	IV σ̄	IV SD	IV TY P>950 mb σ̄	IV STY P<950 mb σ̄
1 x 1 (r ∿ 0–1.4°)	(1)	54	5.4	3.6	48	5.2	2.8	39	4.9	2.4	88	4.6	2.5	4.6	4.5
	(2)	68	74.6	27.5	48	79.2	18.7	41	80.1	26.5	92	91.4	14.1	89.1	92.3
	(3)	68	30.6	32.7	48	32.0	29.4	41	34.6	32.0	92	68.3	30.8	61.0	71.7
3 x 3 (r ∿ 0–4.2°)	(1)	54	3.2	1.7	48	2.1	0.9	39	2.2	1.1	88	4.5	2.4	3.7	4.5
	(2)	68	49.9	24.5	48	46.9	20.9	41	47.5	24.5	92	62.8	23.1	61.2	65.1
	(3)	68	16.1	13.7	48	10.7	12.7	41	13.2	13.1	92	32.8	20.3	28.9	33.8
5 x 5 (r ∿ 0–7.1°)	(1)	54	1.9	1.0	48	1.3	0.5	39	1.4	0.7	88	2.5	1.3	2.0	2.8
	(2)	64	32.9	18.0	48	30.3	18.1	40	30.9	18.5	90	42.0	20.2	39.8	43.2
	(3)	64	8.5	7.2	48	6.4	9.3	40	7.4	7.6	90	17.0	11.8	14.1	19.0
Outer 8 (r ∿ 1.4–4.2°)	(1)	54	2.9	1.7	48	1.8	1.0	39	2.0	1.1	88	3.8	2.4	3.8	4.6
	(2)	68	46.8	25.5	48	42.9	22.4	41	43.4	25.2	92	59.2	24.7	57.7	61.7
	(3)	68	14.3	13.3	48	8.0	11.3	41	10.5	11.7	92	28.3	19.9	24.9	29.1
Outer 16 (r ∿ 4.2–7.1°)	(1)	54	1.2	0.8	48	0.8	0.5	39	1.0	0.7	88	1.4	1.1	1.3	1.8
	(2)	64	22.7	15.3	48	21.0	18.3	40	21.6	17.2	90	30.6	20.1	27.8	30.9
	(3)	64	4.4	4.1	48	4.0	8.4	40	4.1	5.5	90	8.5	8.9	5.8	10.7

1 = Basic convective element (Data Set B).   2 = Total cirrus (Data Set C).   3 = Coldest shade of cirrus (T ≤210K) (Data Set C).

N = Sample size   σ̄ = Average percent area covered by cloud   SD = Standard deviation of sample.

(a)

(b)

(c)

(d)
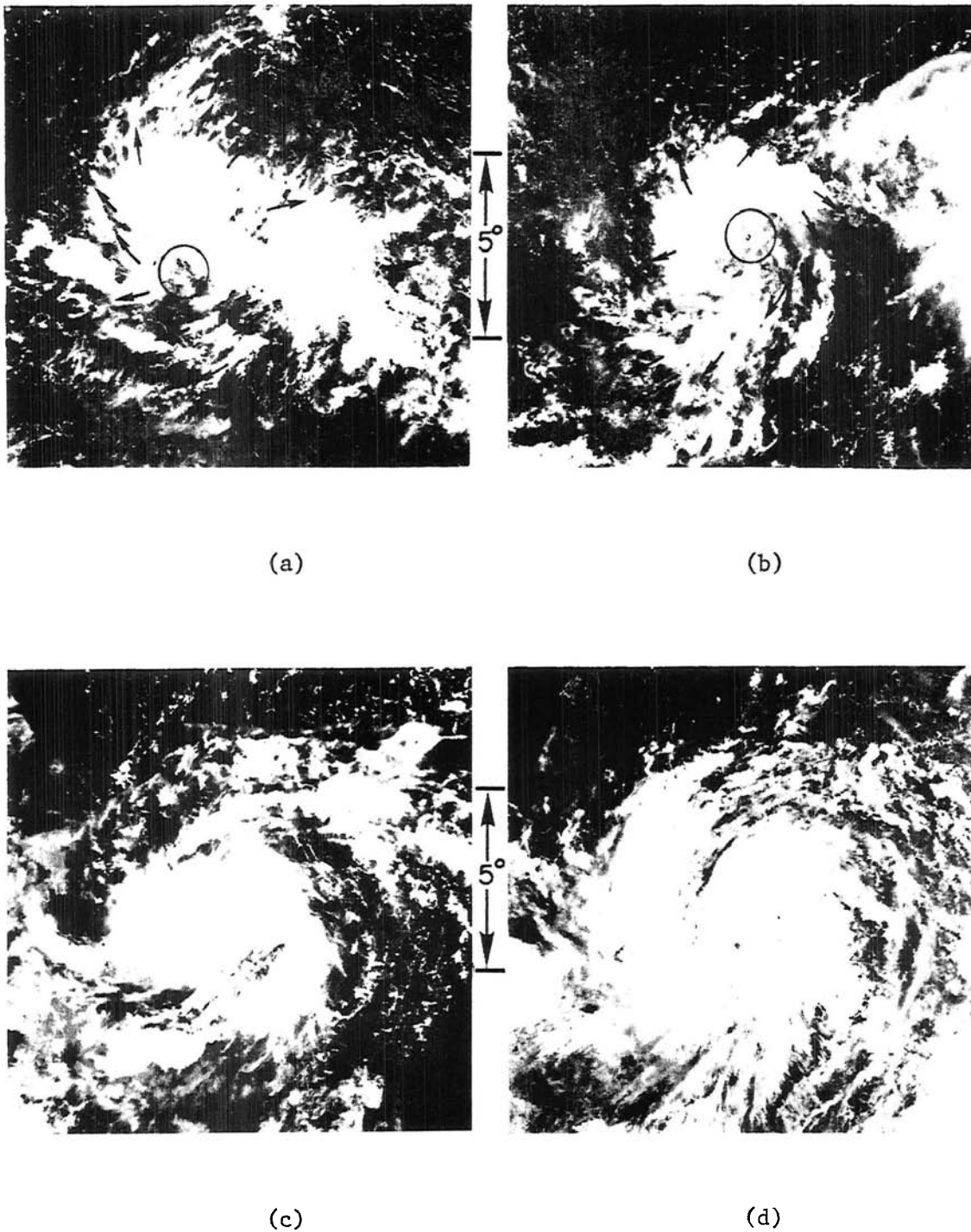
Fig. 20. An example of a storm (Typhoon Ora) which depicts the observed statistical trend of an average storm's life cycle, 1 in = 484 km. (a) Developing cluster (Stage I), 19 June 1972, 0228Z; (b) Tropical depression (Stage II), 22 June 1972, 0327Z; (c) Tropical storm (Stage III), 23 June 1972, 0312Z; (d) Typhoon (Stage IV), 23 June 1972, 2356Z. Circles in first two pictures show where low-level circulation center is located.

(a)　　　　　　　　　　(b)

(c)　　　　　　　　　　(d)
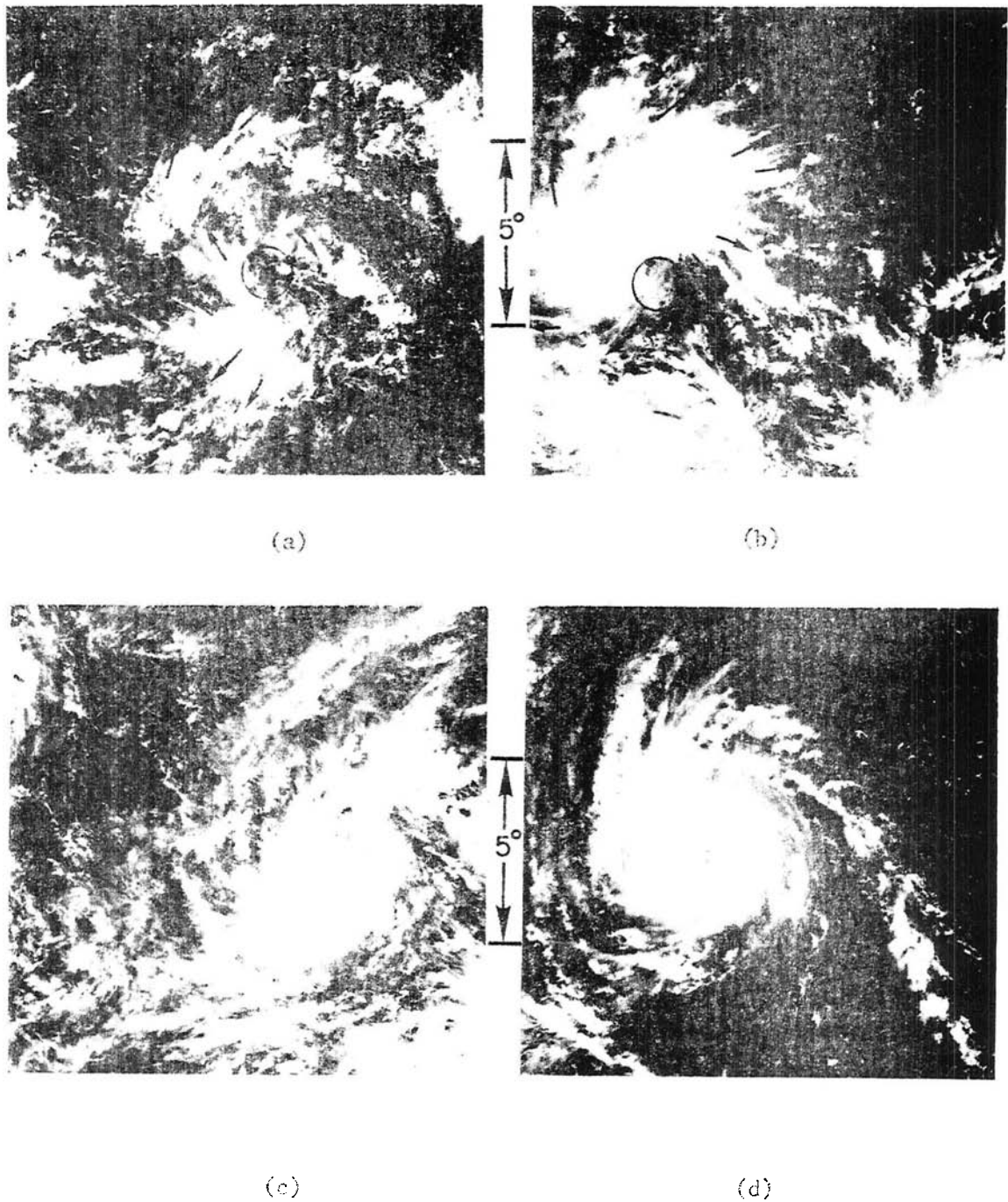
Fig. 21. Same as Fig. 20 except for Typhoon Rita, 1 in = 484 km. (a) Developing cluster (Stage I), 5 July 1972, 0200Z; (b) Tropical depression (Stage II), 6 July 1972, 0146Z; (c) Tropical storm (Stage III), 7 July 1972, 0313Z; (d) Typhoon (Stage IV), 10 July 1972, 0230Z. Circles in first two pictures show where low-level circulation center is located.

different and hence no statistical trend can be ascertained from these values. These mean conditions are illustrated in Figs. 20c, 20d, 21c and 21d. Figures 20c and 21c show developing spiral bands at outer radii with increasing amounts of deep convection and cirrus. Figures 20d and 21d show the typhoon stages of the two storms. Peripheral banding has continued to increase while at the same time inner core convection has become more organized into well defined eye walls. Not only does convection within the inner core continue to increase but, as we have seen, spiral bands begin to form at outer radii with an observed increase in both convection and cirrus production.

Within the storm area (5x5 region) there is a 47% increase in visible deep convection and a 31% increase in the total cirrus from a developing cluster (Stage I) to a super typhoon (STY). The amount of deep convection (3.7%) found within the 3x3 area of a typhoon well with the 4% value reported by Malkus, Ronne and Chaffee (1960).

4.2 Stratifications

Numerous stratifications of the satellite data were made from which composited statistics were computed. These stratifications included: auto-correlation of the cloudiness at one time with the cloudiness at a later time, latitude versus cloudiness, pressure tendency versus cloudiness, and others. The results of nine such stratifications will be discussed:

1) Cluster (Stage I) vs. Typhoon (Stage IV) cloudiness, same storm.

2) Early vs. late clusters (Stage I).

3) Trade wind vs. equatorial trough clusters (Stage I).

4) Deepening vs. filling typhoons (Stage IV).

5) Rapid deepening vs. average deepening typhoons (Stage IV).

6) Past pressure tendency vs. current cloudiness.

7) Past cloudiness vs. current intensity.

8) Cloudiness vs. storm direction of movement.

9) Cloudiness vs. storm speed.

1) <u>Cluster (Stage I) vs. Typhoon (Stage IV) Cloudiness, same Storm.</u>

Cluster cloudiness and later typhoon cloudiness for the same storm show a moderate degree of correlation. The linear correlation coefficient was 0.61 for the 5x5 area. This suggests that small (cloud area) clusters exhibit a tendency to become small (cloud area) typhoons and large clusters similarly tend to become large typhoons. Any such tendency naturally violates the idea that storm cloud diameter and intensity are related. This confirms our earlier observation that average storm radius changes very little with storm stage.

2) <u>Early vs. Late Clusters (Stage I)</u>

Clusters were separated into early and late stages. The former being representative of clusters 3-5 days before they were classified as depressions. The latter were representative of clusters 1-2 days before they become depressions. Early clusters were found to have approximately 8% more cloudiness than late clusters. This result indicates that the concentration of convection may begin early in the life of the developing cluster and continue through the depression stage.

3) Trade Wind vs. Equatorial Trough Clusters (Stage I)

Early in the course of this research it was suspected that trade wind clusters were smaller than clusters forming within the equatorial trough. Hayden (1969), Williams and Gray (1973) and Ruprecht and Gray (1976) have quoted the average area of cloud cluster solid cloudiness as 4-5° in diameter. Earlier, it was shown that equatorial trough (0-12° latitude) clusters in the western north Pacific are (with a change in definition as previously discussed) approximately 10° in diameter. Clusters which developed north of $\sim$ 15 N latitude were considered to be of the trade wind variety. These were compared to those which formed south of N 15. This stratification revealed that trade wind clusters had approximately 40% less cirrus and convection than equatorial trough clusters.

4) Deepening vs. Filling Typhoons (Stage IV) and 5) Rapid Deepening vs. Deepening Typhoons (Stage IV)

More developed storms were examined to determine any relationship which may exist between pressure tendency and cloudiness. Deepening typhoons when compared to filling typhoons were found to have about 23% more cirrus and only 8-10% more deep convection. Rapid deepening typhoons (central pressure falling by greater than 15 mb/12 h) were found to have 8% more convection than deepening typhoons (central pressure falling by less than 15 mb/12).

6) Past Pressure Tendency vs. Current Cloudiness

When past pressure tendency (previous 24 $\pm$ 3½ hours value) was compared to current cloudiness values the correlation was nearly zero. Thus, while current pressure tendency appears somewhat correlated with cloudiness, there is no apparent direct relationship with past tendency and current cloudiness. The storm cloudiness has little

or no memory with regard to pressure tendency. The convection thus appears to respond weakly to current intensity changes but not to prior intensity changes.

An excellent example which illustrates the poor relationship between pressure tendency and changes in convection or cirrus can be seen in Typhoon Gloria (1974). Holliday (Annual Typhoon Report (ATR), 1975; 1976) noted that Gloria of November 1974 displayed unusual intensity fluctuations while in the Philippine Sea. This storm exhibited two intensification periods separated by a 12-h period of weakening. As reported in the 1975 ATR, the storm's central pressure rose from 937 to 955 mb from 5/04Z to 5/16Z, i.e., an 18 mb/12 h filling rate. Following this rapid filling the storm's central pressure began an unusual second deepening. Satellite data revealed a steady but small increase in convection and cirrus from 4/03Z to 7/00Z despite the tremendous short term changes in intensity that were taking place.

7) Past Cloudiness vs. Current Intensity

In order to more fully document the integrated effect of past cloudiness on current intensity a number of storm cases were selected which had two or more observations each separated by 24 hours from the previous observation. The 48 hour past mean convection and cirrus within the 3x3 region for each individual storm period were plotted against current intensity. The results are shown in Figs. 22a and 22b. Only a weak correlation could be found between previous 0-48 h mean cloudiness and current intensity. The linear correlation coefficient relating past deep convection and current intensity was
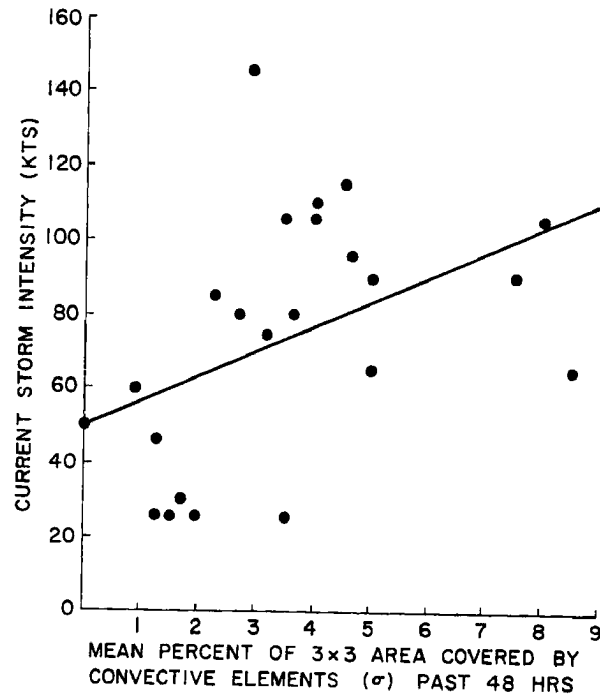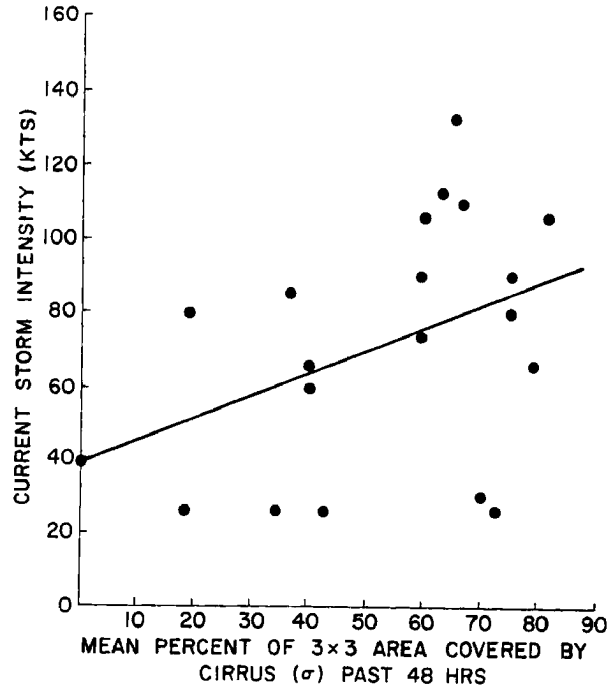
Fig. 22. Previous cloudiness vs. current intensity. (a) Convective
          elements within 3x3 (r ∿ 0-4.2°) region of the storm; (b) Same
          as (a) except for cirrus. σ = fractional area covered by cloud.

0.42. The correlation coefficient relating total cirrus and intensity was 0.36.

8) Cloudiness vs. Storm Direction of Movement and 9) Cloudiness vs. Storm Speed

Several investigators have attempted to relate cloudiness to storm movement. Fett and Brand (1974) devised a technique which provided a 24-h period. This technique was evaluated by this author and his colleagues at the Guam DMSP site in 1973. The results showed no significant improvement over climatology. Based on these results past cloudiness and/or orientation of major cloud features do not appear to be very useful as forecasting tools.

In order to determine what relationship if any exists between current cloudiness and current storm direction or speed, several stratifications were examined. Tropical storm and typhoon cases were combined and divided into two classes based on direction of movement.

1) Storm moving towards $270^{o} \pm 45^{o}$.

2) Storm moving towards $360^{o} \pm 45^{o}$.

A second group consisting of approximately the same number and distribution of storm stages as the previous stratification was likewise divided evenly into three classes based on storm speed.

1) Speed less than or equal to 10 kts,

2) Speed greater than 10 kts but less than or equal to 15 kts and

3) Speed greater than 15 kts.

Composited cirrus and convective element areas were computed for the 3x3 regions of both stratifications. Results are given in Tables 10 and 11. No significant differences in cloudiness could be

TABLE 10

Percent Area Covered (σ) by Cirrus and Convective Elements Within 3x3
(r $\sim$ 0-4.2°) Region for Westerly and Northerly Moving Storms

Cloud Type	Cirrus Cases (Data Set C)	Cirrus (σ)	Convective Cases (Data Set B)	Convective Element (σ)
Storm Direction:				
270° $\pm$ 45°	80	61.2	83	3.5
360° $\pm$ 45°	48	56.7	41	4.0

TABLE 11

Percent Area Covered (σ) by Cirrus and Convective Elements Within 3x3
(r $\sim$ 0 - 4.2°) Region for Three Different Storm Speeds. V_s = speed.

Cloud Type	Cirrus Cases (Data Set C)	Cirrus (σ)	Convective Cases (Data Set B)	Convective Element (σ)
Storm Speed:				
Vs $\leq$ 10 kts	59	61.3	60	3.9
10 kts < V_s $\leq$ 15 kts	40	63.2	43	4.0
V_s > 15 kts	14	58.5	10	4.0

established between storms moving in different directions or between

storms having different speeds. The degree of variability associated

with each class of each stratification appeared to be independent

of direction or speed.

4.3 Distribution and characteristics of basic convective elements (BCE)

In Chapter 2 the meso-convective element was introduced. This

study has revealed that this convective form is a basic or elemental

one in tropical cyclones. This author has observed that deep convective cells over western Pacific tropical waters typically are found to exist as groups of multiple cells of about 20-30 km diameter. This was found to be particularly true of west Pacific tropical cyclones and for this reason the term Basic Convective Element (BCE) was chosen. Gray (1977)[8] has provided several photographic examples of BCE's observed from an aircraft flight he made between Guam and Truk islands in the Marianas (Figs. 23a and 23b). Individual BCE's can easily be visually identified in the four DMSP photos shown in Figs. 24 a, b, c, d. Arrows indicate the location of a number of elements in each of the four figures. Because of entrainment considerations and the fact that boundary layer vertical motions resulting from synoptic scale convergence are not typically sufficient to overcome the stability of the lower level layers without raining downdrafts (Lopez, 1973a,b) it is reasonable in this oceanic region to expect multiple cell complexes rather than individual convective cells standing by themselves. We have seen that 4-5% of the 3x3 area of the Stage IV storm is covered by BCE's (Table 9). It is estimated, based on a visual count of sampled storms, that there are perhaps 5-10 individual updraft cells covering an area of $\sim$ 10% of the BCE. This means that $\sim$ 0.5% of the 3x3 area is covered by deep penetrative convective cells. The mean vertical motion for the typhoon at 300 mb is approximately 200 mb d^{-1} within the 0-4° region as reported by W. Frank (1976). If all the up motion above 300 mb is in Cb updrafts (Frank, 1976) then (with 0.5% of the area in updrafts) the average Cb

---

[8]Personal communication.

(a)
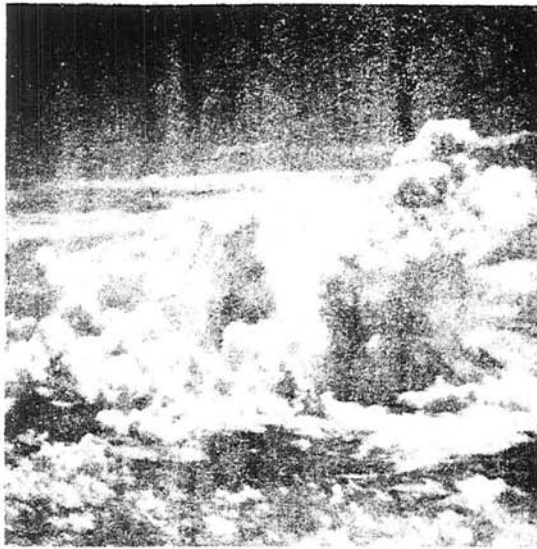
(b)

Fig. 23. Two examples of basic convective elements (BCE) photographed in June 1970 by W. Gray while on flight between Guam and Truk islands.

(a)
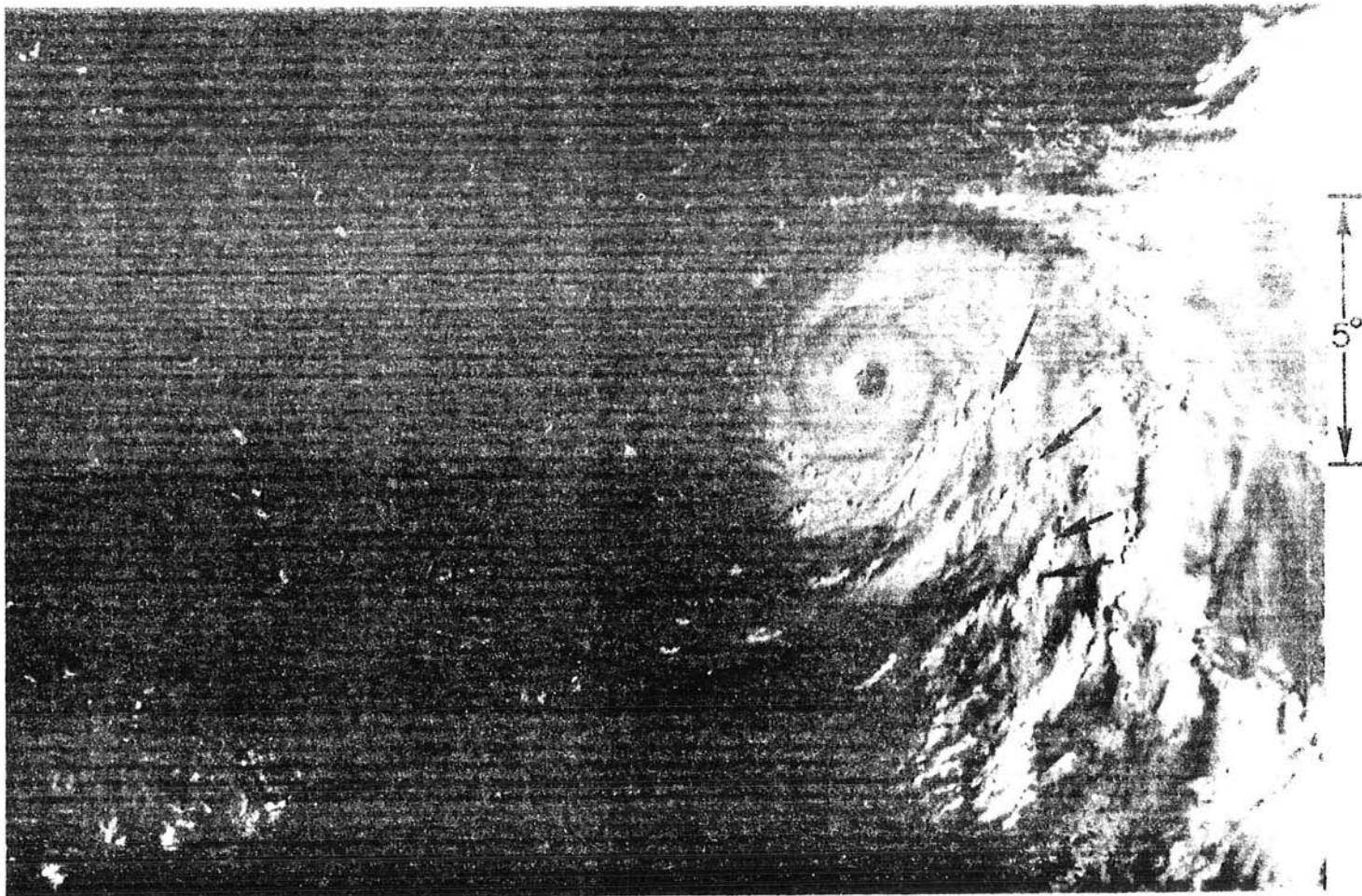
Fig. 24. Four typhoon cases with individual basic convective elements (BCE's) indicated by arrows. 1 in = 380 km. (a) Typhoon Wendy (Stage IV), 7 September 1971, 2107Z; (b) Same as (a) except for 8 September 1971, 2040Z; (c) Typhoon Pamela (Stage IV), 7 November 1972, 0012Z; (d) Same as (c) except for 7 November 1972, 0404Z.

Fig. 24. Continued.

(b)
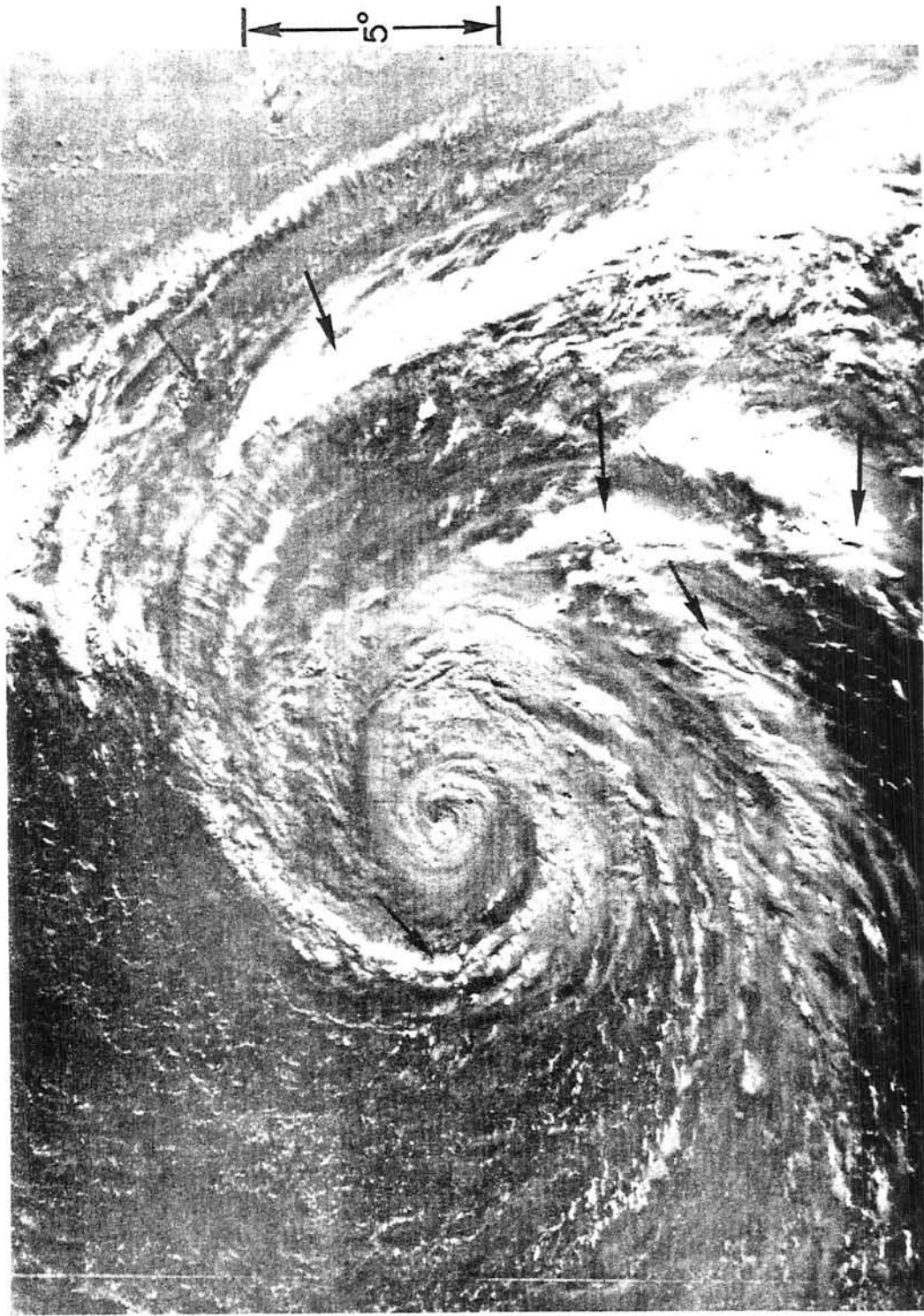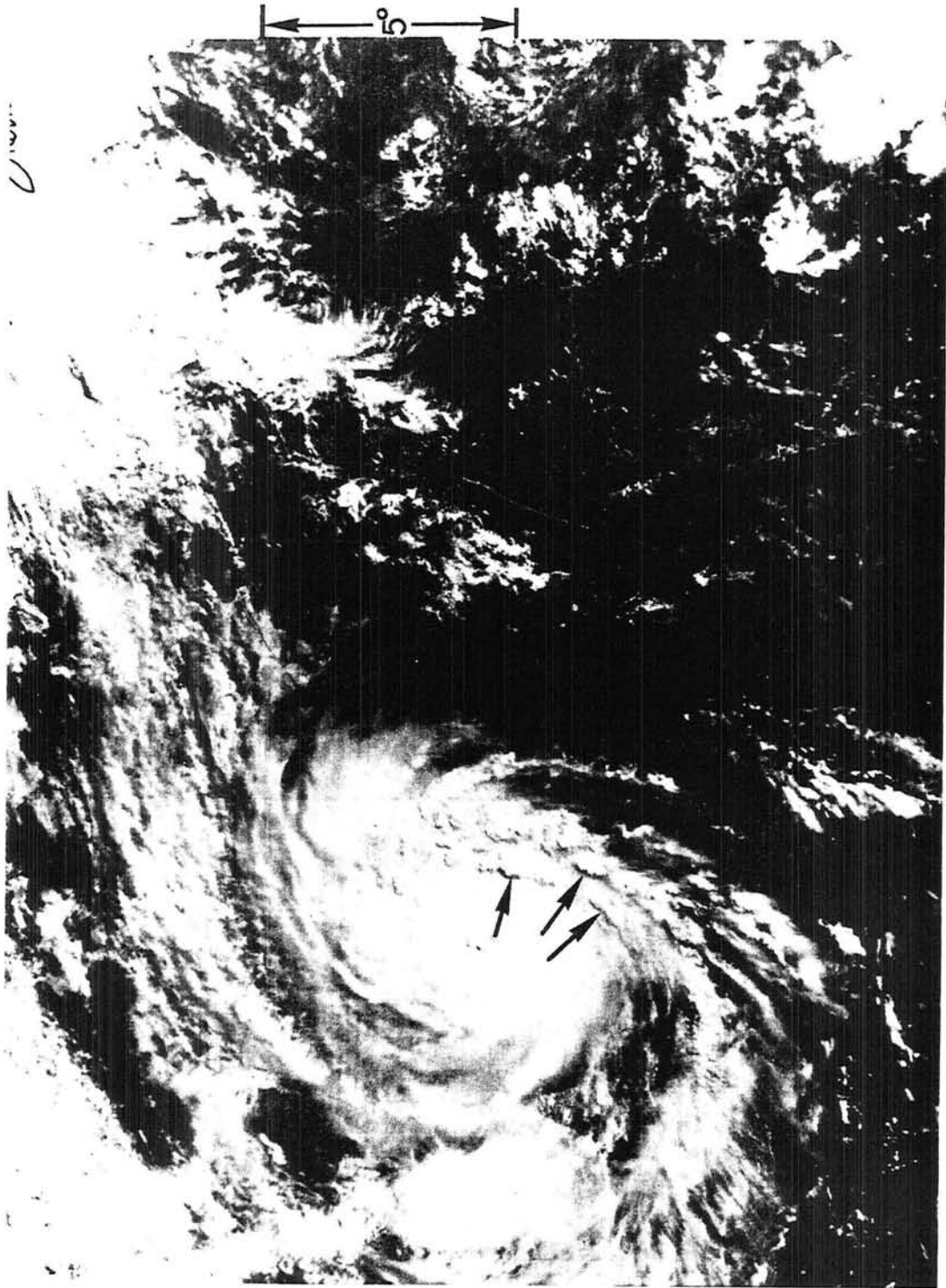
(c)

Fig. 24. Continued.

(d)
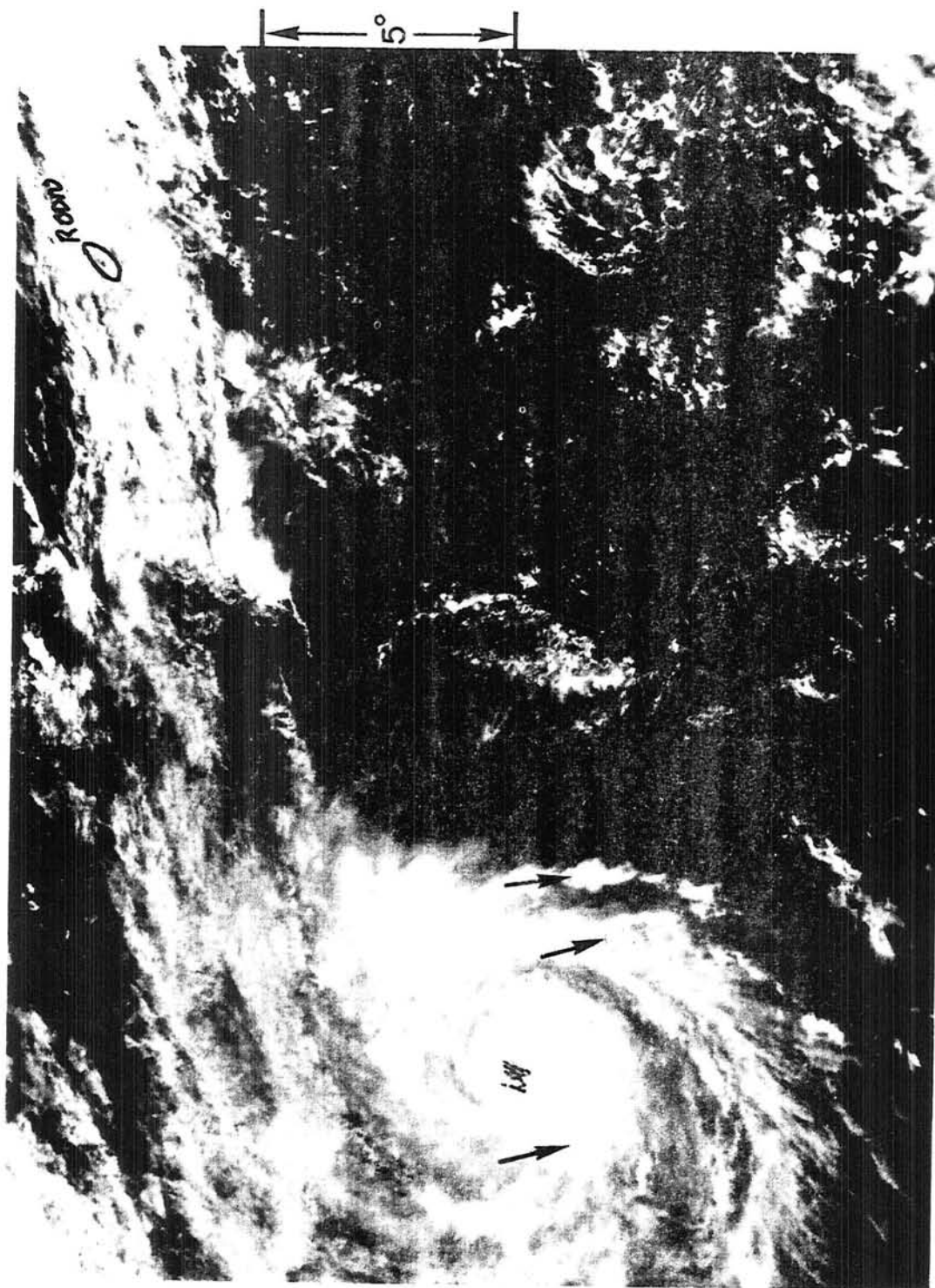
Fig. 24. Continued.

updraft at 300 mb will be approximately 9 m s^{-1}. This estimate agrees
well with the 12 m s^{-1} value estimated by Riehl and Malkus (1961).

The average number of convective elements per storm picture and
per unit area in the 1x1 box, the outer 8 boxes, and the outer 16
boxes (Table 12) reveal the same trends as observed in the percentage
of area covered by the convective elements and the top shade of cirrus
(Table 9). As with the total amount of deep convection in the inner
box we observe a decrease in BCE count with greater storm intensity.
Again this is thought to result from the increasing difficulty in
observing these cells as they become embedded in increasingly denser
cirrus. The average number of BCE's in the outer 16 between storm
stages are not significantly different. This agrees with the observa-
tion in section 4.1 (Table 9) that the σ values for deep convection
between stages in the outer 16 are not significantly different. The
average BCE size for all stages based on data set B (tracing data set)
was approximately 250 n mi^2 or approximately a 30x30 km area. S.
Erickson (1977) has reported finding similar size convective elements
in both his developing and non-developing clusters. He found the
average size to be $\sim$ 26-34 km in diameter.

These large basic convective elements are likely responsible
for most of the vertical energy transport from the lower troposphere
to the outflow region near 150-200 mb. As observed by Lopez (1976)
these elements are frequently irregularly shaped but more often than
not are elliptical or in an elongated band form. This line feature
becomes more apparent with increasing storm intensity.

The percentage of total BCE's found in various parts of the storm
is shown in Table 13. It is seen that there are, in the mean, more

TABLE 12

Average Number of Basic Convective Elements
Per Storm Picture Per Unit Grid Box Area (160 x 170 n mi^2).

Storm Region	I	II	III	IV
Storm Stage:				
1x1 (r ∿ 0-1.4°)	7*	6*	5*	5*
Outer 8 (r ∿ 1.4-4.2°)	3	3	3	4
Outer 16 (r ∿ 4.2-7.1°)	1	1	1	1

*Likely to be an underestimate due to increasing cirrus obscuration
with cyclone intensity

TABLE 13

Percent of Basic Convective Elements in Different Storm Regions. Each
Region Within 5x5 (r ∿ 0-7.1°) Area of Storm

Storm Region	E Half	W Half	N Half	S Half	NW	NE	SE	SE
Stage:								
I	56	44	47	53	19	28	28	25
II	54	46	49	51	21	28	26	25
III	58	42	52	48	19	33	25	23
IV	60	40	47	53	17	30	30	23

E = 0-180°   w = 180-360°   N = 270-90°   S = 90-270°

NW = 270-360°   NE = 0-90°   SE = 90-180°   SW = 180-270°.

convective elements to the east of the storm center than to the west.

Likewise there are more cells to the south than to the north. The

northwest quadrant of the storm reflects a primary minimum in con-

vection with the southwest quadrant being a secondary minimum. Con-

vection in the northeast and southeast quadrants is equally distributed.

These results compare favorably with those based on objective measure-

ments of total cloudiness given in Chapter 3.

4.4 Incipient circulation centers as regions of dynamically forced
     subsidence

In an earlier section it was shown that 25% of all developing

cluster circulation centers were found outside (exposed) of the cluster

itself. Half of these were identified with what was called a cradle

type of banding feature (Fig. 9). The low level circulation center

was still visible but was partially surrounded by the main body of

cluster cloudiness.

An estimated 50% of circulation centers within the cluster (embed-

ded) could be identified with a relative minimum in both deep convection

and cirrus. This was true when the best track positions were based

on aircraft reconnaissance. This feature varied from less than 1°

latitude diameter to several degrees diameter. When an upper level

anticyclone was present over the cluster, the embedded circulation

center was typically found near the anticyclone's center. Had more

of the cluster centers been based on aircraft reconnaissance, it is

expected that the cloud free regions would have more frequently

coincided with the circulation centers. There undoubtedly were cases

of clusters which, due to their advanced stage of development, did

not exhibit this feature. In such cases, and when no aircraft position

was available, the center of cloud mass would most likely have been chosen as the circulation center.

Figures 25, 26, 27, and 28 illustrate these two classes (exposed and embedded) of circulation centers. Figure 25 clearly shows the exposed low level circulation center. Figure 26 depicts the case where the exposed circulation center is cradled by the cloud cluster. Figures 13, 20a, 21a, 27, and 28 are examples of embedded circulation centers. Both types are associated with areas of depressed convection and cirrus and both show that these centers coincide quite well with the position of the upper level anticyclone.

The IR pictures which accompany Figs. 27 and 28 are shown in Figs. 29 and 30. A point worth noting is that the circulation center may be hidden somewhat in visual pictures by thin cirrus. As seen in these figures the IR can, in such cases, be used quite effectively to locate regions of forced subsidence. Many additional examples are given in Appendix B and in the report by S. Erickson (1977).

A substantial number of storms which begin with an exposed circulation center outside of or near the periphery of the cluster retain this feature throughout their lives. Approximately 10-15% of all centers associated with tropical depressions and tropical storms were of this nature. Some 5% of typhoon centers were near the edge of the storm's cirrus canopy or fully exposed. However, the majority of the latter were associated with filling or dissipating typhoons which had encountered a strong upper-level shearing environment (indicated by strong unidirectional flow of cirrus) which in turn removed the cirrus overlaying the low level eye of the storm.
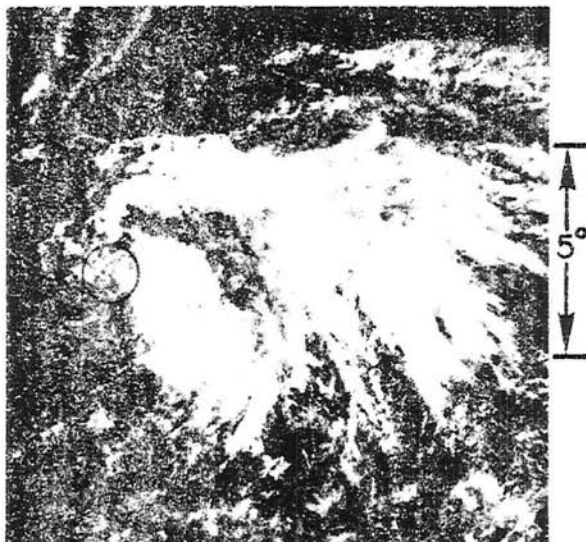
Fig. 25. Example of an exposed low-level circulation center outside the cloud cluster. Center within the circle. Developing cluster stage of tropical storm Viola, 22 July 1972, 0118Z, 1 in = 484 km.
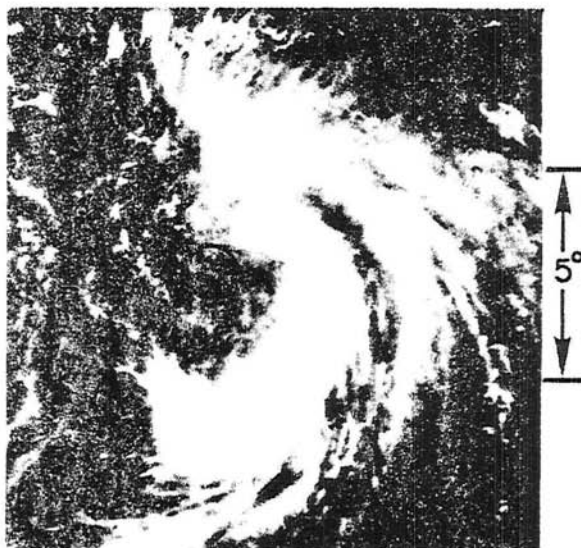
Fig. 26. Example of an exposed low-level circulation center associated with cradle type banding. Developing cluster stage of Typhoon Iris, 10 August 1973, 0313Z, 1 in = 484 km.
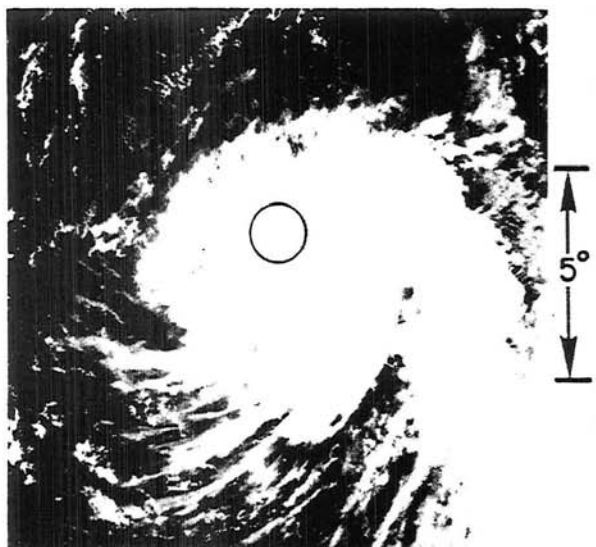
Fig. 27. Example of an embedded circulation center within the circle associated with a region of suppressed cloudiness. Developing cluster stage of Typhoon Pamela, 31 October 1972, 0222Z, 1 in = 484 km.
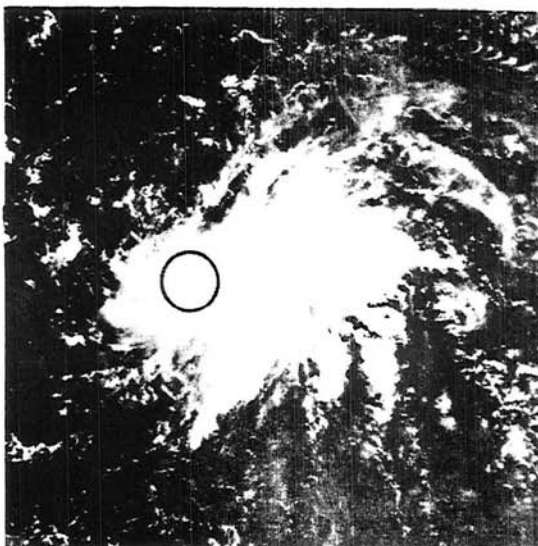
Fig. 28. Same as Fig. 27 except for developing cluster stage of Tropical Storm Viola, 21 July 1972, 0133Z, 1 in = 484 km.
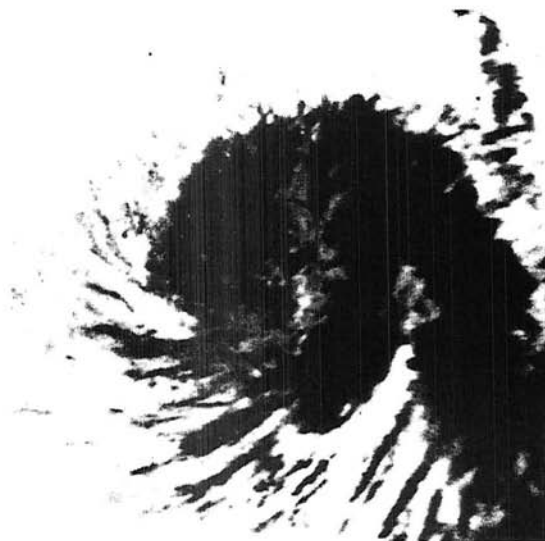
Fig. 29. Infrared picture of Fig. 27. Circulation center within the circle, 1 in = 484 km.

Fig. 30. Infrared picture of Fig. 28. Circulation center within the circle, 1 in = 484 km.

It is postulated that the circulation center develops in a region of dynamically forced subsidence which results from the convergence of the outflow from a number of surrounding deep convective cells (Fig. 31). This subsidence causes an upper level warming which produces a small surface pressure drop. The lower tropospheric circulation is thereby established. This leads to a concentrating of low level mass and moisture convergence and an increase of convection. In this manner the amount of convection near the low level vortex center increases.

It is further postulated that this particular genesis trigger mechanism, which is only one of several other important mechanisms (Gray, 1975; Zehr, 1976), is common to all tropical cyclones regardless of their geographical region of genesis. For example, Sadler (1967a, 1967b, 1976) has often discussed the role of the position of an upper-level trough northwest of a developing cluster in the trade wind region. He has argued that these clusters frequently have an origin from cells in the upper-tropospheric trough. In his 1967 papers he proposed that the upper-trough circulation gradually "penetrated" to the surface and development followed. In his 1976 paper he proposed that the upper-level cell does not penetrate into the near surface layer but rather induces a surface disturbance by the upper divergence east of the cell. This is a tenuous argument. However, with his postulated model, it is reasonable to assume that if the outflow from say the northwest quadrant of the trade wind cluster impinges upon the southwesterly flow from the trough (see Fig. 32), a region of forced subsidence could be established. It should be noted in this regard that trade wind tropical storms seldom develop until
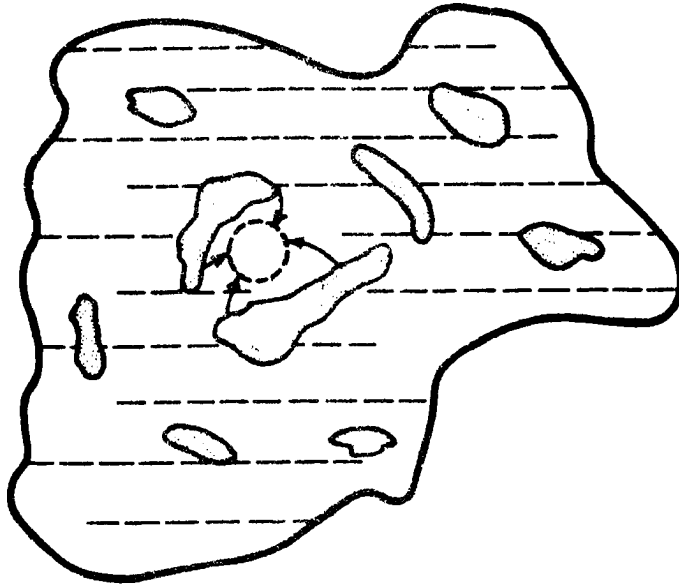
Fig. 31. Illustration of a region of dynamically forced subsidence embedded within a developing cluster. Arrows show outflow from convection elements (shaded). Dashed circle represents the area of maximum upper level convergence.
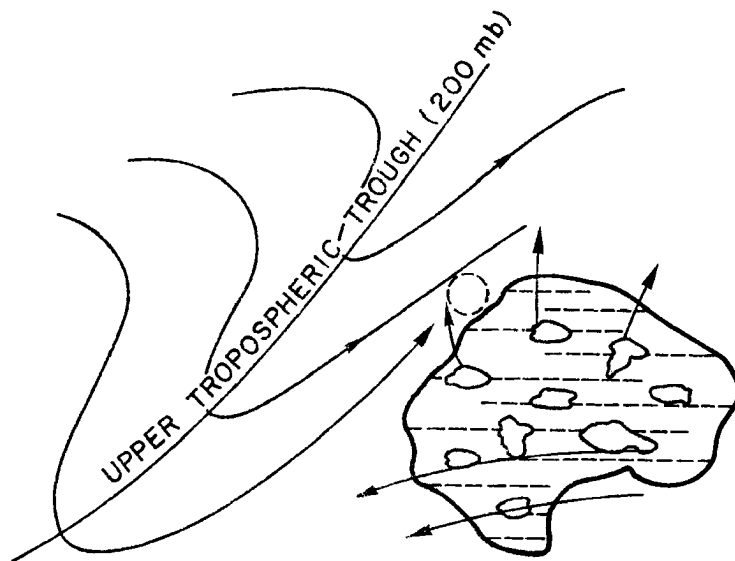
Fig. 32. Same as Fig. 31 except dynamically forced subsidence in an exposed clear region surrounding the cluster. Dashed circle represents area of maximum convergence between outflow from convective elements and southwesterly flow from upper level trough.

they become located near an upper-level trough to their northwest

(Sadler, 1967a, 1967b; Gray, 1977). Lopez (1973b) has similarly specula-

ted on this genesis mechanism. He states:

> "there are reasons to believe that the broadscale
> flow at the level of the disturbance's outflow
> (approximately 200 mb) might be the controlling
> factor. Thus, if the wind pattern at that level
> allows the outflow from the disturbance to be
> spread over a broad region, only gentle subsidence
> and warming will occur. However, if the upper
> air wind pattern restricts the outflow, strong
> local subsidence and considerable warming might
> develop near the disturbance. The convective
> activity would then organize itself around the
> resulting warm core low-pressure region."

More recently Gray (1977) and S. Erickson (1977) have discussed this

genesis mechanism.

Recent observational studies using GATE cluster data support this

hypothesis. Grube (1977a)[9] has recently examined temperature deviations

in the 400 to 150 mb layer taken from several GATE ship 3-h resolution

resports. Combining radar and SMS satellite data with high frequency

rawinsonde data she has observed several cases of warming (2-3 C per

3-6 hs) in this layer in apparently clear regions adjacent to deep

convective cells. Martin et al. (1977) have observed significant

regions of upper level convergence ($4 \times 10^{-5} \text{ s}^{-1}$) on the sides of a

GATE cluster using cirrus cloud vectors measured from SMS data. The

implications of dynamically forced upper-level warming with regard to

current parameterization of cumulus heating will be discussed in

section 6.2

---

[9]Personal communication.

4.5 Variability

Perhaps the single most important result from the analysis of individual satellite pictures in this study has been the documentation of the variable nature of both deep convection and cirrus associated with the tropical cyclone. Figures 33-42 illustrate this variability. We find it within the same storm and between storms. Figures 33-38 illustrate cloud variability within the same storm while Figs. 39-42 illustrate the variability between storms. Figures 33-35 show the various stages in the life of three storms. Storms which begin, for example, as small clusters may evolve into large sprawling typhoons. Likewise, large clusters may become typhoons with small regions of cloudiness. Clusters with little convection may eventually contain enormous spiral arms with numerous convective elements, and fully developed storms may contain little convection. This author flew into a fully developed typhoon in 1971 (shown in Fig. 24a approximately 6 hours prior to the flight) which had 130 knot maximum sustained winds. Radar and visible observations revealed no significant eye wall convection upon penetrating the eye. W. Gray[10] reports that during a similar reconnaissance flight into an Atlantic hurricane in 1964 with maximum sustained winds of $\sim$ 80 kts, the inner region convection did not go above 8-10 thousand feet but that some 100-120 n mi east of the storm center cells were found to 18,000 feet. As shown in these figures, storms may change their appearance from stage to stage, one day to the next, or even during the course of a day.

---

[10]Personal communication.

(a)

(b)

(c)

(d)
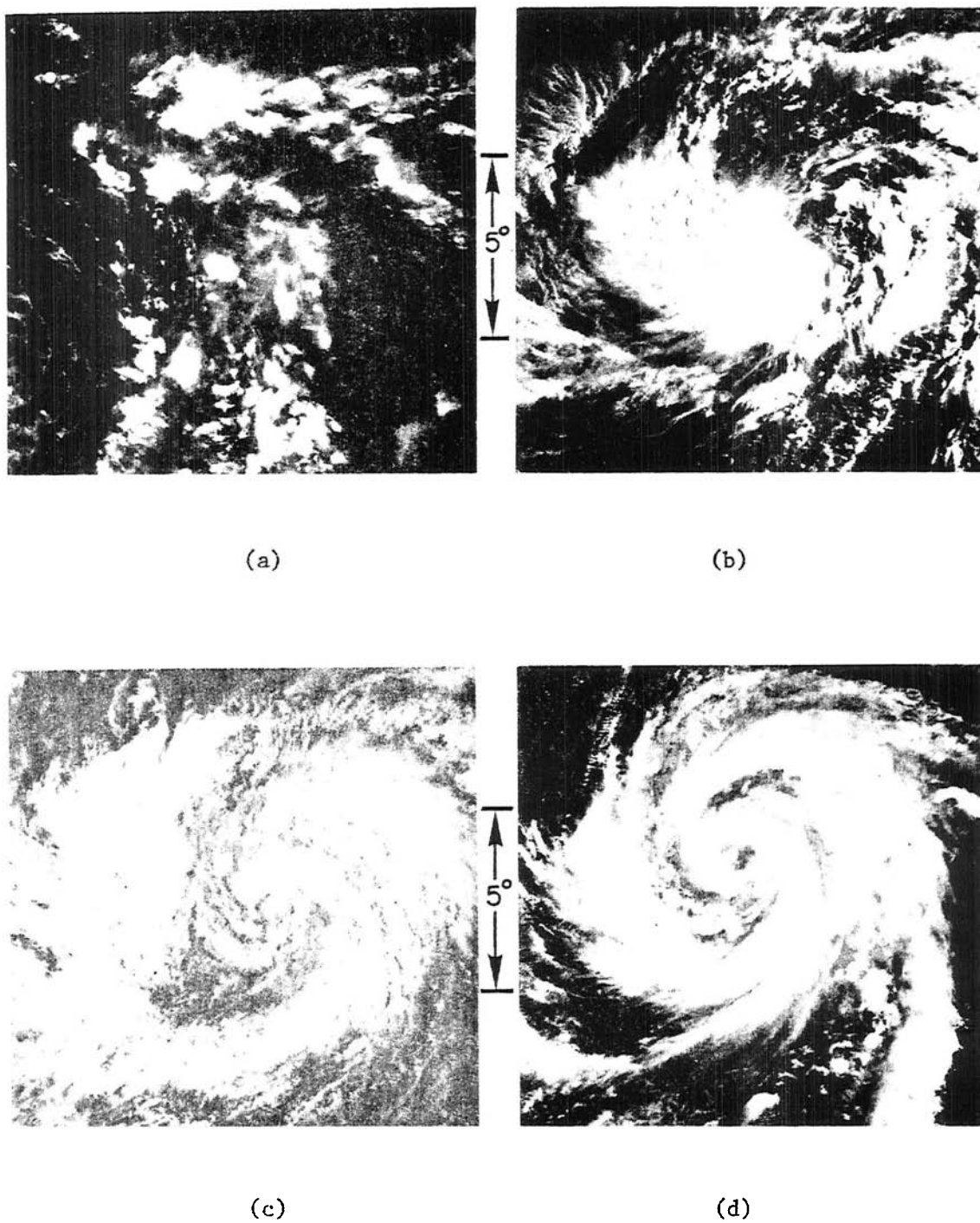
Fig. 33. An example of the variability in cloudiness associated with
Typhoon Lola, 1 in = 484 km. (a) Developing cluster (Stage I),
26 May 1972, 0128Z; (b) Tropical depression (Stage II), 29 May
1972, 2151Z; (c) Tropical storm (Stage III), 30 May 1972,
2124Z; (d) Typhoon (Stage IV), 1 June 1972, 0143Z.

(a)

(b)

(c)

(d)
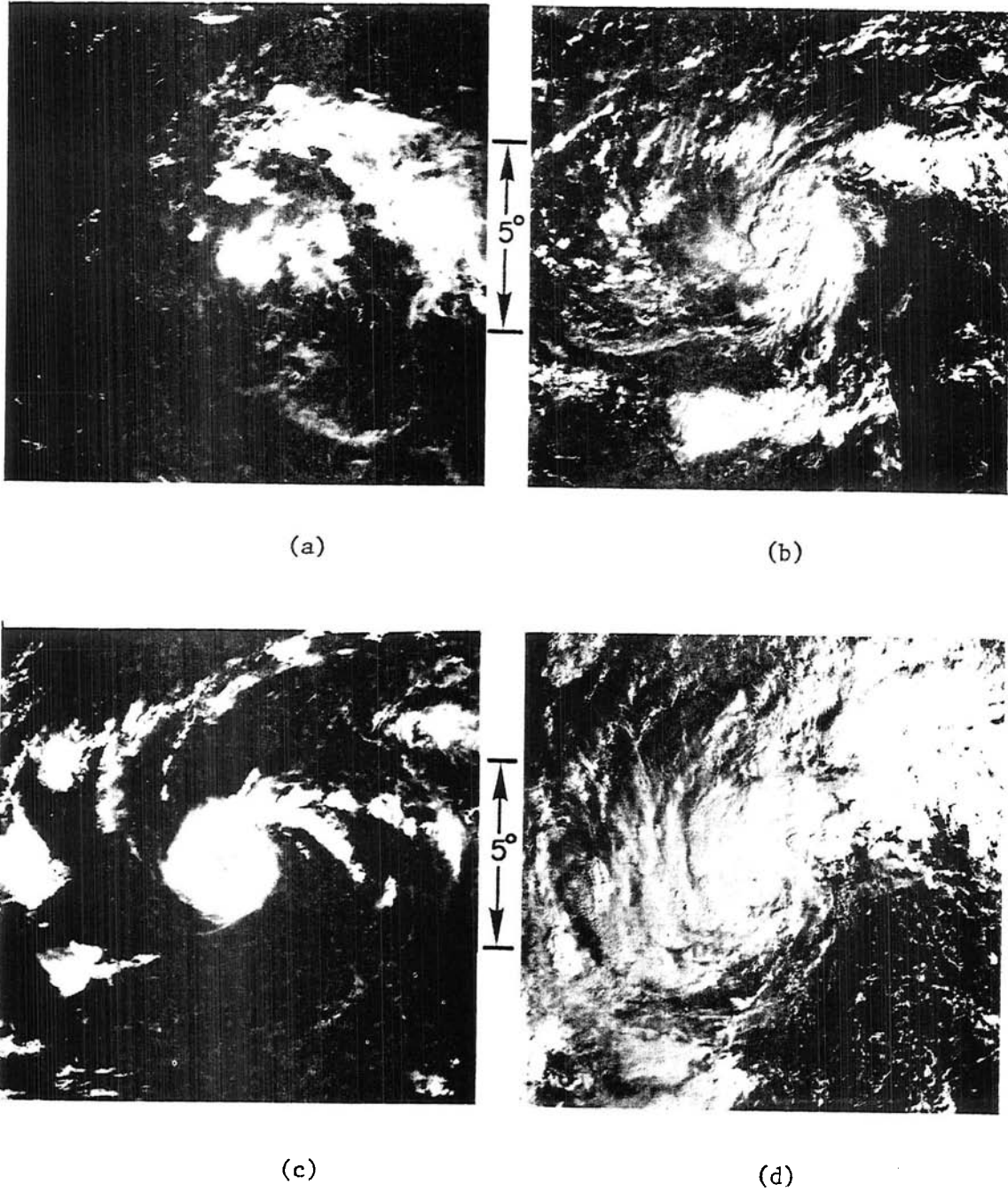
Fig. 34. Same as Fig. 33 except for Typhoon Kit, 1 in = 484 km. (a) Developing cluster (Stage I), 3 January 1972, 0159Z; (b) Tropical depression (Stage II), 4 January 1972, 2240Z; (c) Tropical storm (Stage III), 6 January 1972, 0251Z; (d) Typhoon (Stage IV), 6 January 1972, 2324Z.

(a)

(b)

(c)

(d)
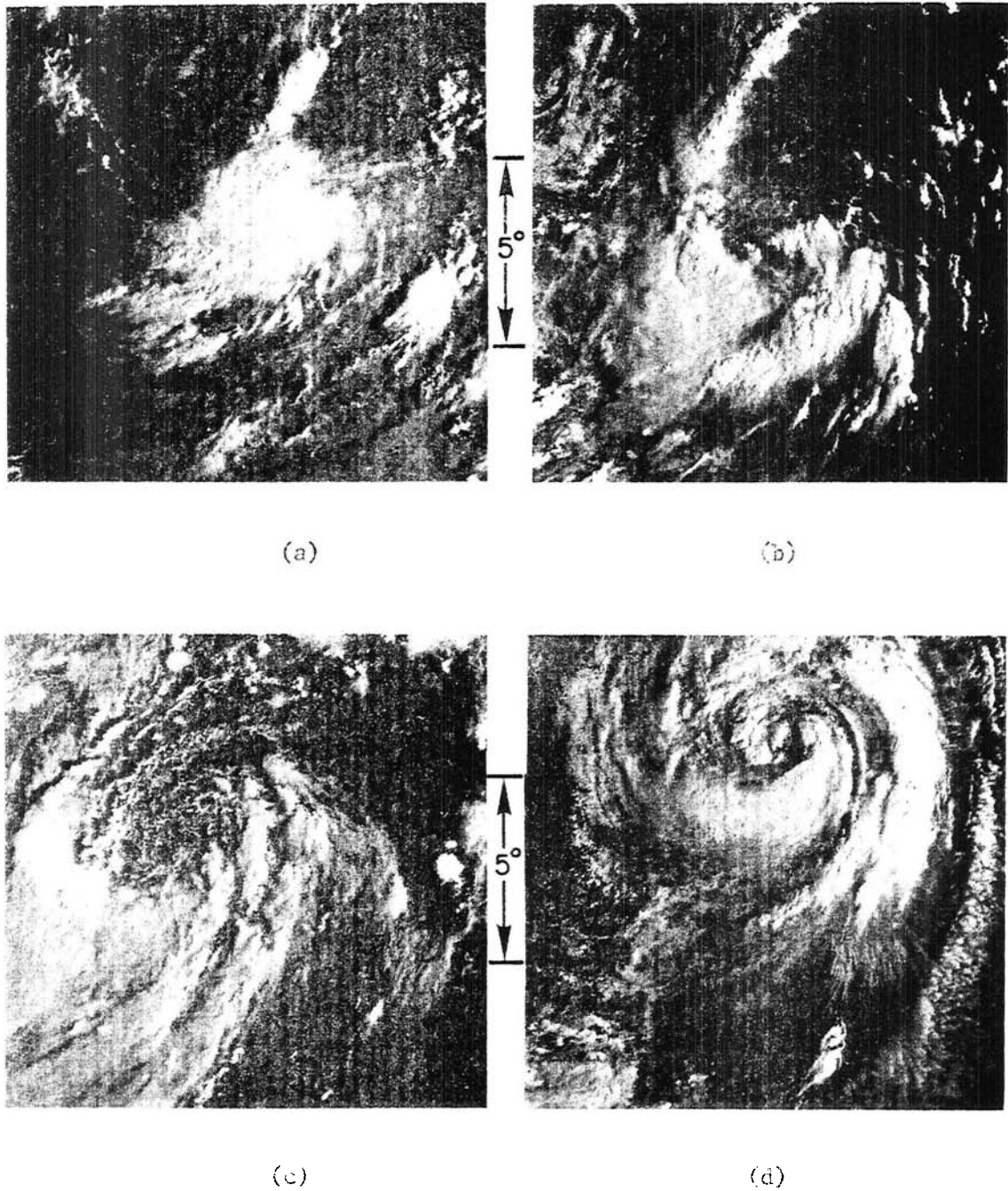
Fig. 35. Same as Fig. 33 except for Typhoon Agnes, 1 in = 484 km. (a) Developing cluster (Stage I), 13 September 1971, 2326Z; (b) Tropical depression (Stage II), 14 September 1971, 2259Z; (c) Tropical storm (Stage III), 15 September 1971, 2232Z; (d) Typhoon (Stage IV), 17 September 1971, 2319Z.
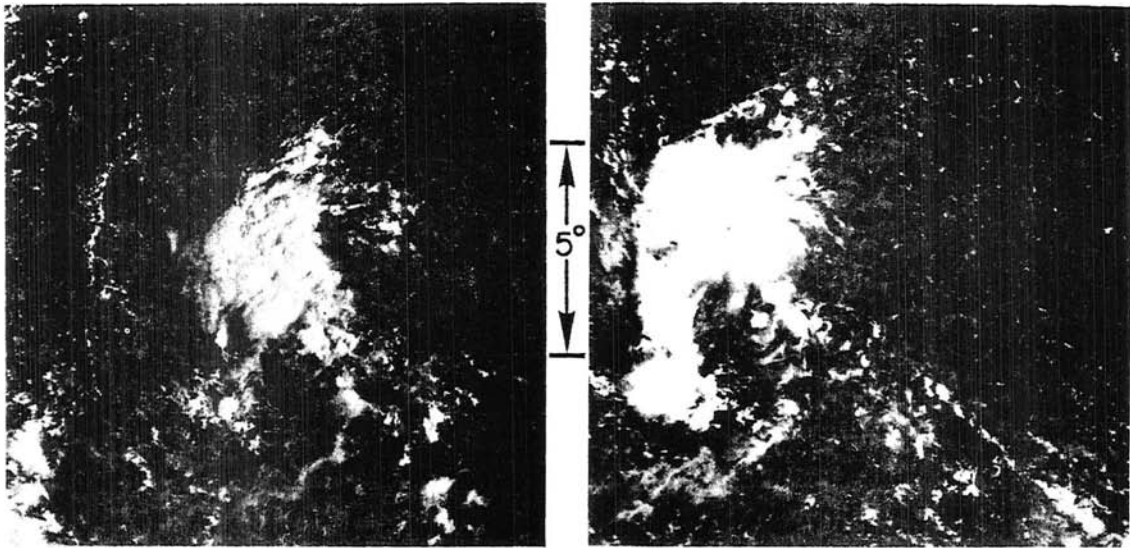
(a) (b)

Fig. 36. An example of the diurnal variability in cloudiness associated with a developing cluster, 1 in = 484 km. (a) Stage I of future Typhoon Flossie, 5 September 1972, 2211Z; (b) Same as (a) except for 6 September 1972, 0205Z, or 4 hours later.
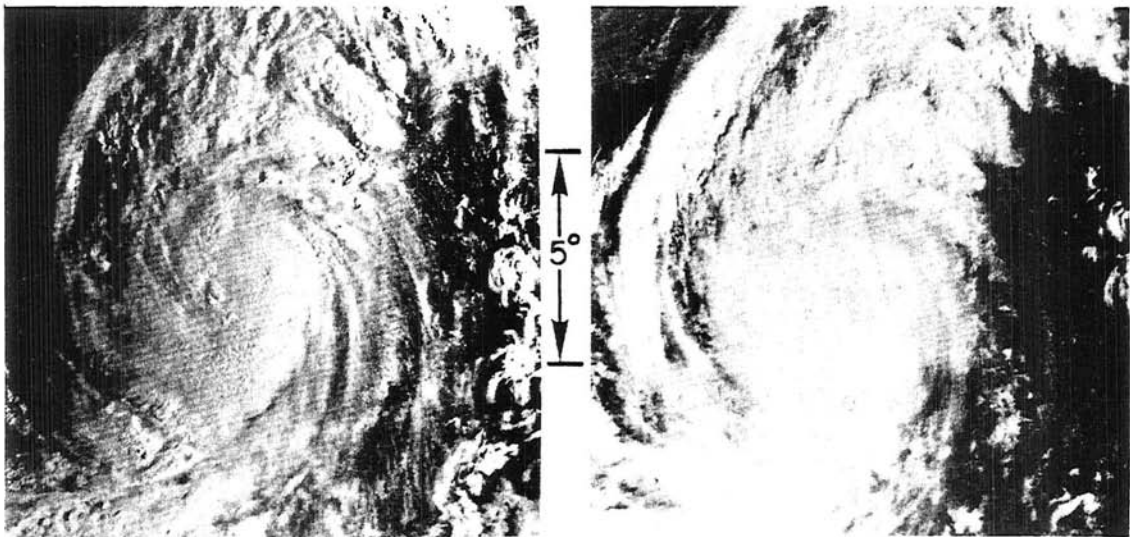
(a) (b)

Fig. 37. An example of the diurnal variability in cloudiness associated with a typhoon, 1 in = 484 km. (a) Typhoon Bess, 10 October 1974, 2227Z; (b) Same as (a) except for 11 October 1974, 0003Z, or 1½ hours later.
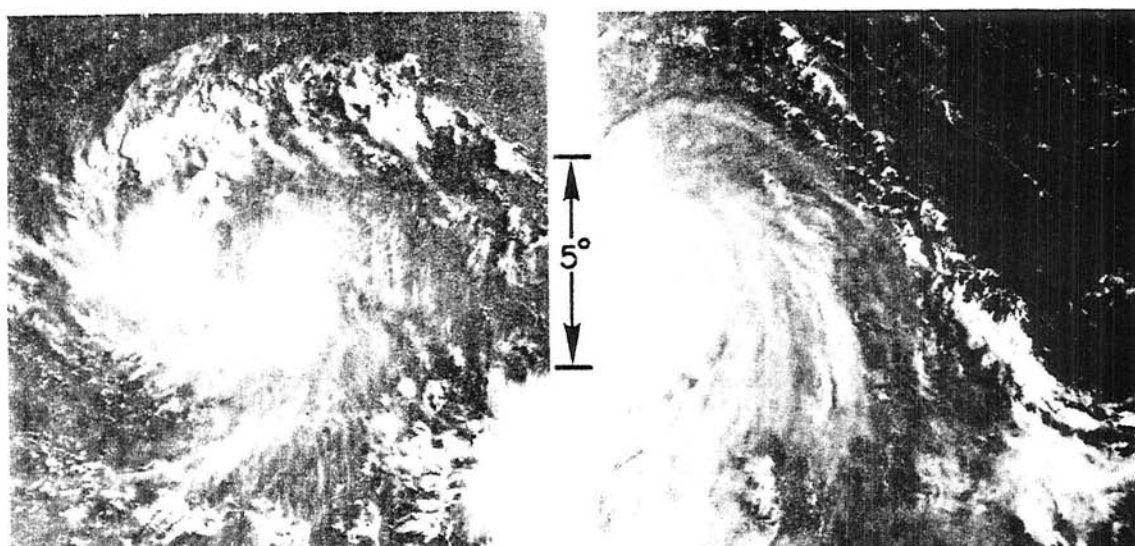
(a)

(b)
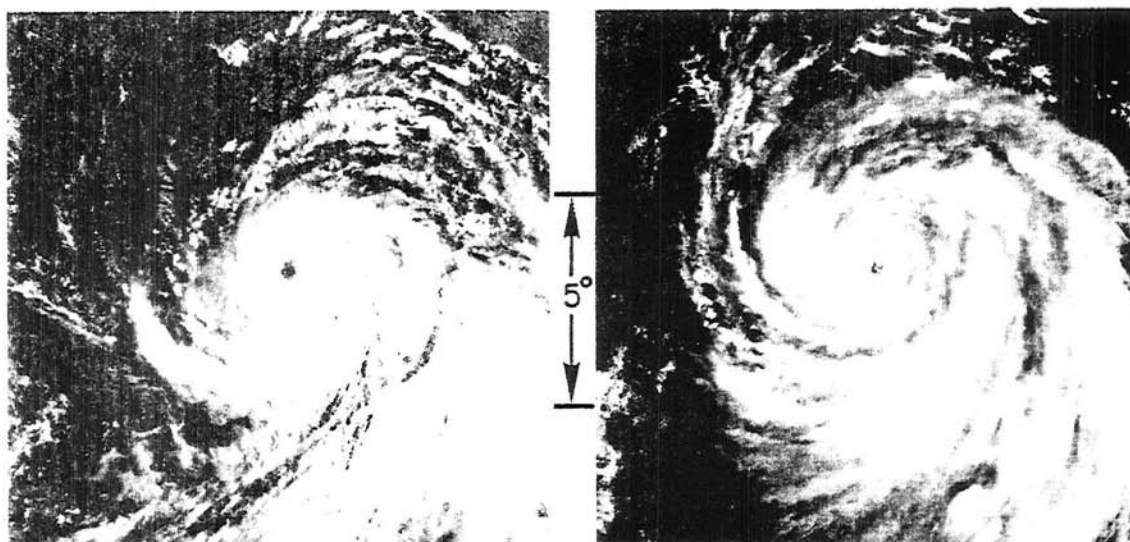
(c)

(d)

Fig. 38. An example of the day to day variability in cloudiness observed while the storm was a typhoon, 1 in = 484 km. (a) Typhoon Betty 10 August 1972, 2215Z; (b) 11 August 1972, 2147Z; (c) 12 August 1972, 2302Z; (d) 15 August 1972, 0400Z.

(a)

(b)

(c)

(d)
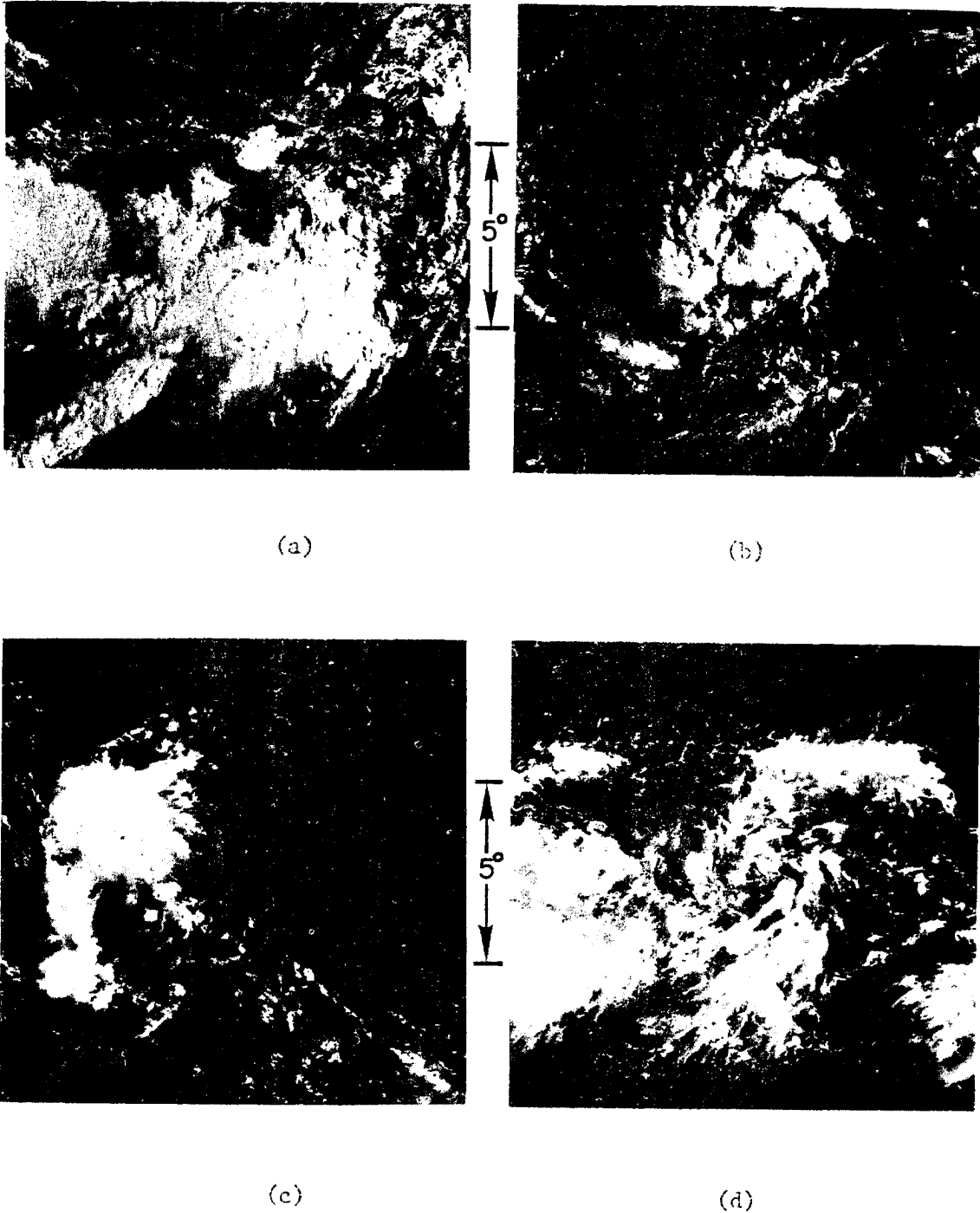
Fig. 39. Variability in cloudiness among clusters (Stage I), 1 in =
484 km. (a) Developing cluster (Stage I of future Tropical
storm Winnie), 28 July 1972, 2308Z; (b) Same as (a) except for
Stage I of future Typhoon Dinah, 23 May 1971, 2233Z; (c)
Same as (a) except for Stage I of future Typhoon Flossie, 6
September 1972, 0205Z; (d) Same as (a) except for Stage I of
future Typhoon Helen, 9 September, 1972, 0303Z.

(a)

(b)

(c)

(d)
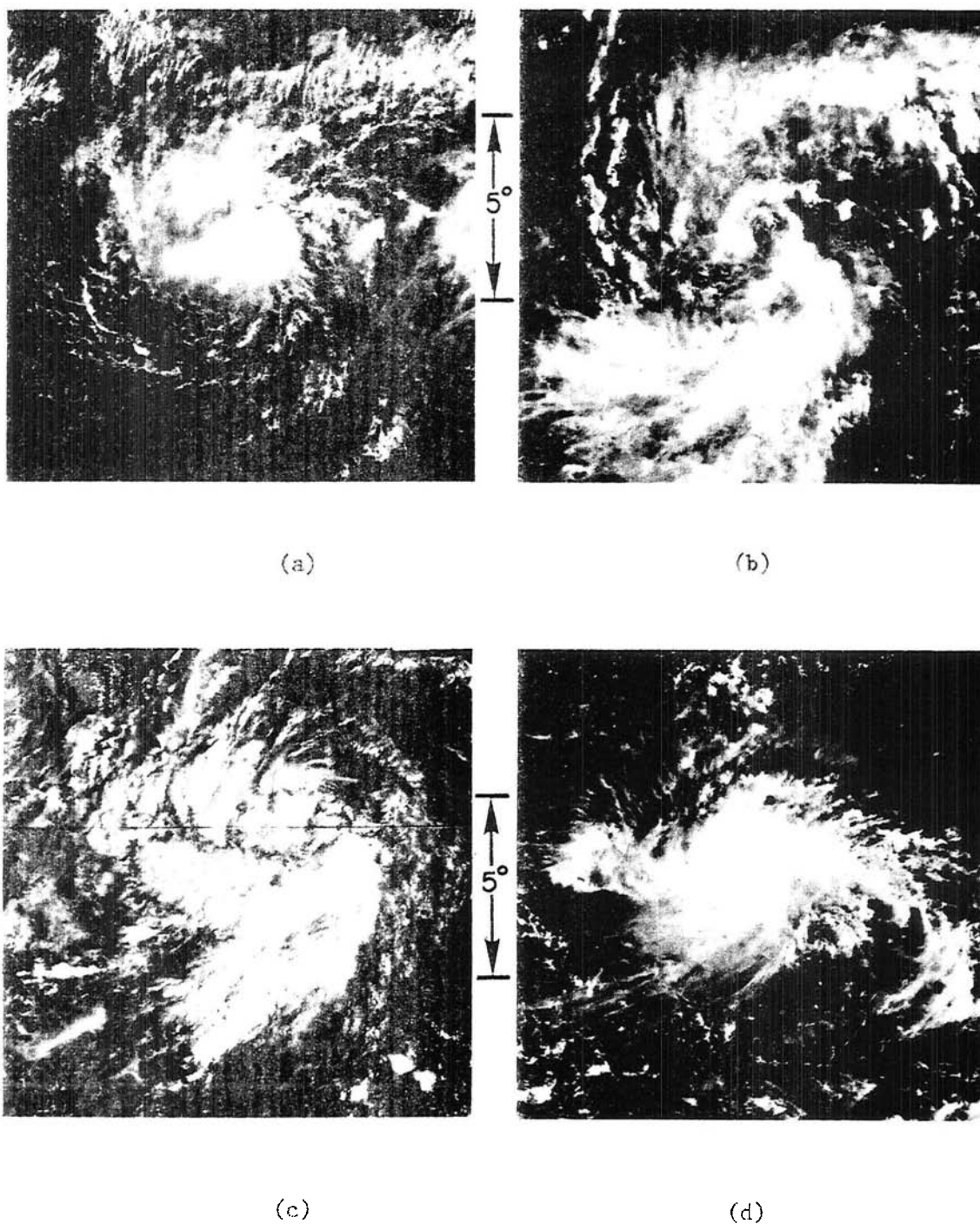
Fig. 40. Variability in cloudiness among tropical depressions (Stage II), 1 in = 484 km. (a) Tropical depression (Stage II of future tropical storm Violet), 16 December 1972, 0125Z; (b) Same as (a) except for Stage II of future Typhoon Betty, 9 August 1972, 0203Z; (c) Same as (a) except for Stage II of future Typhoon Hester, 18 October 1971, 2242Z; (d) Same as (a) except for unnumbered storm of 2 June 1972, 0311Z.

(a)

(b)

(c)

(d)
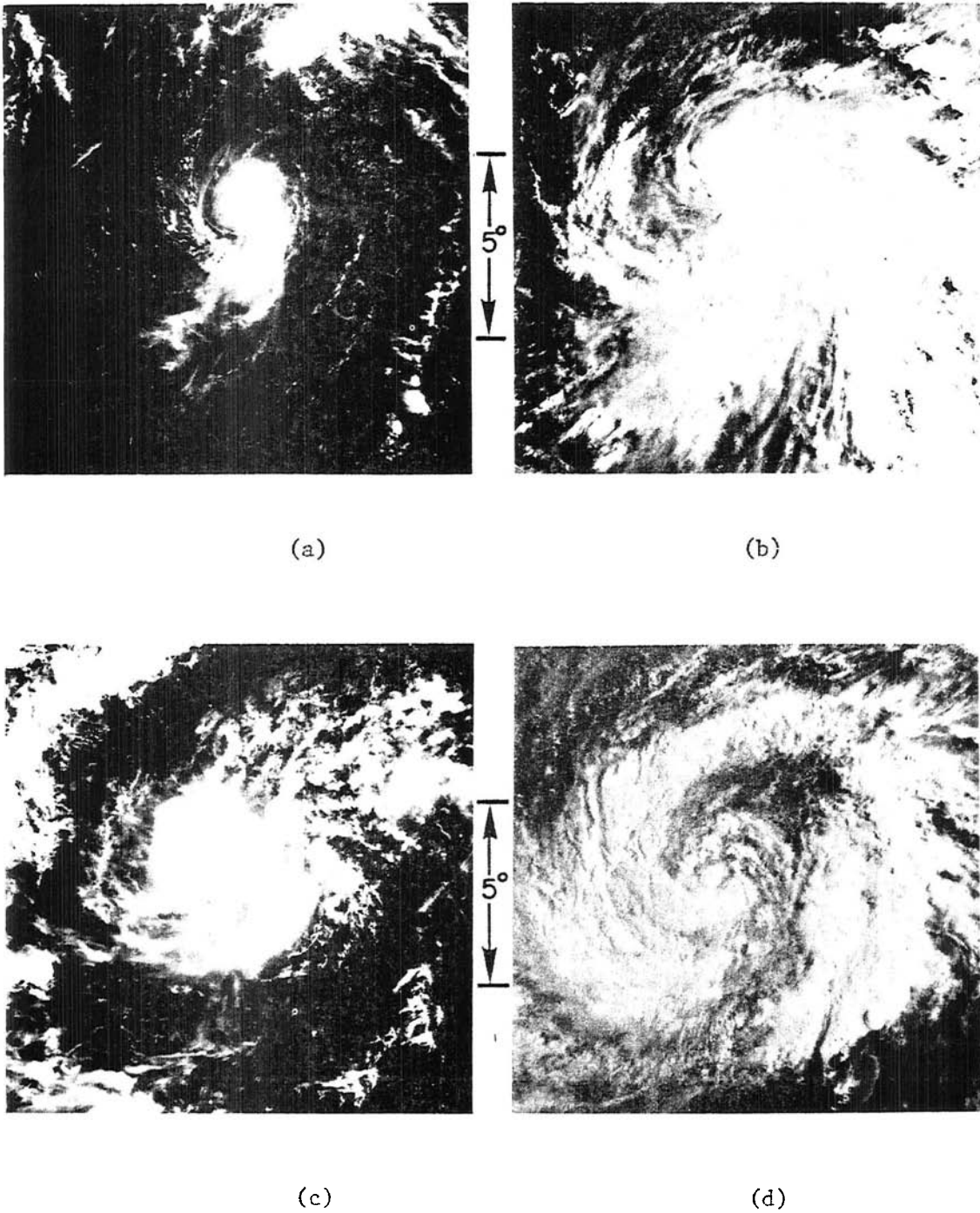
Fig. 41. Variability in cloudiness among tropical storms (Stage III),
1 in = 484 km. (a) Tropical storm (Stage III of Tropical
Storm Doris), 27 August 1972, 0106Z; (b) Same as (a) except
for Stage III of future Typhoon Alice, 31 July 1972, 2146Z;
(c) Same as (a) except for Stage III of future Typhoon
Therese, 2 December 1972, 0306Z; (d) Same as (a) except for
Stage III of future Typhoon Lola, 30 May 1972, 2124Z.

(a)

(b)

(c)

(d)
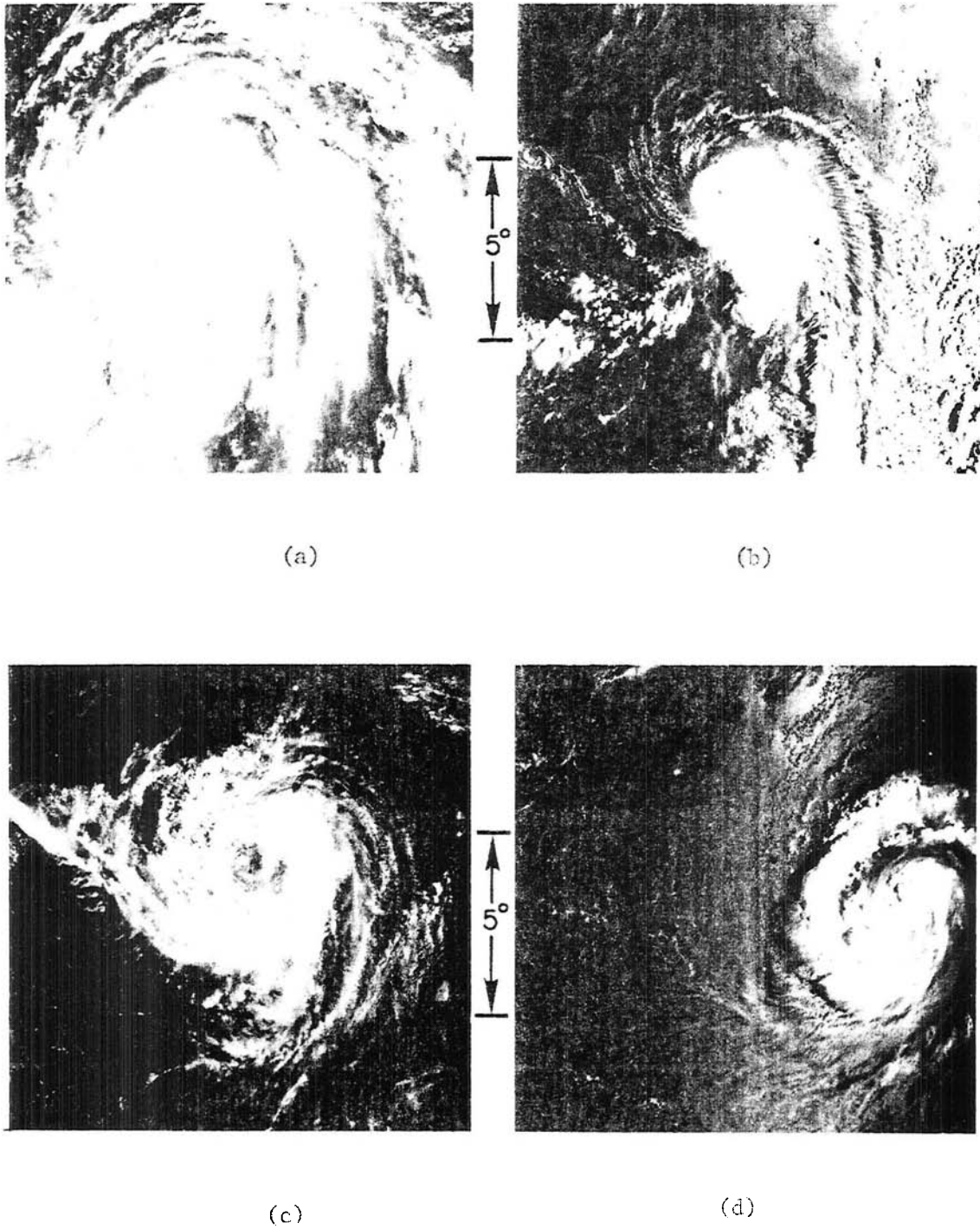
Fig. 42. Variability in cloudiness among typhoons (Stage IV), 1 in = 484 km. (a) Typhoon (Stage IV of Carmen), 16 October 1974, 0013Z; (b) Same as (a) except for Mary, 18 July 1971, 2041Z; (c) Same as (a) except for Alice, 7 August 1972, 0232Z; (d) Same as (a) except for Trix, 21 August 1971, 2206Z.

Figures 36a and 36b are morning (AM)[11] and afternoon (PM)[12] photos of a Stage I cluster on the same day, while Figs. 37a and 37b are consecutive AM pictures of a Stage IV storm. The former shows a 35% per $3\frac{1}{2}$ hour increase in cirrus while the total cirrus for the typhoon case increases by 14% per $3\frac{1}{2}$ hours. Table 14 gives the average percent increases in total cirrus for the composite of all tropical cyclones between the morning and afternoon pictures. Essentially no difference in the diurnal variation was found between storm stages. For the 5x5 area there is approximately a 28% per $3\frac{1}{2}$ hour increase in cirrus from morning to early afternoon for the typhoon stage. Using an area change of 28% per $3\frac{1}{2}$ hours gives an amplitude change of 2.1 per 14-h period. Whereas the Browner paper (Browner et al., 1977) speculated that the magnitude of the oscillation decreases as the storm intensifies, this study shows essentially no change in amplitude with storm intensity. There is also a trend for less deep convection in the afternoon suggesting a maximum activity in deep convection in the morning hours with a minimum in the late afternoon or evening (Table 15). The PM increase in cirrus may be explained as a result of the lag time necessary to advect the cirrus from the storm's interior to outer radii, where the greatest percent increases are observed, or it may be partly a result of an increase in absorption of solar radiation within the cirrus layer.

---

[11]AM is used in this context to refer to ascending nodes before local noon. These were normally between 0800 and 1000 local time.

[12]PM is used in this context to refer to ascending nodes after local noon. These were normally between local noon and 1400 local time. The average difference between AM and PM satellite data used in this study was 3.5 hours.

TABLE 14

Diurnal Change in the Percent Area Covered (σ) by Total Cirrus

Storm Region	AM (Ave. σ)	PM (Ave. σ)	% Change in Ave. σ per 3.5 hour
5x5	31.7	37.0	17
3x3	49.9	56.0	12
1x1	79.9	84.5	6
Outer 8	46.2	52.4	13
Outer 16	21.5	26.3	22

Ave. PM-AM Difference Equals 3.5 Hour.

Note: AM and PM are defined in footnotes 11 and 12.

TABLE 15

Diurnal Change in the Percent Area Covered (σ)
by Deep Convective Elements

Storm Region	AM (Ave. σ)	PM (Ave. σ)	% Change in Ave. σ Per 3.5 Hour
5x5	1.8	1.7	-6
3x3	3.1	2.8	-10
1x1	6.2	4.9	-21
Outer 8	2.7	2.5	-7
Outer 16	1.1	1.1	0

Ave. PM-AM Difference Equals 3.5 Hour.

Note: AM and PM are defined in footnotes 11 and 12.

It is not known whether the observed hourly percentage changes in cirrus and deep convection are constant and can be extrapolated with confidence over time periods greater than the typical 3.5 hours separating daytime satellite pictures. It may be entirely coincidental

that the extrapolated amplitude change calculated for a 14-h period
($\sim$ 0300 to 1700 LT) agrees with the value reported by Browner et al.
(1977).

Diurnal variations in the deep convection and precipitation asso-
ciated with western Pacific cloud clusters have been well documented by
(Ruprecht and Gray, 1976; Gray and Jacobson, 1977). Fingerhut, 1977
has modeled these diurnal differences for a cloud cluster. Their main
results showed a morning maximum in both deep convection and precipita-
tion with an early evening minimum. The cluster divergence profiles
also revealed substantial (2:1) diurnal variations which agree with the
convective variations.

Gray and Jacobson (1977) have postulated that diurnal changes in
net radiative cooling between clusters and their surrounding clear re-
gions force the lower tropospheric convergence and upper tropospheric
divergence. It is reasonable to assume that such a mechanism is at work
in tropical storms and typhoons as well as clusters since all of these
systems have well defined cirrus canopies.

This research indicates that cloud-cloud free radiational differ-
ences may play an important role in cyclone cloud modulation. There
was, however, no evidence of a cyclone intensity change to accompany the
change in cirrus or deep convection. Frank (1976) and Sheets (1972)
have similarly verified that only small ($\lesssim$ 10%) diurnal variations are
likely in typhoon-hurricane maximum winds.

It is not at all unusual to find major structural changes from
day to day in a given storm. Figures 38a to 38d represent four days
in the life of a typhoon. During this period it is transformed from
a cradle type of banding to a very symmetrical storm with quasi-circular

bands of convection about an eye. It would be difficult, given these four pictures, to tell they were all of the same storm.

Variability among storms of the same stage is illustrated in Figs. 39 to 42. Clusters and depressions can be very small or very large, show banding features or be devoid of any organization. The tropical storm and typhoon examples show both large and small storms, ones with banding and ones with no banding, storms with little or no deep convection and storms with enormous amounts of convection and cirrus.

Figures 43a through 43d show the percent deviation from the mean for the area covered by deep convection (Data Set B) within the 3x3 area for each of the four storm stages. Figures 44a-44d show the same for all cirrus (Data Set C). The mean positive and negative deviations for each case are also indicated. All cases have been included and have been randomly ordered. It is evident that there is considerable variability in cloudiness associated with the four storm stages. There can be small or large typhoons, small or large tropical depressions and so on. When similar graphs were made for small storms and for large storms of the same intensity, they revealed that the degree of variability in both groups was essentially the same. For example, typhoons were divided into two groups depending on whether the average radius of their major cloud features was greater or less than 3°. Figures 45a and 46a show the variability associated with the small group. Figures 45b and 46b show the variability associated with the large group. The percent deviation from the mean in each group is seen to be relatively constant.
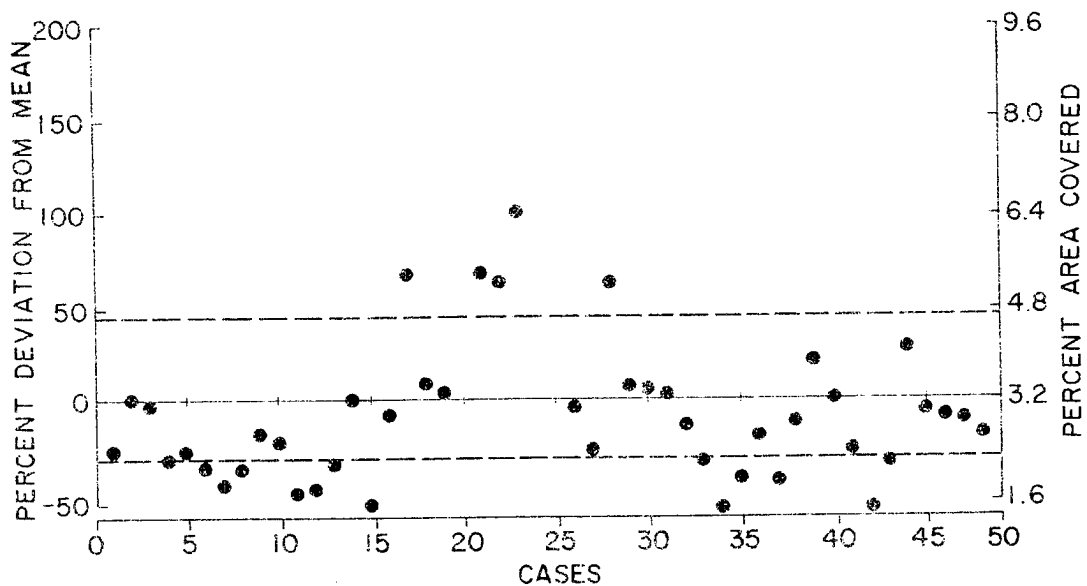
(a)
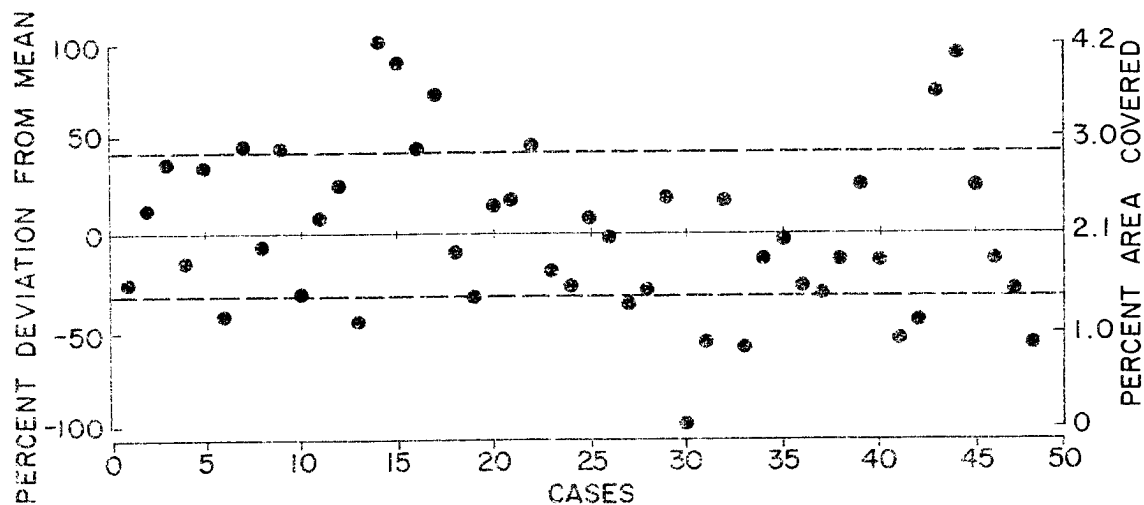
(b)

Fig. 43. Percent deviation from the average area of all deep convective
elements within the 3x3 (r ∿ 0-4.2°) region of different storms.
The order of the cases is random. (a) Developing cluster
(Stage I); (b) Tropical depression (Stage II); (c) Tropical
storm (Stage III); (d) Typhoon (Stage IV). Dashed lines above
and below the mean show the mean positive and negative devia-
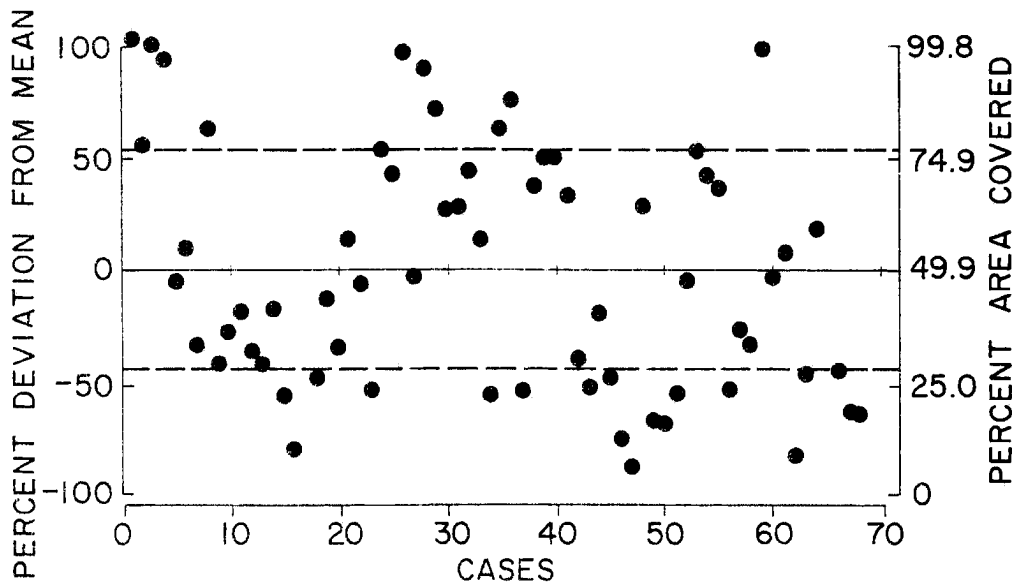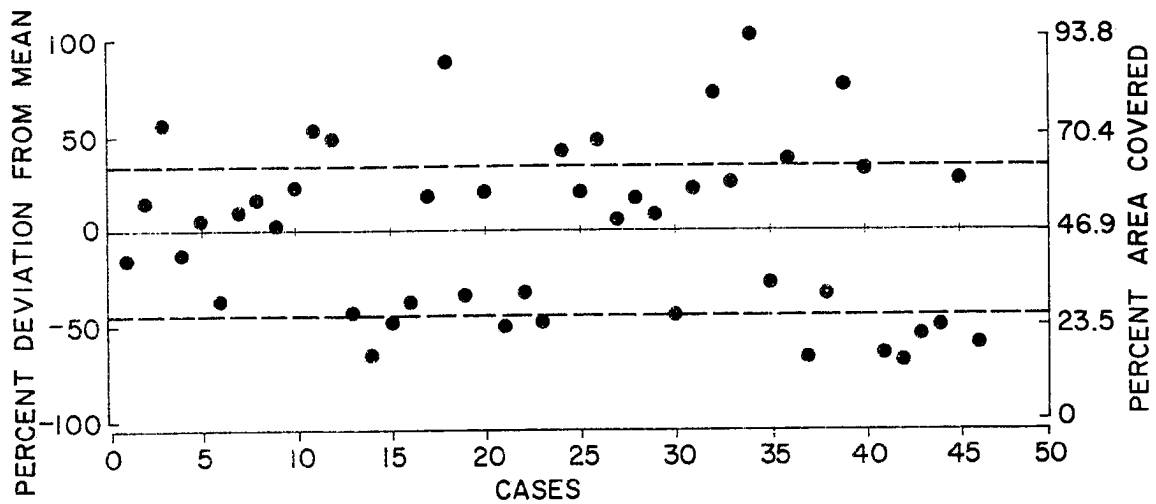tions respectively.
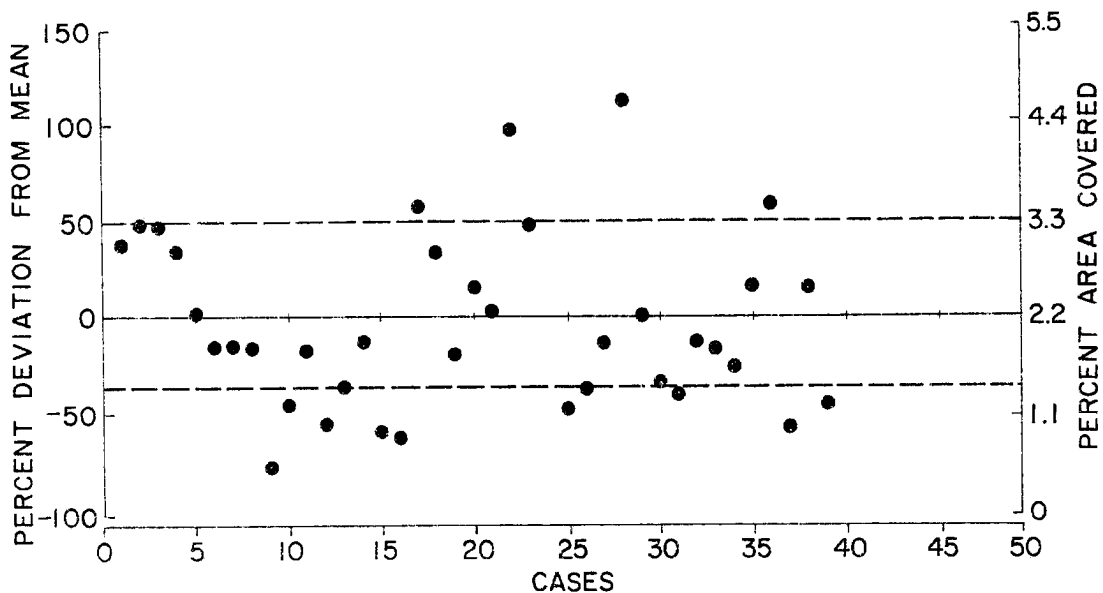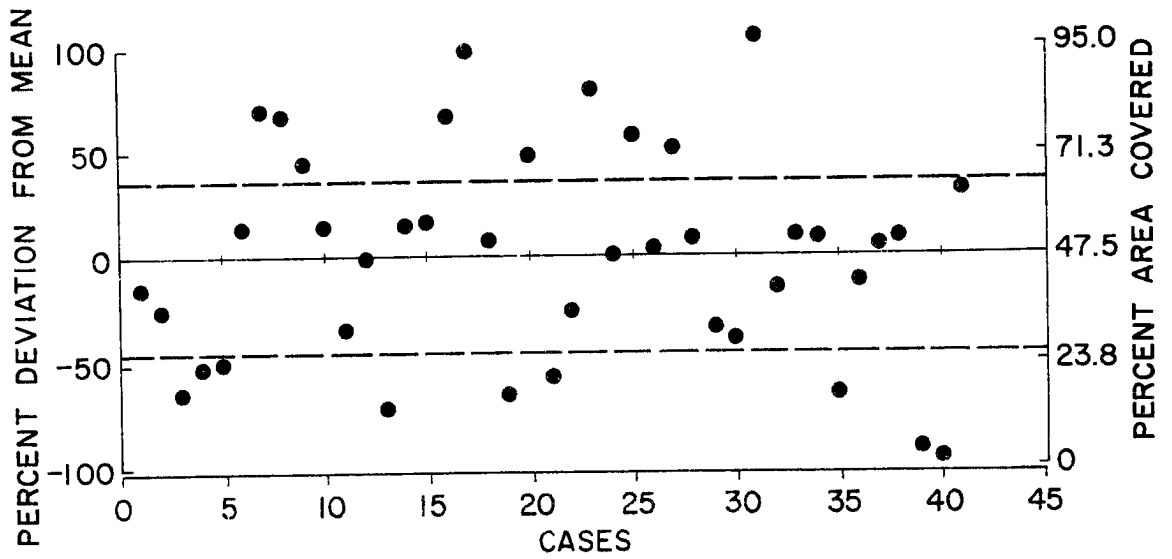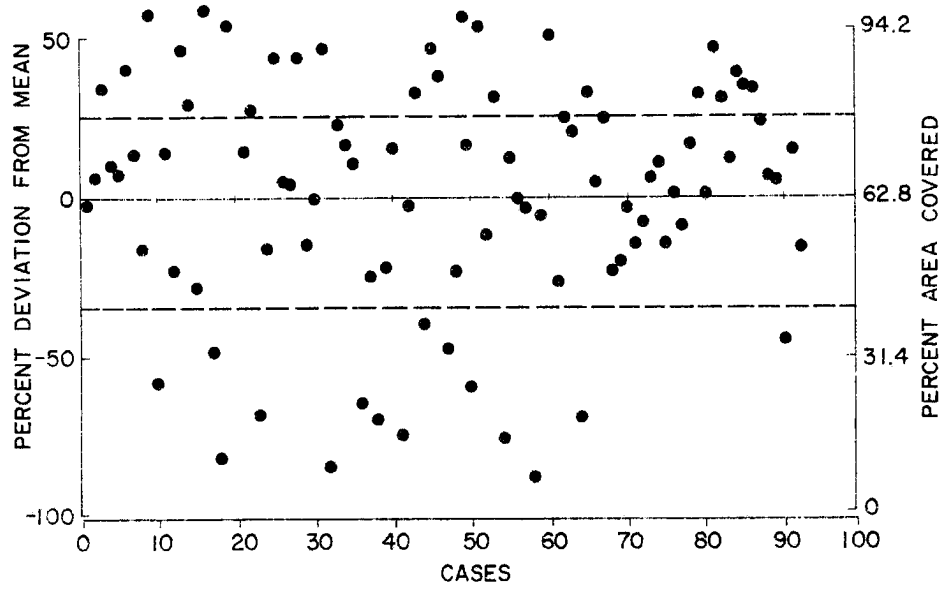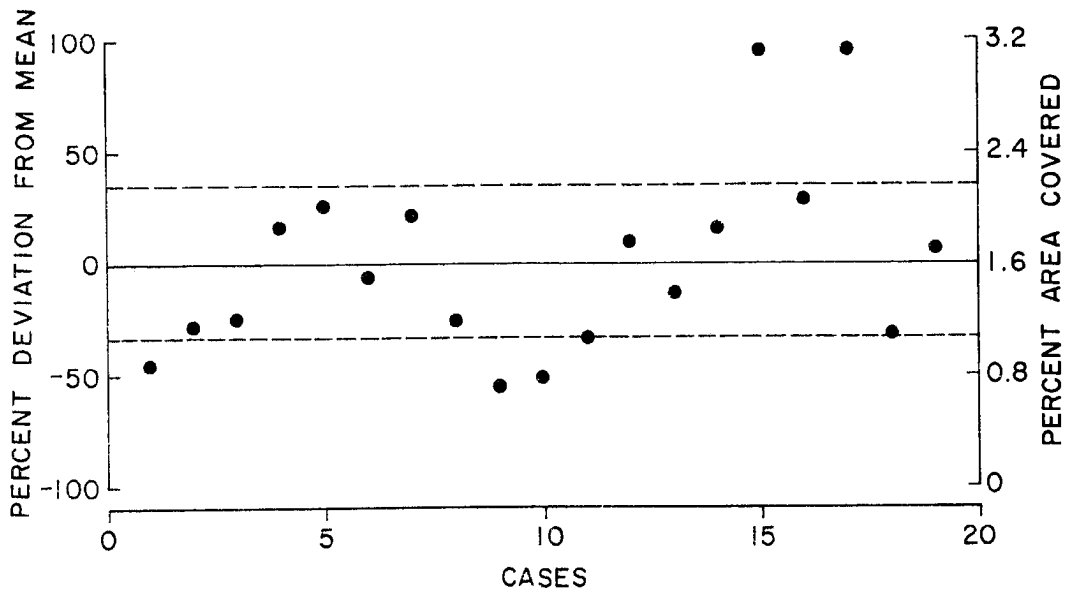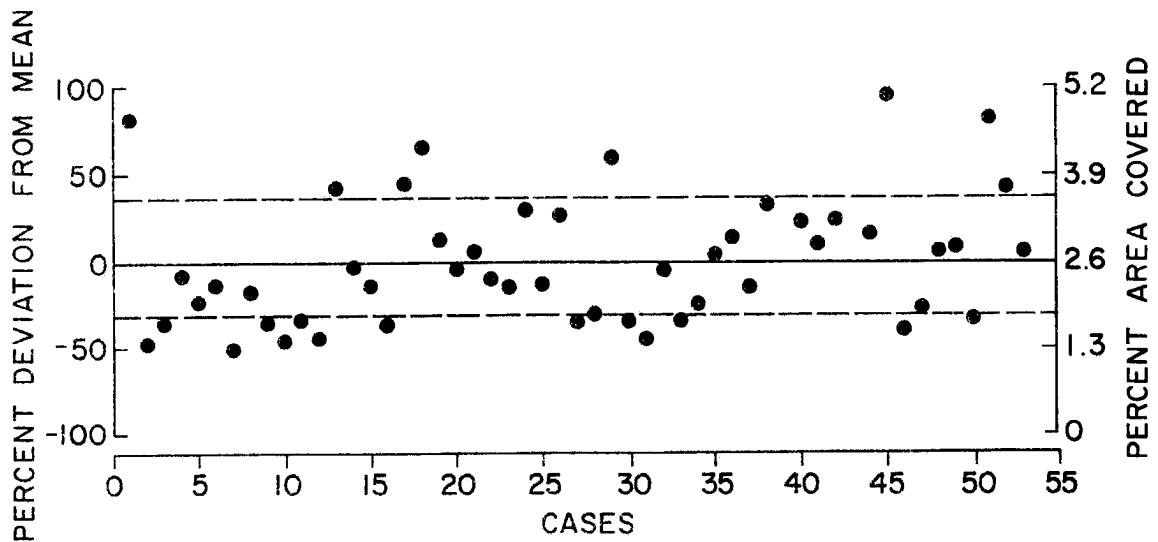
(c)
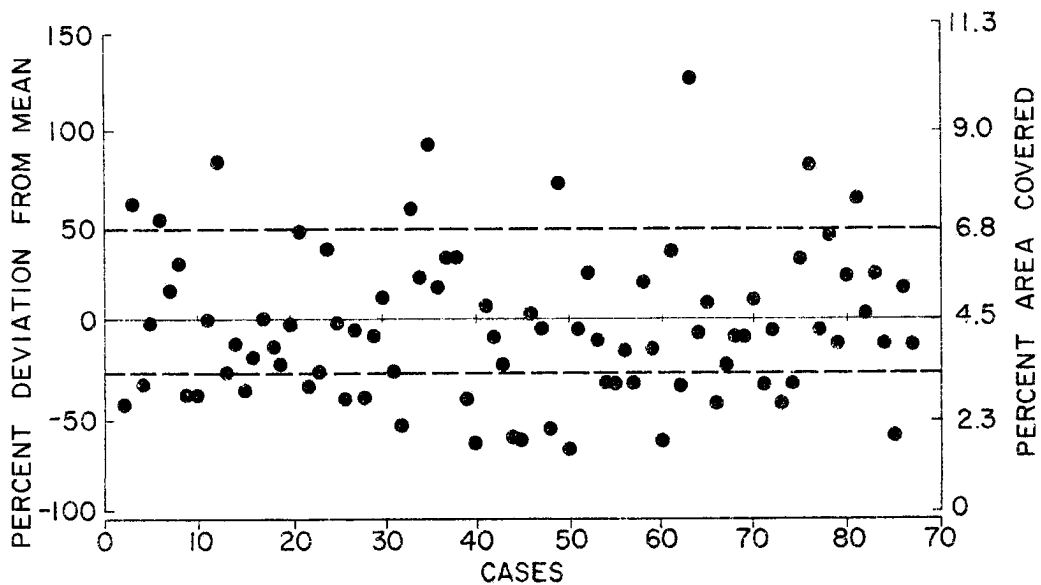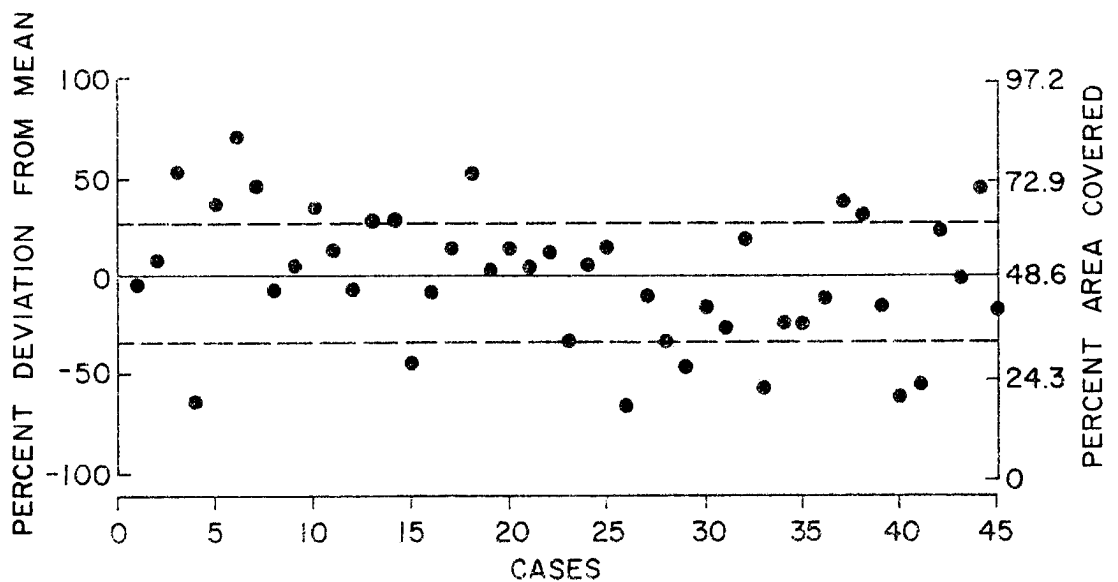

(d)

Fig. 43. Continued.

(a)

(b)

Fig. 44. Percent deviation from the average area of total cirrus within
the 3x3 (r ∿ 0-4.2°) region of different storms. The order of
the cases is random. (a) Developing cluster (Stage I); (b)
Tropical depression (Stage II); (c) Tropical storm (Stage III);
(d) Typhoon (Stage IV). Dashed lines above and below the mean
show the mean positive and negative deviations respectively.

(c)

(d)

Fig. 44. Continued.

(a)

(b)

Fig. 45. Percent deviation from the average area of all deep convective elements within the 5x5 (r ∿ 0-7.1°) region of different storms. The order of cases is random. (a) For typhoons with radius of storm cloudiness less than 3°, (b) for typhoons with radius of storm cloudiness greater than 3°.
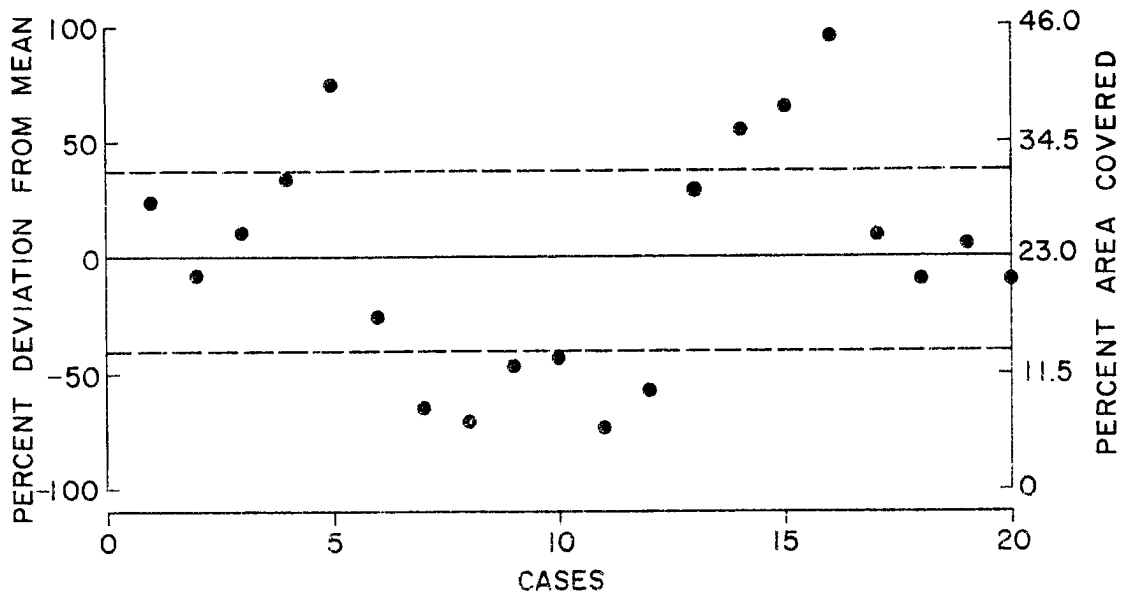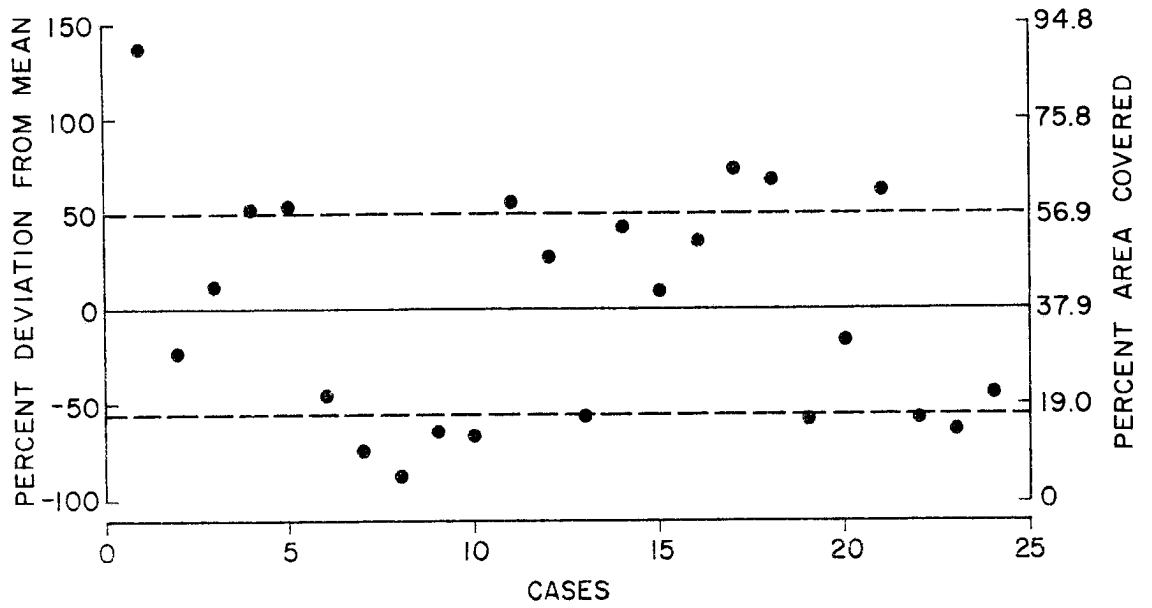
Fig. 46. Percent deviation from the average area of cirrus within the 5x5 (r ∿ 0-7.1°) region of different storms. The order of cases is random. (a) For typhoons with radius of storm cloudiness less than 3°, (b) for typhoons with radius of storm cloudiness greater than 3°.

The diurnal variability discussed earlier was not taken out of the above analyses. In order to determine what effect, if any, the observed diurnal differences would have on the observed variability discussed thus far in this section, a sample of cases from each of the four storm stages was separated into two groups based on the local time of each satellite picture. Only pictures with local times within one-half hour either side of 0800 LT comprised the first group, while pictures with local times within one-half hour either side of 1100 LT comprised the second group. The results are shown in Figs. 47a and 47b for the developing cluster (Stage I) total cirrus amounts within the 3x3 ($r \sim 4.2^{\circ}$) region. Similar results were obtained for the other three storm stages. These figures show that although the afternoon mean of cirrus is significantly larger than the morning mean[13], the percent deviation about each of these means is roughly the same. The variability in total cirrus among all observed tropical depressions, consequently, cannot be attributed to diurnal differences.

4.6 Summary

Each of the intensity estimation models that have been developed since 1964 relies heavily on the <u>amount of either deep convection or cirrus</u> and <u>banding features</u> as indicators of storm intensity. However, as we have seen, the reliability of these models is being questioned. It is now believed that it is the extreme variability in tropical cyclone cloudiness amounts diurnally, day to day, and storm to storm which is most responsible for the problems of the satellite cloud

---

[13]These means represent only sample statistics and for this reason may differ slightly from those given in Table 13.

(a)
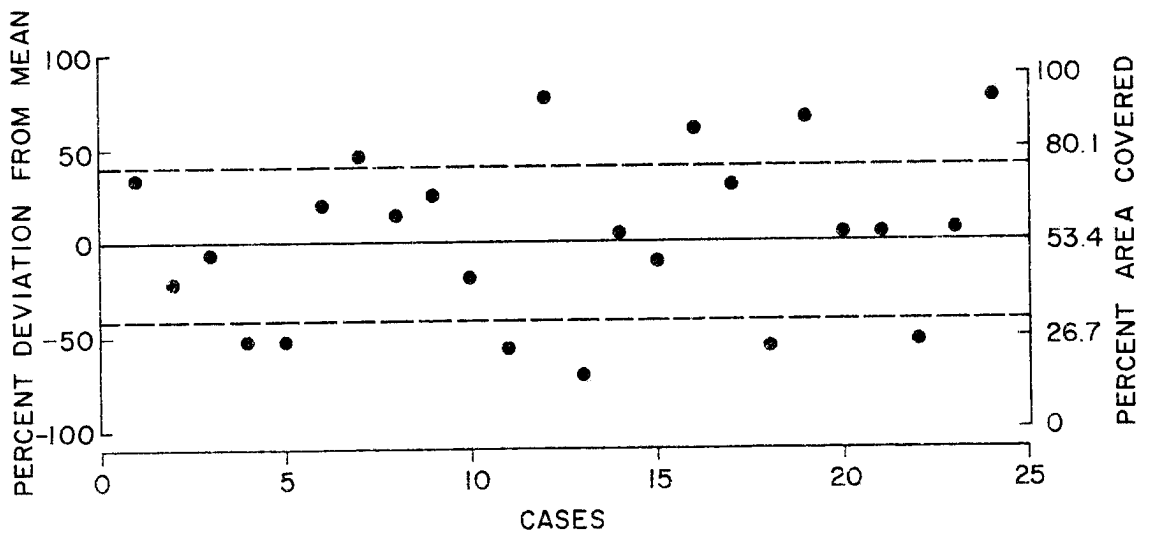
(b)

Fig. 47. Percent deviation from the average area of cirrus within the
3x3 (r ~ 0-4.2°) region of developing clusters (Stage I)
(a) For morning (0800 LT ± 30 min) pictures only. (b) For
afternoon (1100 LT ± 30 min) pictures only.

models. Furthermore, as we noted in Chapter 3, there is also a considerable degree of variability in the banding features of storms, that feature which has been most responsible for the success of the models.

It is concluded that convection and cirrus production and to a large extent the banding characteristics of storms are not at all well related to storm intensity except in the statistical sense that we have observed in Table 8 and which was discussed in section 4.1.

5. WIND AND THERMODYNAMIC CHARACTERISTICS OF THE TROPICAL CYCLONE AS REVEALED IN RAWINSONDE DATA

It was pointed out in the introduction that tropical cyclone studies based solely on satellite data lacked a certain degree of "ground truth" which could be provided with more conventional forms of meteorological data. This data could include aircraft reconnaissance dropsonde information, land and/or aircraft radar and rawinsonde reports. This author has utilized the large amount of west North Pacific rawinsonde data, western Atlantic hurricane research flight data, and West Indies rawinsonde data available on W. Gray's project. This information has been previously reported on in papers by Gray (1973), Shea and Gray (1973), Williams and Gray (1973), Ruprecht and Gray (1976), W. Frank (1976), Zehr (1976) and others involved in the compilation and analysis of these rawinsonde data sets at Colorado State University.

Vertical motion, tangential wind, moisture and temperature data have been analyzed from these data sources, and they document and support many of the conclusions reached in the previous chapter. As discussed in Section 2.2, Stages I, II, III and IV will be used when describing rawinsonde results obtained from Zehr's (1976) pre-tyhpoon class and Frank's (1976) tropical depression, tropical storm, and typhoon classes, respectively. Again it should be noted that occasionally the super-typhoon class, STY, will be used when describing results obtained from Frank's super-typhoon class. These results in several instances have been compared with Erickson's (1977) developing cluster stage (ES1) and with data provided by John McBride and Edwin Núñez, graduate students in the department of Atmospheric Science, for West Indies tropical depressions (WI2), tropical storms (WI3), and hurricanes (WI4).

5.1 Vertical motion

Near the 300 mb level the mean vertical motion within a specified area of a tropical cyclone ($\bar{\omega}$) is essentially due to the total up motion in cumulonimbus clouds (Frank, 1976) or $\omega = \sigma \, \omega_{Cb}$ where ω_{Cb} is the mean upward motion of the cumulonimbus clouds and σ, as previously defined is the percent of the specified area covered by Cb clouds. At lower tropospheric levels the mean vertical motions result only partially from convective clouds since substantial contributions are made by shallow cumulus clouds and return flow subsidence. In order to relate vertical motion to deep convection or cirrus, a mean vertical motion for the 150-300 mb layer was computed from Zehr's developing cluster stage and Frank's tropical depression, tropical storm, typhoon and super-typhoon classes (Zehr, 1976; Frank, 1976). The best comparisons between these data sets and the cloudiness distributions discussed earlier could be made when the 0-2°, 0-4° and 0-6° rawinsonde composited values were compared with the 1x1 ($r \sim 0$-1.4°), 3x3 ($r \sim 0$-4.2°) and 5x5 ($r \sim 0$-7.1°) regions, respectively.

Table 16 lists these vertical motion values for each of the 5 stages. There is an obvious agreement between these values and the cloud statistics given in Chapter 4. The 0-2° region shows a continual increase in $\bar{\omega}$ as the storm intensifies from a cluster (Stage I) to a depression stage (Stage II). From the depression stage on the 0-4° and 0-6° areas both show increases.

The 2-4° region shows a substantial decrease in mean vertical motion from Stage I to Stage II. The latter value is felt to be too small, but no explanation could be found. The vertical motion increases within this band during the later stages of the storm.

TABLE 16

Mean Vertical Motion (150-300 mb) in mb d^{-1} for Each Stage Based on West North Pacific Rawinsonde Data Provided by Zehr (1976) and Frank (1976)

Storm Stage	I	II	III	IV	STY
Storm Region:					
0-2°	-151 (5.4)	-200 (5.2)	-240 (4.9)	-304 (4.6)	-370
0-4°	-145 (3.2)	-55 (2.1)	-101 (2.2)	-147 (4.5)	-179
0-6°	-99 (1.9)	-58 (1.3)	-76 (1.4)	-86 (2.5)	-96
2-4°	-143 (2.9)	-7 (1.8)	-55 (2.0)	-95 (3.8)	-115
4-6°	-62 (1.2)	-60 (0.8)	-56 (1.0)	-37 (1.4)	-30

Note: Figures in parenthesis are the mean percent areas covered by clouds taken from Table 9.

Cloud statistics for the outer 8 ($r \sim 1.4-4.2°$) as reported in Table 9 show a similar trend, and although the differences seem small, they were found to be statistically significant between consecutive storm stages.

The 4-6° region shows a continual decrease in $\bar{\omega}$ from cluster to super-typhoon. These results agree with W. Frank's recent quantitative documentation of the moat region (Frank, 1976). The previous discussion in Sections 4.1 and 4.3 indicated no significant change in BCE area or BCE count within the outer 16 ($r \sim 4.2-7.1°$) region for storms more intense than tropical depression (Stage II). Cloud statistics therefore seem to imply an early establishment of the moat (from Stage I to Stage II) with little change in the amount of deep convection within the moat as the storm intensifies.

Table 17 presents results based on the most recent rawinsonde data provided by Erickson (1977), McBride, and Núñez as described above.

TABLE 17

Mean Vertical Motion (150-300 mb) in mb d^{-1} Based on Supplementary Rawinsonde Data for West North Pacific and West Indies (Caribbean, Gulf of Mexico and Bahamas).

Storm Stage	ES1	WI2	WI3	WI4
Storm Region:				
0-2°	*	-137	-101	-284
0-4°	-148	-52	-92	-127
0-6°	-116	-30	-41	-68
2-4°	*	-24	-88	-68
4-6°	-90	-12	-1	-85

ES1 = Erickson's (1977) W. Pacific developing cluster stage corresponds to Stage I.
WI2 = West Indies tropical depression corresponds to Stage II.
WI3 = West Indies tropical storm corresponds to Stage III.
WI4 = West Indies hurricane corresponds to Stage IV.
* = Data not available.

While several obvious descrepancies exist between the results given in Table 17 and in Table 16, there is good agreement overall. Apparently there is overall less vertical motion in Stage II than in Stage I cyclones. This is an observational result from both oceans.

5.2 Tangential wind and relative vorticity

A rather extensive cyclone exists in the lower troposphere and extends outward to a radius of 1000 km or more. From about 2° radius outward, a large anticyclone overlays the lower level cyclone. The cyclone deepens and intensifies with decreasing radius. The anticyclone deepens and intensifies with increasing radius.

Figures 48, 49 and 50 give the vertical profiles of the tangential wind (V_{θ}) for the five storm stages at three radii. It is obvious that
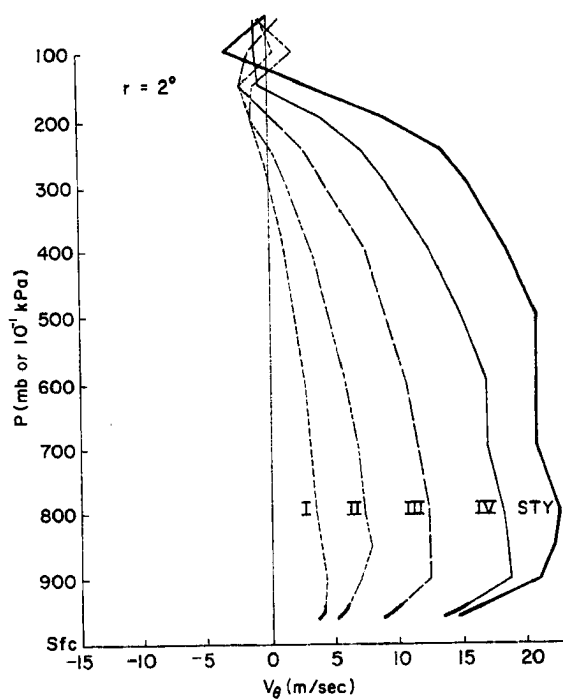
Fig. 48. Tangential wind profiles at r = 2° for five storm stages: I, II, III, IV and Super-Typhoon (STY).

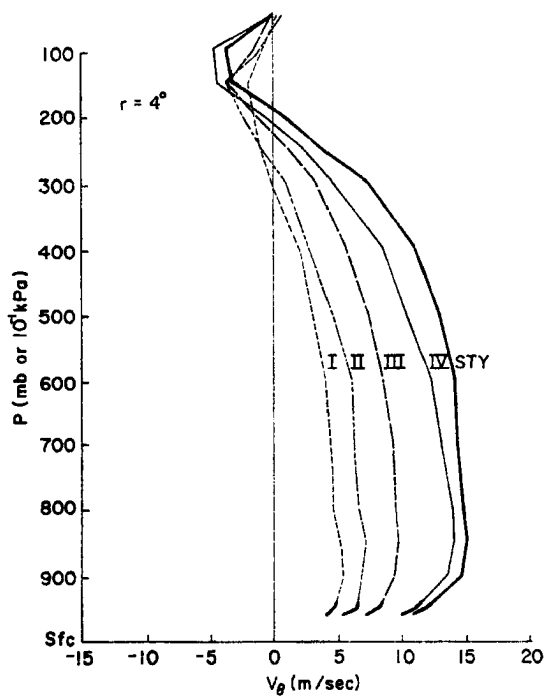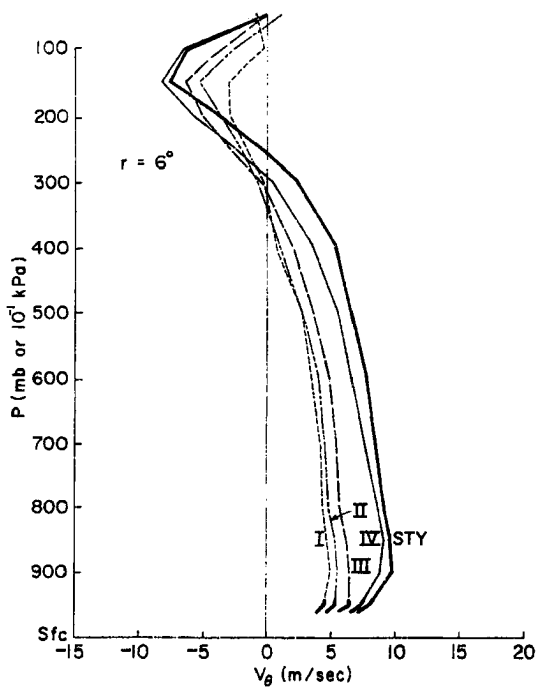Fig. 49. Same as Fig. 48 except for r = 4°.

Fig. 50. Same as Fig. 48 except for r = 6°.

there are rather significant differences in V_θ between storm stages. We note that in all stages a maximum in the low level winds occurs not at the surface but rather above the frictional influences of the boundary layer somewhere between 900 and 800 mb. The anticyclone maximum appears to be near 150 mb.

From the tangential wind profiles, mean relative vorticities, $(\bar\zeta)$, within $2°$, $4°$, and $6°$ for the surface to 300 mb layer and for the 900 mb level were calculated using the cylindrical expression for relative vorticity:

$$\bar\zeta \simeq 2\, \bar{V}_\theta / r$$

where $\bar{V}_\theta$ is the mean tangential wind at radius r. These values are given in Tables 18, 19 and 20. The relative vorticities at 900 mb are seen to be representative of the deep layer values.

5.3 Discussion of vertical motion and vorticity

Most of the cyclone intensification models have been based on the Theory of Conditional Instability of the Second Kind (CISK) as formulated by Ooyama (1964) and Charney and Eliassen (1964). Simply stated, CISK type parameterizations have assumed that cumulus heating is directly proportional to the total moisture convergence into the system or to the vertical motion at the top of the boundary layer. For quasi-balanced flow, vertical motion at the boundary layer top should be approximately proportional to the vorticity at this level, the so called "Ekman pumping effect." Therefore, as the storm intensifies, there should be greater amounts of moisture convergence and subsequent cumulus heating. This direct realization of latent

TABLE 18

Mean Relative Vorticity ($\bar{\zeta}$) from 0-2° (x 10^{-5} s^{-1})

Storm Stage	I	II	III	IV	STY
Relative Vorticity					
$\bar{\zeta}$ (sfc-300 mb)	2.5	4.8	8.7	13.5	17.1
$\bar{\zeta}$ (900 mb)	3.8	6.4	11.3	17.1	19.0

TABLE 19

Mean Relative Vorticity ($\bar{\zeta}$) from 0-4° (x 10^{-5} s^{-1})

Storm Stage	I	II	III	IV	STY
Relative Vorticity					
$\bar{\zeta}$ (sfc-300 mb)	1.6	2.9	3.4	4.8	5.5
$\bar{\zeta}$ (900 mb)	2.4	3.0	4.3	6.1	6.6

TABLE 20

Mean Relative Vorticity ($\bar{\zeta}$) from 0-6° (x 10^{-5} s^{-1})

Storm Stage	I	II	III	IV	STY
Relative Vorticity					
$\bar{\zeta}$ (sfc-300 mb)	1.0	1.1	1.3	1.8	2.1
$\bar{\zeta}$ (900 mb)	1.5	1.7	1.9	2.7	3.0

heat should manifest itself in increased amounts of deep convection.

However, while $\bar{\zeta}$ and $\bar{\omega}$ at 900 mb increase greatly, (Tables 18, 19,

20) with storm stage there is very little corresponding change in the

amount of deep convection (Table 9). These results are also reflected

in Table 21. The ratio of vertical motion to vorticity of the boundary

layer top (assumed here at 900 mb) changes little with storm stage

as expected from direct boundary layer pumping. However, the ratio

of vertical motion at 300 mb (which is mostly in deep convection as

discussed earlier) to vorticity at 900 mb shows a substantial de-

crease with storm stage. The 900 mb vorticity increases much more

rapidly than the upper level vertical motion or amount of deep con-

vection. Vorticity and/or vertical motion at the boundary layer top

and the amount of deep convective cloudiness thus appear not to be

well related for the different storm stages. It also seems likely

that cumulus parameterization schemes employing heating functions

which are proportional to the mean vertical motion at the top of the

boundary layer (and thus to the vorticity) may not realistically be

modeling the magnitude of release of latent heat by deep convection

for the different cyclone stages. This subject needs further study.

5.4 Temperature

Besides the strong differences in tangential wind or relative

vorticity observed between storm stages, we also observe a very

substantial increase in the strength of the upper level warm core

with increasing storm intensity. This is consistent with the hydro-

static relationship. Figure 51 shows the temperature anomaly profiles

for five storm stages. The maximum anomaly is observed to occur

near 250 mb for each of the stages. For the fully developed typhoon

TABLE 21

Vertical Motion-Relative Vorticity Ratios from 0-2° by Storm Stage

	(1)	(2)	(3)	(4)	(5)
	$\overline{\zeta}_{900}$	$\overline{\omega}_{900}$	$\overline{\omega}_{300}$	$\overline{\omega}_{900}/\overline{\zeta}_{900}$	$\overline{\omega}_{300}/\overline{\zeta}_{900}$
Storm Stage					
I	3.8	-51.4	-215	-16	-65
II	6.4	-121	-309	-22	-56
III	11.3	-225	-300	-23	-31
IV	17.1	-350	-411	-24	-28

(1) Mean relative vorticity (x $10^{-5}s^{-1}$) at 900 mb.

(2) Mean vertical motion (mb d^{-1}) at 900 mb.

(3) Mean vertical motion (mb d^{-1}) at 300 mb.

(4) Ratio of (2) to (1) in units of mb.

(5) Ratio of (3) to (1) in units of mb.
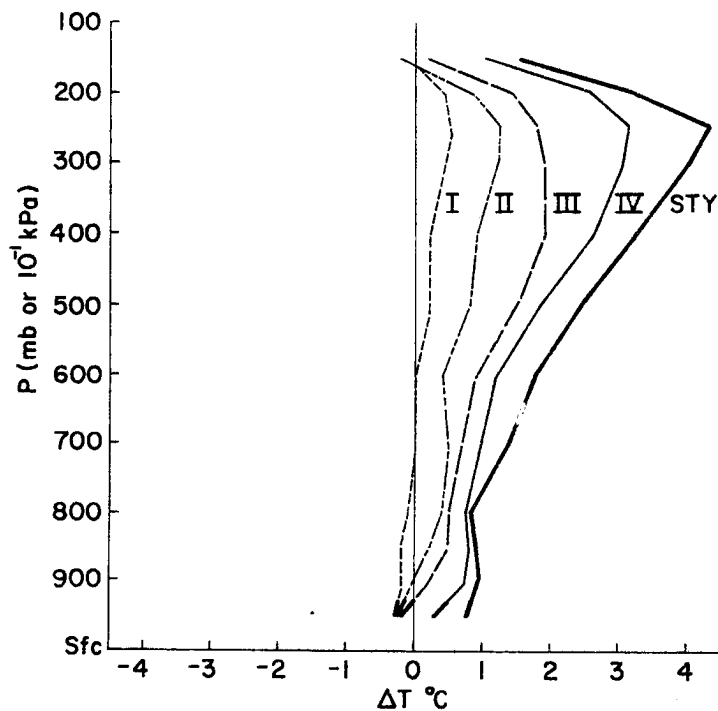
Fig. 51. Temperature anomaly profiles for five storm stages I, II, III, IV, and STY. $\Delta T = \overline{T}_{(0-3^{\circ})} - \overline{T}_{(3-7^{\circ})}$ for stages I, II, III. $\Delta T = (0-3^{\circ}) - 8^{\circ}$ for stages IV and STY.

the mean maximum anomaly may be near 15 C based on the results obtained from flight data by Shea and Gray (1973). For the developing cluster this anomaly may be only 0.5 C. With stronger systems the temperature anomaly may be an underestimate because the extreme warm core is not sampled. Large temperature anomalies, associated with typhoons, of the magnitude given above have been obtained by Simpson (1952) and shown by Riehl (1954), Hawkins and Rubsam (1968), Hawkins and Imbembo (1976), and most recently by Frank (1976).

The statistical relationship between the upper level temperature anomaly and the mean tangential wind in the 900-700 mb layer is given in Fig. 52. The percentage increase in the anomaly is seen to be very well correlated with the percentage increase in the mean tangential wind. This implies that if we were able to obtain an accurate mean temperature anomaly by aircraft or satellite through the life of the storm, we should be able to obtain reasonably accurate estimates of the radial profile of tangential wind. This has an obvious practical application with regard to storm reconnaissance. Up to now aerial reconnaissance has been performed at lower mid tropospheric and lower tropospheric levels. Maximum sustained winds are often difficult to obtain in the more intense storms, as these winds are found within the highly turbulent eye-wall regions of the storm. Reconnaissance of the upper-level (250-300 mb) temperature field would significantly reduce the hazards of low-level penetrations and may provide more conservative and accurate wind estimates than are presently available from direct aircraft measurement.
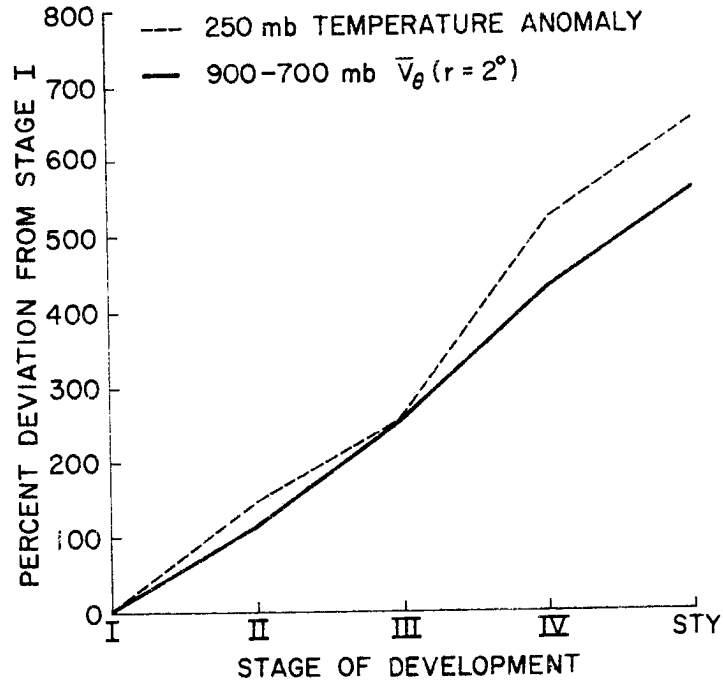

Fig. 52. The 250 mb temperature anomaly and 900-700 mb tangential wind at $r = 2°$, each expressed as a percent deviation from the corresponding developing cluster (Stage I) values.

The 300-200 mb mean temperature within the storm's inner core is very well related to the mean 850 mb height (Fig. 53). It might be possible through a measure of the upper level temperature gradients to estimate the surface winds through low level height gradients. It can be noted that Kidder (1977)[14] has recently analyzed temperature data over tropical cyclones retrieved from the 5 channel Scanning Microwave Spectrometer (SCAMS) on NIMBUS VI. The SCAMS has a field of view or spatial resolution of approximately a 78 n mi diameter circle. Temperature values are therefore smoothed considerably. Even allowing for the large smoothing, Kidder has observed temperature differences between storm and storm environment within the 250-100 mb layer as

---

[14]Personal communication.
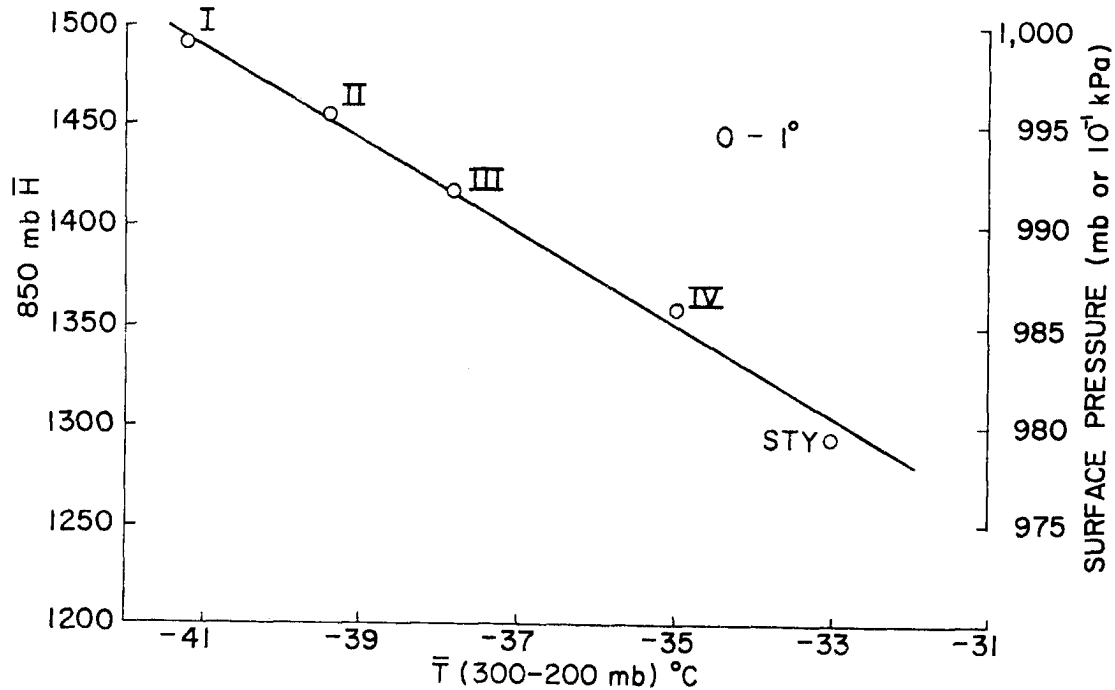
Fig. 53.   The mean 300-200 mb temperature from 0-1° vs. mean 850 mb height from 0-1°.

large as 5 C. He has also observed that the anomaly increases as the

storm intensifies from a cluster to a typhoon.

5.5 Moisture

Mean relative humidity values, $\overline{RH}$, were computed for each level

from the surface to 300 mb using the Zehr (1976) and Frank (1976) data

sets. Significant differences in relative humidity should

reflect significant differences in vertical motion and convection. Both

sets used only the 12Z (∿ 22 LT) $\overline{RH}$ values to avoid the instrument

errors in humidity measurements caused by solar heating of the sensors

(Ruprecht, 1975).

Table 22 gives the $\overline{RH}$ values at 500 mb for four storm stages and

three radial bands. Table 23 gives the $\overline{RH}$ values for the surface to

300 mb layer. It is felt that overall the moisture field agrees quite

TABLE 22

Mean 500 mb Relative Humidity

Storm Stage	I	II	III	IV
Storm Region:				
0-2°	69	70	72	81
2-4°	65	60	62	64
4-6°	59	58	54	53

TABLE 23

Mean Sfc-300 mb Relative Humidity

Storm Stage	I	II	III	IV
Storm Region:				
0-2°	72	74	78	83
2-4°	71	70	70	72
4-6°	68	67	66	65

well with the convection patterns. The $\overline{RH}$ increases in the 0-2° region
while the 2-4° band reflects the decrease in convection from cluster
to depression stage followed by an increase. In the 4-6° band the $\overline{RH}$
decreases from the cluster stage to typhoon stage. The inner core
$\overline{RH}$ values (0-1°) for the cluster are less than the 2° $\overline{RH}$ as shown in
Table 24 suggesting that the central core may be a drier subsiding re-
gion. This agrees with our earlier observation which relates the
developing vortex to a region of dynamically forced subsidence.

TABLE 24

Mean Sfc-300 mb Relative Humidity

Storm Stage	I	II	III	IV
Storm Region:				
0-1°	72	76	82	90
2°	74	72	73	77

Frank (1976) has shown a minimum in $\overline{RH}$ (< 40%) west and northwest of the storm center (see Fig. 54). This agrees well with the observation in Section 4.2 that the northwest quadrant of the storm is a primary minimum in amount of convection. Frank's data for the steady state typhoon also shows very large relative humidities, 90% or greater, up through 400 mb within the inner core region (Fig. 55).
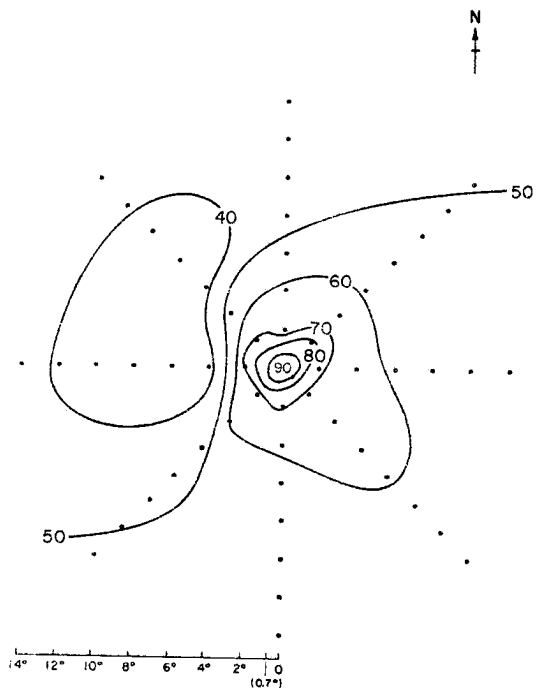
Fig. 54. Plan view of relative humidity at 500 mb for typhoon stage (from Frank, 1976).

I2Z RELATIVE HUMIDITY
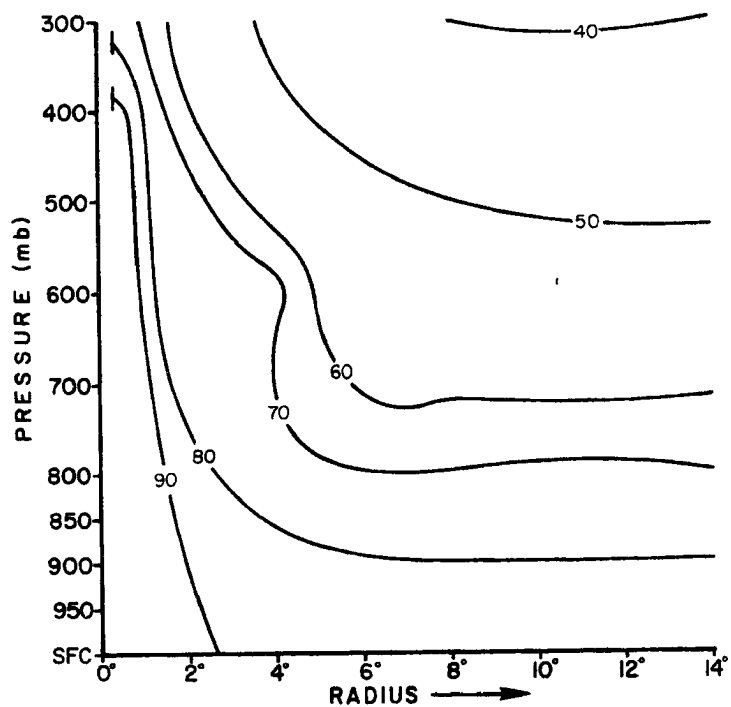
Fig. 55. Relative humidities of the typhoon stage at 1200Z (from Frank, 1976).

6. SUMMARY AND DISCUSSION

6.1 Summary of satellite and rawinsonde analysis

Convection as measured from the tracing data set or inferred from the top shade of IR, total cirrus, total cloudiness and BCE population all indicate that the average tropical cyclone goes through a two stage growth process. As the developing cluster begins to intensify there is an overall decrease in peripheral cloudiness with a concentration of inner core deep convection. As the storm intensifies beyond the depression stage, there is an overall increase in both deep convection and cirrus (Table 9). Due to an insufficient number of consecutive day storm cases it was not possible to determine what percentage of developing clusters display these characteristics. It is believed, however, that the concentration of convection is probably a consistent feature in most developing clusters (S. Erickson, 1977). Satellite analysts and tropical forecasters involved in monitoring cloud clusters may find that this tendency for concentration of convection is a useful tool in diagnosing those clusters which have the greater potential for development.

Although the growth curve in cloudiness is present in the statistical sense, we have seen that due to the pronounced variability in cloudiness any attempt to forecast growth or intensity based on an individual cyclone picture could be subject to significant inaccuracy. For instance, we have seen that there is a marked diurnal variability in both cirrus and deep convection. Such variability has been partially responsible for the difficulties experienced by the various cloudiness-intensity estimation techniques. For while there may be rather large

109

changes in cloud amount and/or organization during a 24-h period, no evidence of corresponding significant intensity change is noted. The results of this research clearly demonstrate that knowledge of storm cloud region size, amount of convection or cirrus, or spiral banding features is not sufficient for accurate intensity determination.

The results of individual satellite picture analyses in Stages I and II have confirmed the relationship between potential storm circulation centers and areas of depressed cloudiness.

Although it is not possible to examine individual storm variability with the rawinsonde data, the composited data agrees well with the composite satellite analysis. The changes in vertical motion at the base of the outflow level of the storm agree with changes in convection and cirrus production. Near the storm core, relative humidity increases with storm stage. The inner core relative humidity of the developing cluster (Stage I) indicates a subsiding region slightly drier than its surrounding environment. Diurnal variations in $\overline{RH}$ which might have been used to support the observed diurnal variability in cirrus and convection could not be determined because of the inaccuracies in the 00Z ($\sim$ 10 LT) $\overline{RH}$ values.

The most significant differences between storm stages were found in the composited temperature and tangential wind or vorticity fields. The percentage change in the 250 mb temperature anomaly between storm core and environment was found to be highly correlated with the percentage change in low level mean tangential wind. The implications for this with regard to satellite applications and storm forecasting are explored in Chapter 7.

Figures 56, 57 and 58 show the percentage changes in the various satellite determined cloud parameters and rawinsonde parameters during the life of the mean storm. The most striking feature here is the comparison between the very large increases in vorticity and the rather conservative changes in convection and cirrus. Thus, while there is a very weak correlation between the two, the overall conclusion that must be drawn is that deep convection is not directly related to vorticity.

6.2 Why variability and only weak vorticity-cloudiness relationships should be expected

Gray (1972, 1973) has frequently pointed out that the primary role of cumulus condensation is to provide potential energy to the rising air parcel and not to directly warm the environment. The small required extra temperature excess of 1-2° which the parcel has over the environment for buoyancy does not warm the surroundings unless it directly mixes out from the cloud. The cumulus parcel rises until it loses its temperature excess and its buoyancy. It then mixes with the environment at roughly the same temperature. Condensation heating is realized through mass subsidence in the clear environment outside the cloud. This concept of condensation warming explains why latent and sensible heating are often not directly related.

Lopez (1973b) has argued that "the degree of the resultant warming depends, however, on the scale on which the compensating sinking occurs. If the subsidence takes place over a broad region, a slight warming is experienced, which is probably used to compensate for the radiational cooling of the area". Typically most upper level enthalpy increase from subsidence goes to balance radiational cooling and is too weak to
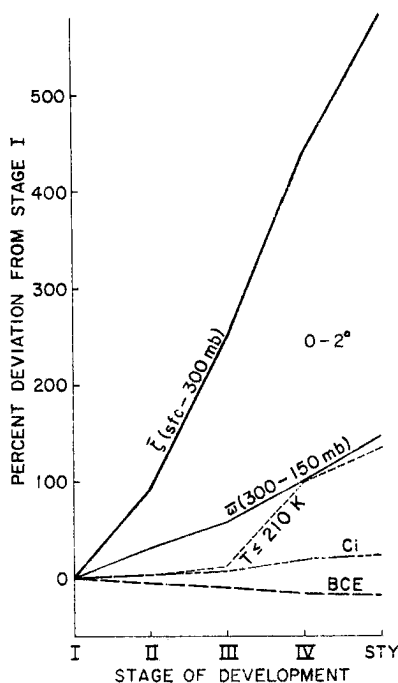
Fig. 56. Mean relative vorticity from the surface to 300 mb, mean
vertical motion from 300 to 150 mb, percent area covered by
basic convective elements (BCE), percent area covered by all
cirrus (Ci), and percent area covered by the coldest cirrus
(T ≤ 210 K) each expressed as a percent deviation from the
corresponding developing cluster (Stage I) values. For r =
0-2°.

produce the necessary pressure falls at the surface which would lead to

cyclone genesis.

A favorable arrangement of convective cells which could lead to

local regions of larger upper-level convergence may result in an upper

level forced subsidence warming. If present in a condition of weak ven-

tilation and occurring over a reasonable time period (3-10 hours), it

may be sufficient to produce the necessary local enthalpy increase and

surface pressure falls to form a cyclone center. This mechanism appears

to be related not to the overall amount of convective activity but

to the favorable positioning of the deep convective elements. Varia-

bility in cloudiness among storms with the same intensity should there-

fore be expected. Numerical modeling schemes which hope to model

113
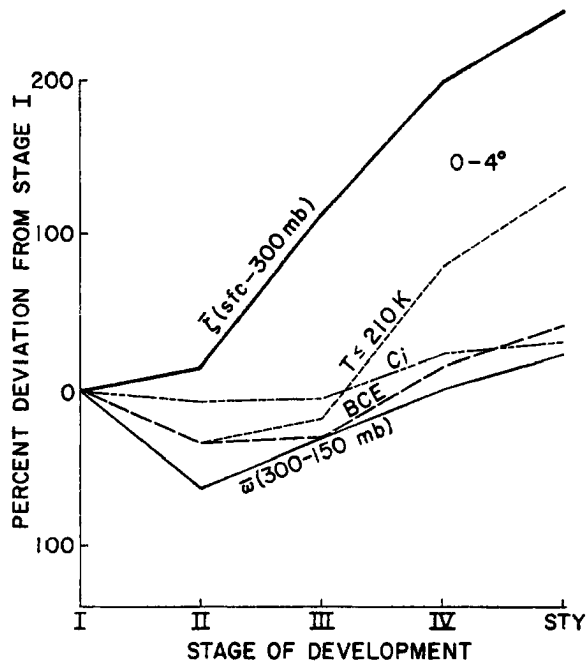
Fig. 57. Same as Fig. 56 except for r = 0-4°.

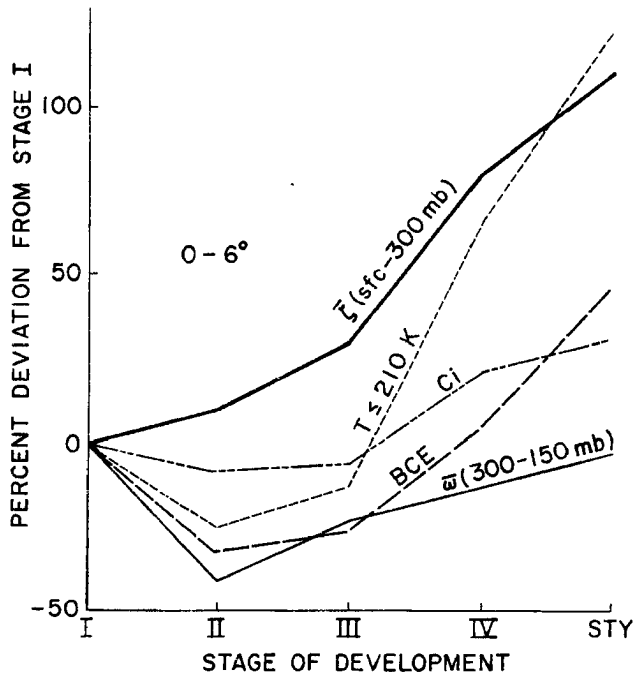
Fig. 58. Same as Fig. 56 except for r = 0-6°.

tropical cyclone genesis should likely not rely on the magnitude of the direct released latent heat but more importantly on the favorable positioning of the Cb convection and the indirect warming of the cumulus through locally forced return flow subsidence between groups of Cb elements.

Anthes (1974) has performed a scale analysis of the horizontal equations of motion over four subdivisions of the hurricane domain. He demonstrated that the only terms which could be neglected in the tangential wind equations (for a deep layer averaged outside the eyewall) were the eddy viscosity terms. All nondimensional coefficients in the equation were found to be so small that V_θ varied with a time scale on the order of 4-6 days. Therefore, one should expect that whatever may be the cause of significant changes in cirrus or deep convection on a time scale considerably less than several days, the mid-tropospheric tangential circulation will be slow to change.

During the period 1971-1974, this author observed no less than four typhoons which traveled across Southeast Asia from the Vietnam coast to the Bay of Bengal. These storms lost most of their deep convection and banding features yet retained their upper-level warm core and much of their deep tropospheric circulation. Several of these storms were able to redevelop a surface circulation upon entering the warm waters of the Bay of Bengal. Thus, continuously acting deep convection does not appear to be a necessary requirement for large-scale cyclone maintenance.

Lopez (1973b) has shown that it is impossible to generate convective clouds over tropical waters without cloud-base vertical velocities of 1-5 m s^{-1}. This requires the convergence beneath individual

cells to be approximately 5×10^{-3} s^{-1}, roughly 3 orders of magnitude larger than the cluster synoptic convergence. Gray (1973) concluded that frictionally induced low-level convergence by itself could play only a small direct role in maintaining a cluster's cumulus convection and that much local recycling of mass within the cluster must be occurring. A primary role for this mass convergence is to provide water vapor convergence.

Therefore, considering the different time scales upon which the deep tropospheric vorticity field and individual convective elements act and the small direct role that low-level forcing has in convective initiation it is not unreasonable to expect a weak vorticity-deep convection relationship at individual time periods.

6.3 Causes of variability in tropical cyclone cloudiness

This subject is not well understood and requires further investigation. At least three general areas of influence are likely to be important:

1) Environmental Influences,

2) Diurnal Influences, and

3) Natural Variability.

1) Environmental Influnces

The varying proximity of tropical cyclones to traveling mid-latitude systems may result in momentum pulses and/or divergence/vorticity changes which manifest themselves in changes in cloudiness (Mak, 1969). N. Frank (1969) has noted "extreme" day-to-day variability of cloudiness associated with cloud clusters in the eastern Caribbean. He considered this an important factor in explaining the discrepancies often found to exist between classical ideas, such as the easterly wave, and

observations. He has suggested that some of this variability may be directly related to the flow pattern in the high troposphere. Simpson et al. (1967) concluded that temporary changes in cloudiness "are related to small subtle changes in the wind field at or above 500 mb".

Sadler (1964) has also proposed that an intensifying cyclone may be temporarily or permanently dissipated as a result of the storm coming under the influence of an upper-level trough. Sadler reasoned as did Frank (1969) that there may at first be a temporary blowup in cloudiness as the storm approached the trough and that subsequently the extreme vertical wind shear produced by the tropical upper-tropospheric westerlies overlying the storm would quickly dissipate much of the cloudiness.

Dvorak (1975) has noted that the cyclone's cloud features change with the cyclone's changing environment. Environmental changes such as unidirectional flow aloft or "blocking" may produce short period or permanent changes in the cyclone's cloudiness. Blocking is indicated when the cyclone's cloudiness becomes elongated perpendicular to its direction of movement. The convective clouds ahead of the storm become suppressed. Results of this study also support the observations of N. Frank (1969) and Dvorak (1975). It was observed that the presence of an upper-level trough north or northwest of a westerly moving cyclone produced temporary (24-36 h) changes in the cyclone's cloud pattern and increases in cloud amount to the north and northwest of the storm. Typically a circular shaped storm becomes more elongated in a northeast-southwest direction.

Stability changes as a result of cyclone movement over a colder sea surface or as a result of advection of cooler air into the system should likely alter or suppress convection. Sadler (1964) has also

observed that eastern Pacific storms are smaller than those in the western Pacific. He attributes this variability in size to the restricted area of warm water over which the eastern Pacific storms form and to the relatively close proximity of very cold water on either side of the formation area. Dvorak (1975) has mentioned that changes in cloudiness may occur as a storm moves nearer a region of stratocumulus. Stratocumulus clouds are often found over colder sea surface temperatures.

Proximity of a cyclone to land may result in a modification of the storm's cloudiness due to land-sea induced circulation changes. It is a well observed fact that due to such circumstances there may be devastating effects on the structure and amount of deep convection and cirrus in tropical cyclones (Dvorak, 1975). Brand and Blelloch (1973) have noted that storms approaching the Philippines show an average increase in intensity 48-24 hours prior to landfall. A number of storms used in this study passed through the Philippines. As best as could be determined, there were intensity increases prior to landfall. More importantly, perhaps, was the significant decrease in the organization and amount of deep convection during the same time intervals of intensification in each storm. Thus, the increased intensity was not associated with an increase but rather a decrease in deep convection.

2) Diurnal Influences

Diurnal radiative effects appear to be reflected in diurnal cloudiness changes. Diurnal variability in cloudiness is considered to be related to diurnal variations in cloud-cloud free radiation differences as discussed briefly in an earlier chapter. Figure 59 shows the observed diurnal difference in cloud cluster divergence discussed by Gray and
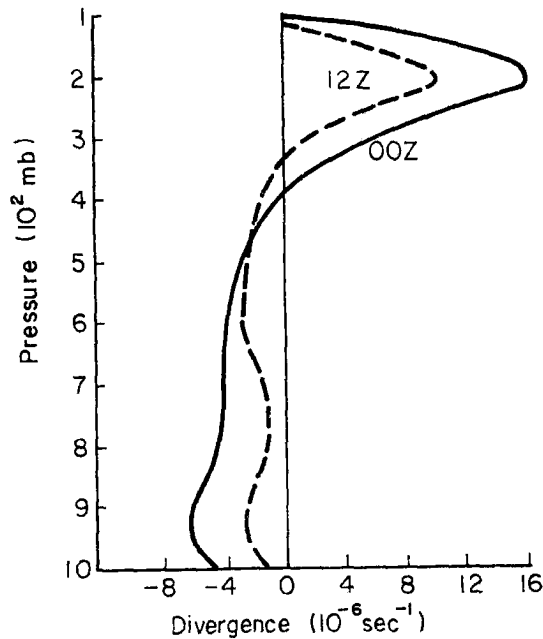
Fig. 59. Cloud cluster divergence (from Gray and Jacobson (1977).

Jacobson (1977). Nearly a 2 to 1 difference was found. The estimated
net radiational warming of cluster and clear region for both day (00Z)
and night (12Z) are given in Fig. 60. These differences in cluster and
surrounding region solar absorption were hypothesized by Gray and
Jacobson (1977) to produce a significant modulation of cluster inward-
outward height gradients and consequently the observed cluster mass
divergence profiles.

3) Natural Variability

Natural variability may arise as a result of mutually interacting
clusters competing for existing moisture and vorticity sources as they
vary in their relative positions. Observations from this research re-
veal that much of the variability in developing cluster size and cloud-
iness is random and natural. Some clusters are naturally small while
others forming under apparently similar environmental conditions were
found to be much larger. As pointed out earlier, there was a tendency

**ESTIMATED NET
RADIATIONAL WARMING**
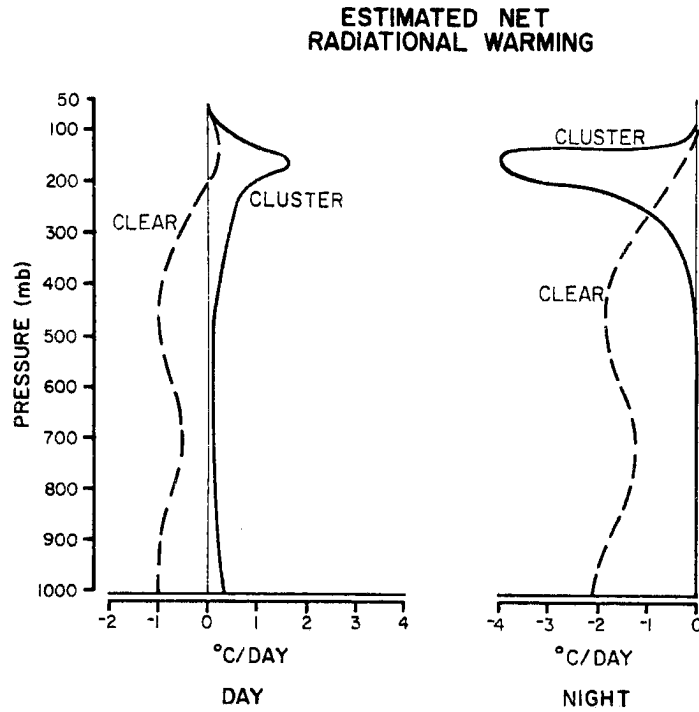
Fig. 60. Estimated typical day and night net radiational warming within
the cloud cluster and in the surrounding clear or mostly clear
regions (from Gray and Jacobson, 1977).

for small clusters to develop into small typhoons and for large clusters

to become large typhoons. Therefore, some of the natural variability

in clusters, perhaps resulting from a competition among adjacent

clusters for existing vorticity and moisture sources, carries over into

the typhoon stage.

7. CONCLUSIONS

The use of individual high resolution, high contrast positive transparency satellite photos has revealed several important physical characteristics of tropical storm cloudiness and genesis. Composited satellite-determined cirrus and deep convection well document the large variability of tropical storm deep convection. Rawinsonde composites have been used to support the results obtained from the satellite study.

7.1 Results

The most striking result to come from the analysis of physical and cloud characteristics was the observed deep convective cloud variability for all classes of cyclone intensity. On the basis of a number of previous cloudiness - storm intensity models, (Fett, 1964; Fritz et al., 1966; Dvorak, 1975) it was expected that significant differences between storm stages would be found in physical characteristics such as storm dimensions and banding features as well as cloud characteristics such as percent of area covered by cirrus and deep convective cloud types. Tropical cyclone dimensions and cloud amounts, however, showed little difference from one intensity stage to the next but did show considerable variability within a given stage. The percentage of storms which showed some degree of banding increased rather substantially from the developing cluster to the typhoon ($\sim$ 25% to $\sim$ 75%). It is for this reason that previous cloudiness-intensity models have been as useful as they are. Even so, this feature is highly variable with many advanced stage storms showing little or no banding.

It was found that deep convection in the tropical cyclone occurs in multi-cellular complexes. Since these appear to be an elemental convective form they were termed "Basic Convective Elements" (BCE). Their average size was found to be approximately 200-250 n mi^2 (15 x 15 n mi). It is believed that the multiple constraints of entrainment drying, low-level layer stability, mass recycling, and synoptic scale forcing, etc. all act to impose this mode of convection over tropical waters.

From an analysis of individual satellite pictures of developing clusters, it was observed that 25% of incipient circulation centers were exposed, i.e. found in the clear region outside or along the periphery of the cluster. Approximately 50% of identifiable circulation centers[15] within the cluster were associated with areas of suppressed cirrus and convective cloud types. These areas were typically defined by an arc of BCE's. It is hypothesized that both types of circulation centers are associated with an upper-level type of dynamically forced subsidence resulting from either the convergence between the outflow from a group of BCE's and the environmental flow (Fig. 32) or from the convergence between the outflow from adjacent embedded BCE's (Fig. 31).

The analysis of wind and thermodynamic parameters derived from the rawinsonde composites supported the satellite findings. The statistical tendency for a decrease in cloudiness at outer radii (2-6°) from the Stage I to the Stage II cyclone was confirmed by the observed decrease in vertical motion at the outflow level. At 4-6° this

---

[15]Confirmed by aircraft reconnaissance investigative flight data as discussed in Chapter 2.

decrease in vertical motion and cloudiness continues through the life of the storm suggesting an early formation of a largely "cloud-free" moat region between 4 and 6°.

Tropospheric vorticity values increase by over 400% in the inner core $(0-2^{\circ})$ of the storm between Stages I and IV while during the same period cirrus cloud amounts increase by less than 25%. Convective elements increase by 30-40%. Thus, there is only a weak cloudiness-vorticity relationship. Upper tropospheric temperature anomalies (storm core minus environment) increase dramatically with intensity and as expected are highly correlated with lower tropospheric height gradients. Relative humidities show a continual moistening of the inner core.

7.2 Implications for modeling

Many cumulus parameterization schemes may be overspecifying the amounts of direct condensation heating. Direct cumulus heating is extremely weak since most of the latent heat is converted into potential energy and exported to the surroundings. It appears that cumulus heating can only be realized indirectly by means of mass subsidence in the environment or locally. The existence of localized regions of dynamically forced subsidence associated with surface circulations strongly suggests that condensation warming results from a mechanism by which cumulus induced subsidence occurs. The role of convective elements in this warming process further suggests that the cyclone development process proceeds independent of the total amount of convection in the cluster and is likely more a result of the favorable positioning of the deep convective elements.

Ooyama (1964), Charney and Eliassen (1964), Ooyama (1969), and most recent modelers of tropical cyclone intensification have developed their models based on an inner core of convection of radius A with upward vertical motion surrounded by a region of compensating subsidence. Linear analysis leads to an eigenvalue equation relating the growth rate of the disturbance (σ) to the parameter A. Solutions are in the form of self amplifying perturbations. Although the solutions and growth rates are realistic, there are many shortcomings of the linearized model, as discussed in detail by Ooyama (1969). It is therefore suggested that models be developed which begin with an inner region of sinking motion ($\sim$ 1-2° diameter) with a variable outer convective region of mean upward motion surrounded by a subsidence region.

Grube (1977b) has recently discussed preliminary results obtained from a 7-layer symmetric cloud cluster model being developed by Finger-hut (1977). Grube has observed cases of upper level warming using GATE data in semi-cloudless areas surrounded by deep convection. The observed warmings (2-3 C/3-6 hs) were too large to be a result of daily solar heating and too brief to be due to advection. She concluded that they resulted from dynamical causes. She assumed that if the convective elements are patterned such that their outflow is trapped, forced convergence and local subsidence warming would occur. Using Fingerhut's model with an assumed inward radial wind of 5 m s^{-1} at 204 mb, she has shown that such a sequence of events are physically sound.

7.3 Implications for tropical cyclone reconnaissance

Tropical cyclone reconnaissance has traditionally relied on aircraft fix data such as storm position and intensity (central pressure, maximum sustained surface wind). In recent years it has become necessary to reduce the amount of aircraft reconnaissance and use satellite information whenever possible. Satellite storm positions can now be made quite accurately. Accurate storm intensity based on satellite determined cloud amounts and/or organization, however, is here questioned. It appears that greater reliability could be placed on measurements of the storm's upper level temperature field.

It is suggested that the possibilities of developing special sensors aboard future satellites be explored which can measure a cyclone's upper troposheric temperature field. At present the SCAMS instrument aboard NIMBUS VI can only provide temperatures in the 250-100 mb layer of the storm. Often this region of the storm is cold core (Frank, 1976) making it difficult to obtain realistic temperature gradients. Instrumentation is required which provides temperatures in the layer of maximum temperature anomaly (250-300 mb). Similar sensors could be placed on aircraft which are capable of overflying a tropical cyclone.

7.4 Further research

More observational data should be sought to confirm the existence of dynamically forced subsidence regions which apparently lead to cyclone center formation. The precise role that this mechanism plays in tropical cyclone genesis should be further explored. The role of the Basic Convective Element in cluster growth and decay

should be explored. Finally, research should continue into more

reliable means of estimating storm strength from the storm's tempera-

ture field.

ACKNOWLEDGEMENTS

The author deeply appreciates the moral support, guidance and continual encouragement given him by his adviser, Professor William M. Gray. The author was fortunate to have had the technical assistance of Mr. Edwin Buzzell, Mr. Roger Whitcomb, Mrs. Barbara Brumit, Mr. Charles Solomon and Mrs. Dianne Schmitz. For their many helpful suggestions and enlightening discussions the author would like to thank Dr. William M. Frank, Mr. William A. Fingerhut, Captain Steven Erickson, Mr. John McBride, Dr. Thomas Vonder Haar, Dr. Peter Sinclair and Dr. David Krueger. He would also like to acknowledge the U.S. Air Force for providing him the opportunity to attend CSU. His deepest gratitude goes to his wife Elaine and Children Amy, Charles, Beth and Mike who made so many sacrifices for him.

BIBLIOGRAPHY

Allison, L. J., G. W. Nicholas and J. S. Kennedy, 1966: Examples of
the meteorological capability of the high resolution infrared
radiometer on the Nimbus I satellite. J. Appl. Meteor., 5,
314-333.

Anthes, R. A., 1974: The dynamics and energetics of mature tropical
cyclones. Reviews of Geophysics and Space Physics, 12, 495-522.

Arnold, C. P., 1972: Circulation center fixes. Unpublished letter
dated 26 July 1972 from C. P. Arnold, Det. 2, 1st Weather
Wing to 1 WWG/DNX.

Arnold, C. P., 1974: Tropical cyclone position and intensity analysis
using satellite data. 1 WW Pamphlet 105-10, Department of the
Air Force, Headquarters 1st Weather Wing, 88 pp.

Arnold, C. P., 1975: Selective reconnaissance program of the western
north Pacific. Bull. Amer. Meteor. Soc., 56, 362-371.

Balogun, E. E., 1973: A study of satellite-observed cloud patterns
of tropical cyclones. Satellite and Mesometeorology Research
Project No. 108, Department of the Geophysical Sciences, The
University of Chicago, 103 pp.

Bandeen, W. R., V. Kunde, W. Nordberg and H. P. Thompson, 1964: TIROS
III Meteorological satellite radiation observations of a tropical
hurricane. Tellus, 16, 481-502.

Brand, S. and J. W. Blelloch, 1973: Changes in the characteristics
of typhoons crossing the Phillipines. J. Appl. Meteor., 12,
104-109.

Brooks, C. E. P. and N. Carruthers, 1953: Handbook of statistical
methods in meteorology. Her Majesty's Stationary Office, London,
412 pp.

Browner, S. P., 1976: Diurnal oscillation of the cloudiness associated
with tropical storms. Paper presented at the 10th Technical
Conference on Hurricanes and Tropical Meteorology, University of
Virginia, Charlottesville, VA, July 6-9, 1976, 15 pp.

Browner, S. P., W. L. Woodley and C. G. Griffith, 1977: Diurnal
oscillation of the area of cloudiness associated with tropical
storms. Mon. Wea. Rev., 105, 856-864.

Chang, C. P., 1970: Westward propagating cloud patterns in the
tropical Pacific as seen from time-composite satellite photo-
graphs. J. Atmos. Sci., 27, 133-138

BIBLIOGRAPHY (cont'd)

Charney, J. C. and A. Eliassen, 1964: On the growth of the hurricane depression. J. Atmos. Sci., 21, 68-75.

Dickinson, L. G., S. E. Boselly and W. S. Burgmann, 1974: Defense Meteorological Satellite Program User's Guide. Air Weather Service Tech. Rept., 109 pp.

Dvorak, V., 1968: Tropical and subtropical disturbance classification from satellite data. National environmental Satellite Center Analysis Branch.

Dvorak V., 1973: A technique for the analysis and forecasting of tropical cyclone intensities from satellite pictures. NOAA Technical Memorandum NESS 45 (Revision of NOAA TM NESS 36). U.S. Department of Commerce, Suitland, MD, 19 pp.

Dvorak, V., 1975: Tropical cyclone intensity analysis and forecasting from satellite imagery. Mon. Wea. Rev., 103, 420-430.

Erickson, C., 1974: Use of geostationary-satellite cloud vectors to estimate tropical cyclone intensity. NOAA Technical Memorandum NESS 59, U.S. Department of Commerce, National Environmental Satellite Service, Washington, DC, 37 pp.

Erickson, S., 1977: Comparison of developing vs. non-developing tropical disturbances. Colo. State Univ., Atmos. Sci. Paper No. 274, Ft. Collins, CO, 85 pp.

Fett, R. W., 1964: Some characteristics of the formative stage of typhoon development: A satellite study. National Conference on Physics and Dynamics of Clouds, Chicago, IL, March 24-26, U.S. Weather Bureau, Washington, DC, 10 pp.

Fett, R. W., 1966: Upper-level structure of the formative tropical cyclone. Mon. Wea. Rev., 94, 9-18.

Fett, R. W., 1967: A note of the stage C - "comma configuration". Annual Typhoon Report, 1967. Fleet Weather Central, Guam, Marianas Islands, 9 pp.

Fett, R. W., 1968: Typhoon formation within the zone of the intertropical convergence, Mon. Wea. Rev., 96, 106-117.

Fett, R. W. and S. Brand, 1974: Tropical cyclone movement forecasts based on observations from satellites. Naval Environmental Prediction Research Facility, Technical Paper No. 1-74, Monterey, CA, 70 pp.

BIBLIOGRAPHY (cont'd

Fingerhut, W., 1977: Model simulation of the tropical cloud cluster and its diurnal variation. (Manuscript available from Dept. of Atmos. Sci., CSU). (To be published in Mon. Wea. Rev.)

Frank, N. L., 1963: Synoptic case study of tropical cyclogenesis utilizing TIROS data. Mon. Wea. Rev., 91, 355-366.

Frank, N. L., 1969: The "inverted v" cloud pattern-an easterly wave? Mon. Wea. Rev., 97, 130-141.

Frank, W., 1976: The structure and energetics of the tropical cyclone. Colo. State Univ., Atmos. Sci. Paper No. 258, Ft. Collins, CO, 180 pp. (To be published in Mon. Wea. Rev., Oct., 1977).

Fritz, S., 1962: Satellite pictures and the origin of hurricane Anna. Mon. Wea. Rev., 90, 507-513.

Fritz, S., L. F. Hubert and A. Timchalk, 1966: Some inferences from satellite pictures of tropical disturbances. Mon. Wea. Rev., 54 231-236.

Fujita, T. and J. E. Arnold, 1964: Detection of hurricanes using TIROS infra-red data. Proc. Symp. Tropical Meteorology, Rotorua, New Zealand, 1963, 582-589.

GARP report on the first session of the study group on tropical disturbances (Madison, WI, 21 October - 8 November 1968), Joint GARP Organization Committee, WMO.

Gray, W., 1972: The magnitude and character of the radiation induced vertical circulation of the troposphere. Conference on Atmospheric Radiation, August 7-9, 1972, Ft. Collins, CO, published by AMS, Boston, MA, 255-259.

Gray, W., 1973: Cumulus convection and larger scale circulations I: Broadscale and mesoscale considerations. Mon. Wea. Rev., 101, 839-855.

Gray, W., 1975: Tropical cyclone genesis. Colo. State Univ., Atmos Sci. Paper No. 234, Ft. Collins, CO, 119 pp.

Gray, W., 1977: Tropical disturbance to cyclone transformation. (submitted to J. Atmos. Sci.).

Gray, W., and D. J. Shea, 1973: The hurricane's inner core region. II Thermal stability and dynamic characteristics. J. Atmos. Sci., 30, 1565-1576.

BIBLIOGRAPHY (cont'd)

Gray, W. and D. Shea, 1976: Data summary of NOAA's hurricane inner-core radial leg flight penetrations 1957-1967, and 1969. Colo. State Univ., Atmos. Sci. Paper No. 257, Ft. Collins, CO, 219 pp.

Gray, W. and R. Jacobson, 1977: Diurnal variation of deep cumulus convection. (submitted to Mon. Wea. Rev.).

Grube, P., 1977a: Personal communication.

Grube, P., 1977b: Influence of deep cumulus convection on upper tropospheric changes in GATE, 18 pp. (Informal report given to GATE Workshop, Boulder, CO, August, 1977).

Hawkins, H. F. and D. T. Rubsam, 1968: Hurricane Hilda, 1964: II. Structure and budgets of the hurricane on October 1, 1964. Mon. Wea. Rev., 99, 427-434.

Hawkins, H. and S. Imbembo, 1976: The structure of a small, intense hurricane - Inez, 1966. Mon. Wea. Rev., 104, 418-442.

Hayden, C. M., 1969: Objective dimensions of Pacific cloud clusters. Paper presented at the 50th Annual Meeting of the American Geophysical Union, Washington, DC, April 21-25, 1969.

Hayden, C. M., 1970: An objective analysis of cloud cluster dimensions and spacing in the tropical north Pacific. Mon. Wea. Rev., 98, 534-540.

Holle, R. L., 1968: Some aspects of tropical oceanic cloud populations. J. Appl. Meteor., 7, 173-183.

Holliday, C. R., 1975: Annual Typhoon Report, 1974. Fleet Weather Central, Guam, Marianas Islands, 9 pp. (Available from Joint Typhoon Warning Center, Guam).

Holliday, C. R., 1976: Double intensification of typhoon Gloria, 1974. Mon. Wea. Rev., 105, 523-528.

Hubert, L. and A. Timchalk, 1969: Estimating hurricane wind speeds from satellite pictures. Mon. Wea. Rev., 97, 382-383.

Jacobson, R. W. and W. Gray, 1976: Diurnal variation of oceanic deep cumulus convection, Paper I: Observational evidence, Paper II: Physical hypothesis. Colo. State Univ., Atmos. Sci. Paper No. 243, Ft. Collins, CO, 106 pp.

Joint Typhoon Warning Center, 1971: Annual Typhoon Report, 1971. Fleet Weather Central, Guam, Marianas Islands, 173 pp. (Available from Joint Typhoon Warning Center, GUAM).

BIBLIOGRAPHY (cont'd)

Joint Typhoon Warning Center, 1975: Annual Typhoon Reports, 1972-1976, Fleet Weather Central, Guam, Marianas Islands, (Available from Joint Typhoon Warning Center, GUAM).

Kidder, S., 1977: Personal communication.

Lopez, R. E., 1968: Investigation of the importance of cumulus convection and ventilation in early tropical storm development. Colo. State Univ., Atmos. Sci. Paper No. 124, Ft. Collins, CO, 86 pp.

Lopez, R. E., 1973a: A parametric model of cumulus convection. J. Atmos. Sci., 30, 1354-1373.

Lopez, R. E., 1973b: Cumulus convection and larger scale circulations, I. Broadscale and mesoscale considerations, II. Cumulus and mesoscale interactions. Mon. Wea. Rev., 101, 839-870.

Lopez, R. E., 1976: Radar characteristics of the cloud populations of tropical disturbances in the northwest Atlantic. Mon. Wea. Rev., 104, 268-283.

Mak, M. K., 1969: Laterally driven stochastic motions in the tropics. J. Atmos. Sci., 26, 41-64.

Malkus, J. S., C. Ronne and M. Chaffe, 1960: Cloud patterns in hurricane Daisy, 1958. Woods Hole Oceanographic Institution Technical Report No. 8, 48 pp.

Malkus, J. S. and H. Riehl, 1964: Cloud structuring and distribution over the tropical Pacific ocean. University of California Press, 229 pp.

Martin, D., D. Suchman and D. Sikdar, 1977: Deep convective mass transport - two estimates from geostationary satellites. Mon. Wea. Rev., (in press).

Merritt, E. S., 1964: Easterly waves and perturbations, a reappraisal. J. Appl. Meteor., 3, 367-382.

Meyer, W., 1973: Data acquisition and processing program: A Meteorological data source. Bull. Amer. Meteor. Soc., 54, 1251-1254.

Oliver, V. J. and R. K. Anderson, 1969: Circulation in the tropics as revealed by satellite data. Bull. Amer. Meteor. Soc., 50, 702-707.

Ooyama, K., 1964: A dynamical model for the study of tropical cyclone development. Geofis. Intern., 4, 187-198.

BIBLIOGRAPHY (cont'd)

Ooyama, K., 1969: Numerical simulation of the life cycle of tropical
    cyclones. J. Atmos. Sci., 26, 3-40.

Riehl, H., 1954: Tropical Meteorology. McGraw-Hill, New York, 392 pp.

Riehl, H. and J. Malkus, 1961: Some aspects of hurricane Daisy, 1958.
    Tellus, 13, 181-213.

Ruprecht, E., 1975: Diurnal temperature corrections for rawinsonde
    humidity sensors. Mon. Wea. Rev., 103, 352-355.

Ruprecht, E. and W. Gray, 1974: Analysis of satellite-observed cloud
    clusters. Colo. State Univ., Atmos. Sci. Paper No. 219, Ft.
    Collins, CO, 91 pp.

Ruprecht, E., and W. M. Gray, 1976: Analysis of satellite observed
    tropical cloud clusters. Papers I and II. Tellus, 28, 319-425.

Sadler, J., 1964: Tropical cyclones of the eastern north Pacific as
    revealed by TIROS observations. J. Appl. Meteor., 3, 347-366.

Sadler, J., 1967a: On the origin of tropical vortices. Working Panel
    on Trop. Dynamical Meteorology, Naval Postgraduate School, Monterey,
    CA, 39-75.

Sadler, J. C., 1967b: On the tropical upper tropospheric trough as a
    secondary sources of typhoons and a primary source of trade wind
    disturbances. Hawaii Institute of Geophysics, University of
    Hawaii, Final Report to Air Force Cambridge Research Laboratories,
    44 pp.

Sadler, J., 1976: Tropical cyclone initiation by the tropical upper
    tropospheric trough. Naval Environmental Prediction Research
    Facility, Technical Paper No. 2-76, Monterey, CA, 103 pp.

Shea, D. and W. Gray, 1973: The hurricane's inner core region, I:
    Symmetric and asymmetric structure. J. Atmos. Sci., 30, 1554-1564.

Sheets, R. C., 1972: Diurnal variation in hurricanes. Project Storm-
    fury Annual Report 1971, U.S. Department of Commerce and U.S.
    Department of the Navy, Miami, FL, Appendix G, 121-126.

Sheets, R. C. and P. G. Grieman, 1975: An evaluation of the accuracy
    of tropical cyclone intensities and locations determined from
    satellite pictures. NOAA Technical Memorandum ERP WMPO-20, U.S.
    Department of Commerce, 36 pp.

BIBLIOGRAPHY (cont'd)

Sikdar, D. and V. E. Suomi, 1971: Time variation of tropical energetics as viewed from a geostationary altitude. J. Atmos. Sci ., 28, 170-180.

Simpson, R., 1952: Exporting the eye of typhoon Marge, 1951. Bull. Amer. Meteor. Soc., 33, 286-298.

Simpson, J., M. Garstang, E. Zipser and G. Dunn, 1967: A study of a non-deepening tropical disturbance. J. Appl. Meteor., 6, 237-254.

Timchalk, A., L. F. Hubert and S. Fritz, 1965: Wind speeds from TIROS pictures of storms in the tropics. Meteorological satellite Laboratory Report No. 33, U.S. Department of Commerce, 33 pp.

Williams, K., 1970: A statistical analysis of satellite-observed trade wind cloud clusters in the western north Pacific. Colo. State Univ., Atmos. Sci. Paper No. 161, Ft. Collins, CO, 80 pp.

Williams, K. and W. Gray, 1973: Statistical analysis of satellite observed trade wind cloud clusters in the western north Pacific. Tellus, 25, 313-336.

Yanai, M., 1961: A detailed analysis of typhoon formation. J. Meteor. Soc. Japan, 39, 187-213.

Yanai, M., 1968: Evolution of a tropical disturbance in the Caribbean Sea region. J. Meteor. Soc. Japan, 46, 86-108.

Zehr, R., 1976: Tropical disturbance intensification. Colo. State Univ., Atmos. Sci. Paper No. 259, Ft. Collins, CO, 91 pp.

APPENDIX A

COMPOSITING PHILOSOPHY AND STATISTICAL TREATMENT OF DATA

A.1 Rawinsonde compositing philosophy

Subjectiveness in the analysis of tropical cyclone case studies has in general led to inconclusive results. A compositing scheme which uses large amounts of rawinsonde data, on the other hand, can for mean-state differences, be quantitative. The rawinsonde compositing scheme used in this paper was introduced by Williams and Gray (1973) from an earlier study by Williams (1970) and is based on the fact that with a deficiency in observations, broad scale dynamics cannot be adequately described at individual time periods. Only from a composite study of many systems, which a priori are assumed to have similar physical processes, is it possible to make quantitative descriptions. Individual rawinsonde observations are seldom, if ever of sufficient quantity or representativeness to accurately describe individual tropical systems. For example, in the study of cloud clusters, their sub-synoptic size with respect to the present trade wind network of rawinsondes makes their description by case study virtually impossible (Ruprecht and Gray 1974). The a priori assumption that basic physical processes of like systems are basically similar is reasonable. At present there are no physical or observational reasons to believe otherwise (Gray, 1975).

A.2 Statistical treatment

If one can separate a population into classes each based on one or more known distinguishing parameters which are significantly different in the mean, it is reasonable to assume that other parameters may exist which show similar differences. The compositing

assumption in the last section that physical processes of like

systems (such as classes or stages) are basically similar does not

necessarily imply that a given physical process can be used to

categorize the system into a given stage or class. The degree to

which a member of a population can be satisfactorily placed into a

sub-class will depend in part, on the degree of variability within

the class. For example, if the variances associated with two or more

normally distributed populations are very small and the mean values

are significantly different, one can place a given member into its

proper class with a high degree of statistical probability. Therefore,

while the compositing method may be very excellent for a study of

the characteristics of a given class, it may be limited in its

ability to distinguish between individual members of the population.

Tropical cyclones[16] as a population can easily be categorized

into four basic classes based on intensity, the latter being

represented by either maximum sustained surface wind, central pressure,

or upper level temperature anomaly. All are, of course, dependent

variables. Maximum sustained surface wind as determined in post

analysis is the most reliable since it is normally based on many

independent observations. There are other parameters such as storm

damage or storm surge with which a storm could be categorized but

with much less accuracy. The four classes referred to above are:

> I) Tropical disturbance or cloud cluster as defined in the
> 1968 GARP report. This stage may or may not be characterized
> by a closed wind circulation. It has been further sub-
> divided into non-developing and developing clusters. The
> latter are typically warm core with a closed circulation and

---

[16]A warm core tropical weather system having a definite organized
circulation.

hence are normally regarded as being the first in the family
of tropical cyclones. They typically have maximum sustained
surface winds less than 20 knots.

II. Tropical depression – the second stage of tropical
cyclone development with maximum sustained surface winds
in the range of 20 to 33 knots inclusive,

III. Tropical storm – the third stage of tropical cyclone
development with maximum sustained surface winds in the
range of 34 to 63 knots inclusive,

IV. Typhoon stage – the fourth stage of tropical cyclone development
with maximum sustained surface winds 64 knots or greater. A
subset of this stage will sometimes be used, called the super-
typhoon (STY) defined as having wind speed greater or equal to
130 knots.

These four basic stages will be referred to as Stage I, II, III or IV

throughout this paper.

With these four classes or stages used in this report the assump-

tion was made that deep convective clouds and the cirrus which they

produce would represent a physical process or parameter which while

similar within a given class would be significantly different between

classes, and that the natural variability within classes would be such

as to permit this parameter to be used to categorize a given tropical

cyclone. This has been the working hypothesis behind all intensity

estimation schemes discussed in the introduction. The hypothesis, how-

ever, has never been fully tested.

All sample statistics were tested for significance using the rou-

tine tests of small sampling theory. If a given hypothesis is, a priori,

assumed true and it is found, based on sampling theory, that certain

sample statistics differ markedly from those expected on the basis of

pure chance, the observed differences are considered significant and the

hypothesis is rejected (Brooks and Carruthers, 1953). Statisticians

generally agree that results significant at the .01 level are highly

significant while results significant at the .05 but not the .01 level are considered probably significant.

In many instances during the course of this research is was necessary to determine whether or not there were any significant differences between composite or mean values. The null hypothesis was that there were no such differences. Tests were then conducted to determine the validity of the null hypothesis. Unless stated otherwise all comparisons between sample statistics such as mean values exhibited differences that were at least probably significant. A similar statistical analysis was accomplished by Williams (1970) for the rawinsonde data. Although similar tests were not conducted by Zehr (1976) and Frank (1976) their data sets are considered to be as reliable and representative as that of Williams.

APPENDIX B

EXAMPLES OF DYNAMICALLY FORCED SUBSIDENCE REGIONS OUTSIDE AND WITHIN
THE DEVELOPING CLUSTER

This appendix contains additional DMSP examples of cloud free or
nearly cloud free regions associated with incipient circulation centers
of developing clusters (Stage I). Some are exposed, being in the clear
region surrounding the cluster, while others depict the embedded type.
All centers are circled. The date, time, latitude and longitude of
storm center, and data type (visual, VHR; infrared, IR) are listed below
for each figure in the appendix. The scale for these figures is 484 km
to an inch.

Figure	Date	Time(Z)	Latitude(N)	Longitude(E)	Data Type
B1	10 SEP 72	0249	14.5	129.8	VHR
B2	10 SEP 72	0249	14.5	129.8	IR
B3	10 SEP 72	2316	15.5	128.6	VHR
B4	10 SEP 72	2316	15.5	128.6	IR
B5	2 JUL 72	2312	8.8	129.2	VHR
B6	2 JUL 72	2312	8.8	129.2	IR
B7	4 JUL 72	0357	10.3	125.6	VHR
B8	4 JUL 72	0357	10.3	125.6	IR
B9	2 JUL 72	2131	8.7	162.9	VHR
B10	2 JUL 72	2131	8.7	162.9	IR
B11	19 JUN 72	2223	10.8	145.1	VHR
B12	19 JUN 72	2223	10.8	145.1	IR
B13	20 JUN 72	0214	10.7	144.8	VHR
B14	20 JUN 72	0214	10.7	144.8	IR
B15	29 MAY 72	0409	16.7	128.3	VHR
B16	29 MAY 72	0409	16.7	128.3	IR
B17	25 SEP 72	2310	13.0	128.0	VHR
B18	25 SEP 72	2310	13.0	128.0	IR
B19	30 AUG 72	0346	11.6	124.1	VHR
B20	30 AUG 72	0346	11.6	124.1	IR
B21	27 NOV 72	0237	9.9	138.5	VHR
B22	27 NOV 72	0237	9.9	138.5	IR
B23	4 JUL 72	2358	11.0	124.8	VHR
B24	4 JUL 72	2358	11.0	124.8	IR
B25	5 JUL 72	0200	9.5	150.2	VHR
B26	5 JUL 72	0200	9.5	150.2	IR
B27	29 AUG 72	0402	9.0	129.1	VHR
B28	29 AUG 72	0402	9.0	129.1	IR

APPENDIX B (cont'd)

Figure	Date	Time(Z)	Latitude(N)	Longitude(E)	Data Type
B29	5 JUL 72	0242	13.4	123.8	VHR
B30	5 JUL 72	0242	13.4	123.8	IR
B31	31 OCT 74	2243	5.0	143.3	VHR
B32	31 OCT 74	2243	5.0	143.3	IR
B33	12 OCT 74	2326	12.5	137.5	VHR
B34	12 OCT 74	2326	12.5	137.5	IR
B35	1 NOV 72	0207	17.5	151.1	VHR
B36	1 NOV 72	0207	17.5	151.1	IR
B37	19 JUN 72	0225	9.4	147.0	VHR
B38	19 JUN 72	0225	9.4	147.0	IR
B39	15 SEP 72	0136	13.5	154.5	VHR
B40	15 SEP 72	0136	13.5	154.5	IR
B41	29 AUG 72	2342	11.3	125.4	VHR
B42	29 AUG 72	2342	11.3	125.4	IR
B43	31 OCT 72	2153	16.8	152.4	VHR
B44	31 OCT 72	2153	16.8	152.4	IR
B45	4 JUL 72	0215	7.4	150.2	VHR
B46	4 JUL 72	0215	7.4	150.2	IR
B47	28 NOV 72	0404	8.5	131.6	VHR
B48	28 NOV 72	0404	8.5	131.6	IR
B49	5 JUL 72	0200	7.2	163.0	VHR
B50	5 JUL 72	0200	7.2	163.0	IR
B51	29 JUL 72	0119	6.0	163.1	VHR
B52	29 JUL 72	0119	6.0	163.1	IR
B53	13 NOV 74	0008	14.3	121.2	VHR
B54	13 NOV 74	0008	14.3	121.2	IR
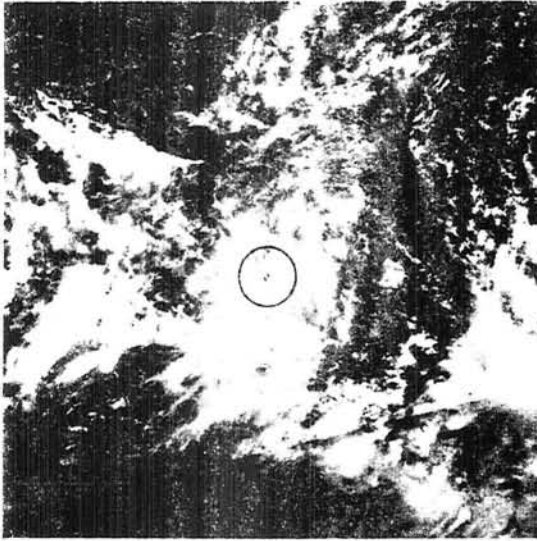
Fig. B1.
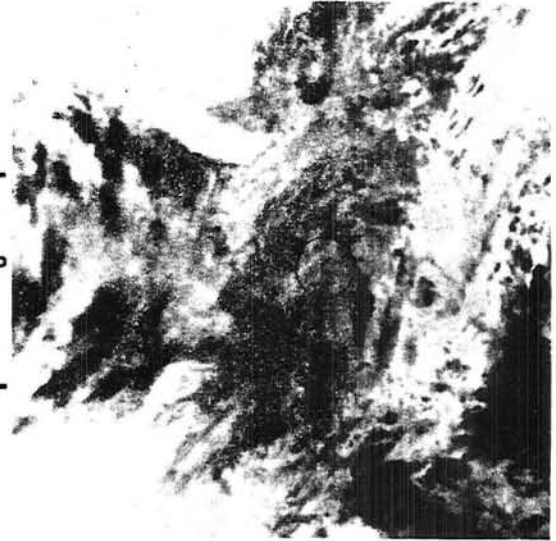
Fig. B2.
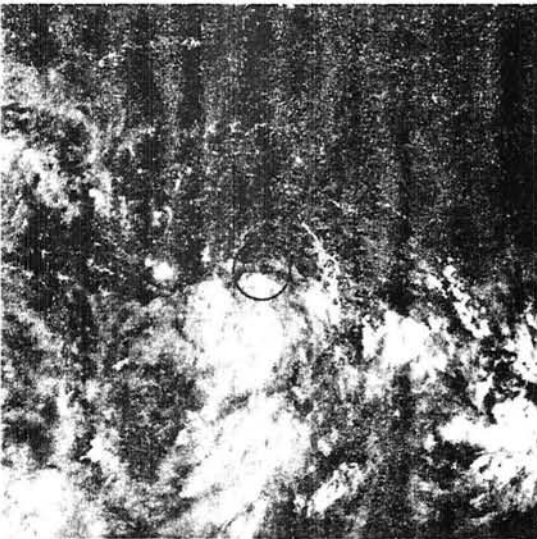
Fig. B3.

Fig. B4.
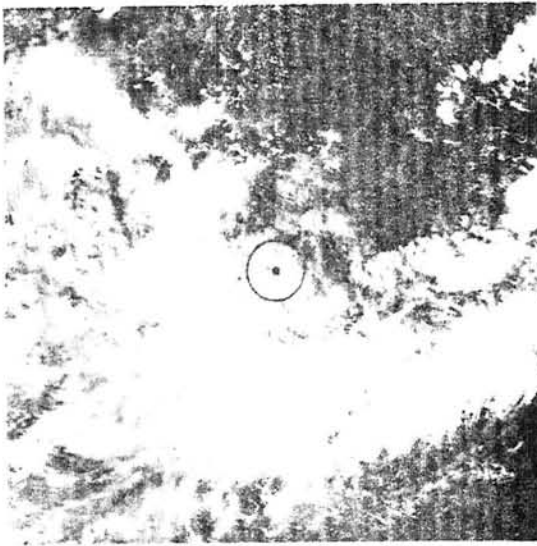
Fig. B5.
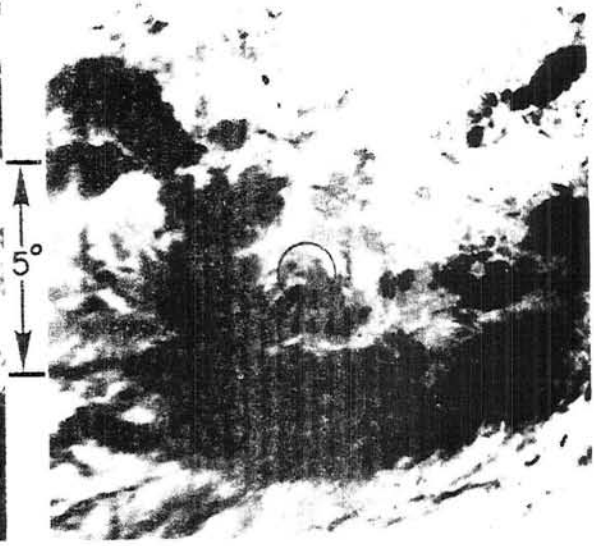
Fig. B6.
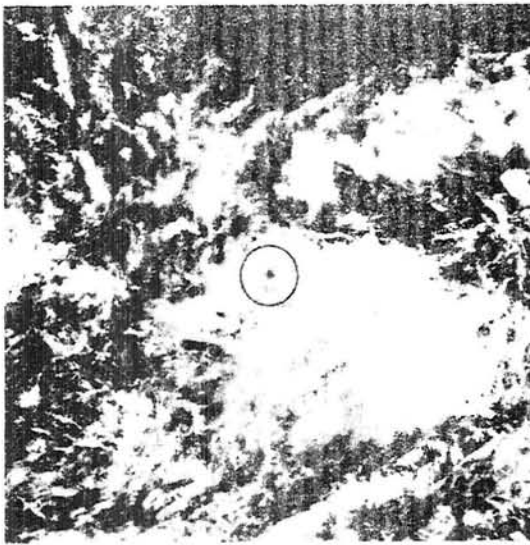
Fig. B7.
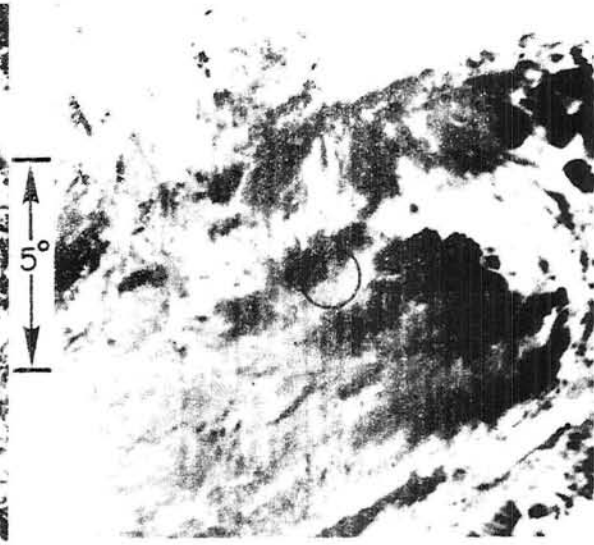
Fig. B8.
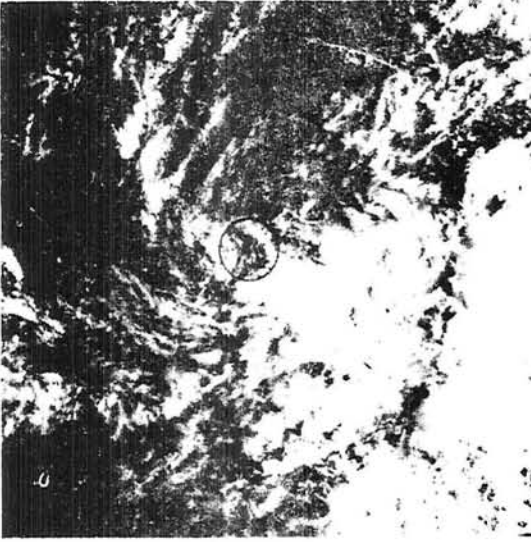
Fig. B9.
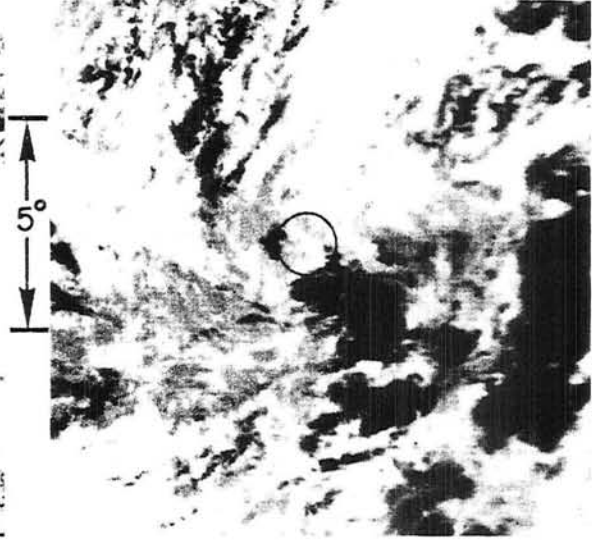
Fig. B10.

Fig. B11.
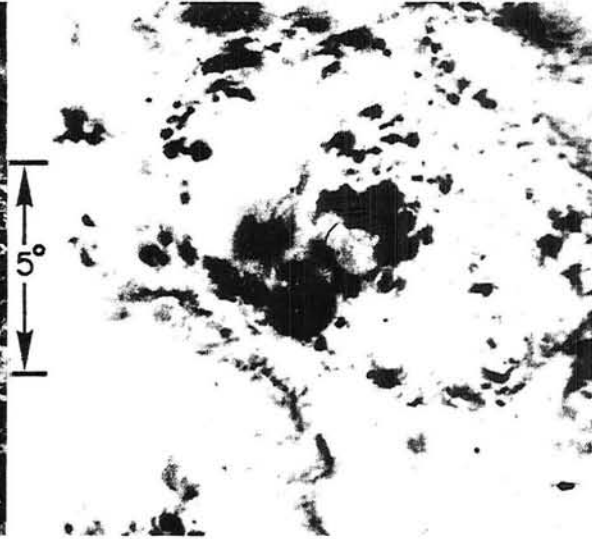
Fig. B12.
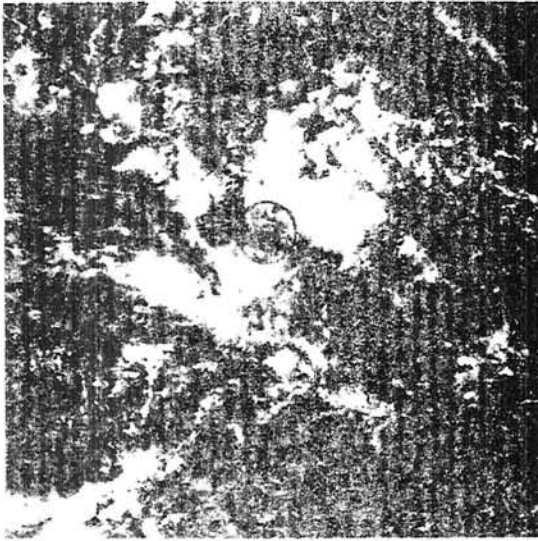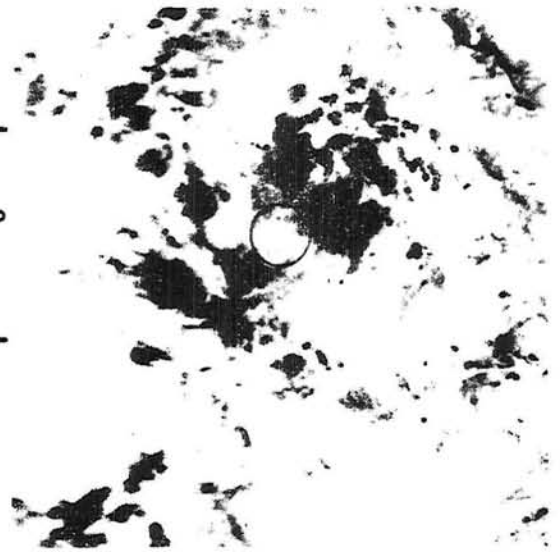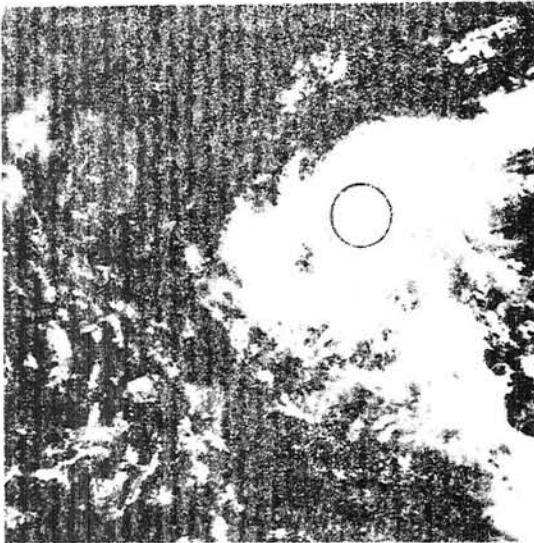
Fig. B13.
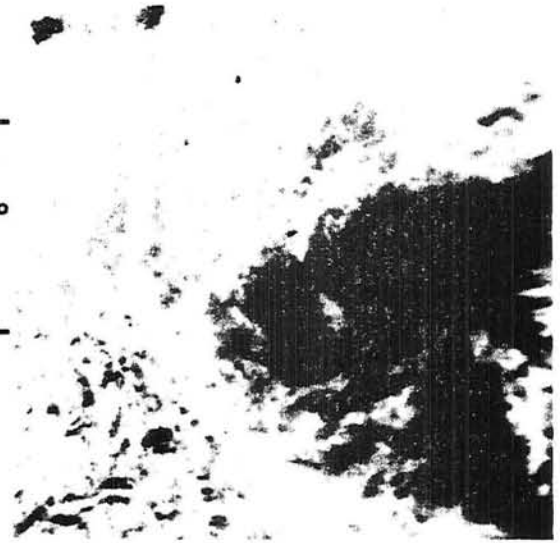
Fig. B14.

Fig. B15.

Fig. B16.

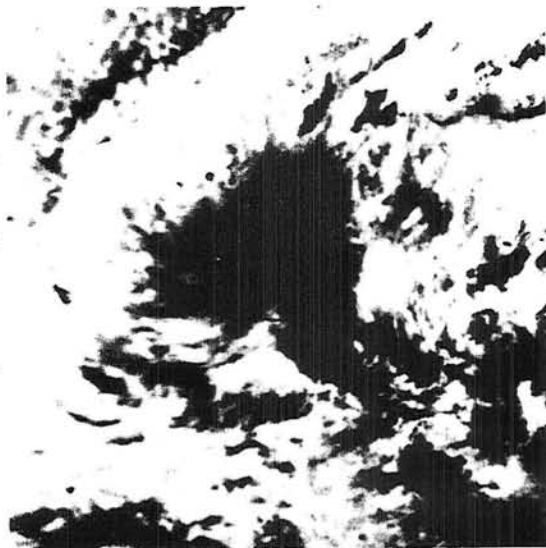Fig. B17.
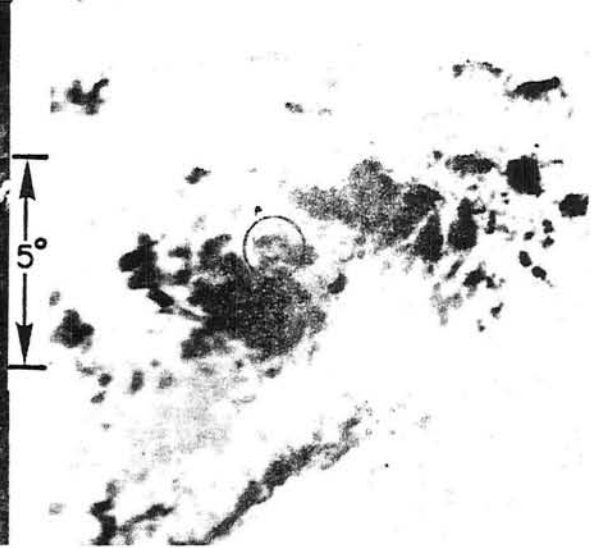
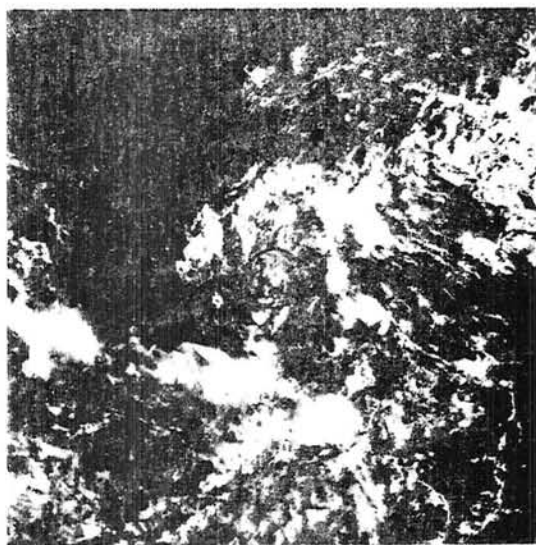Fig. B18.
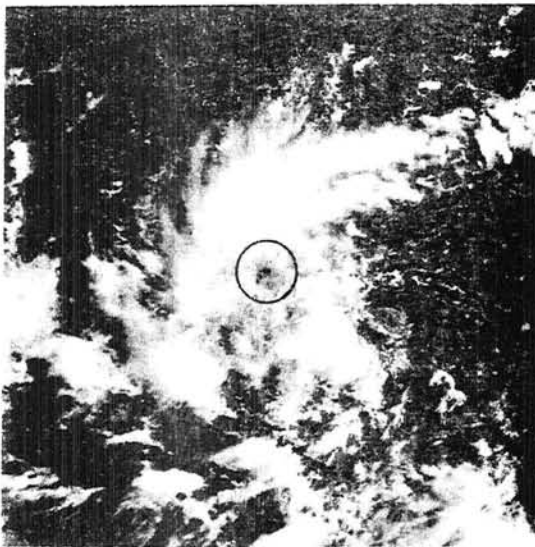
Fig. B19.
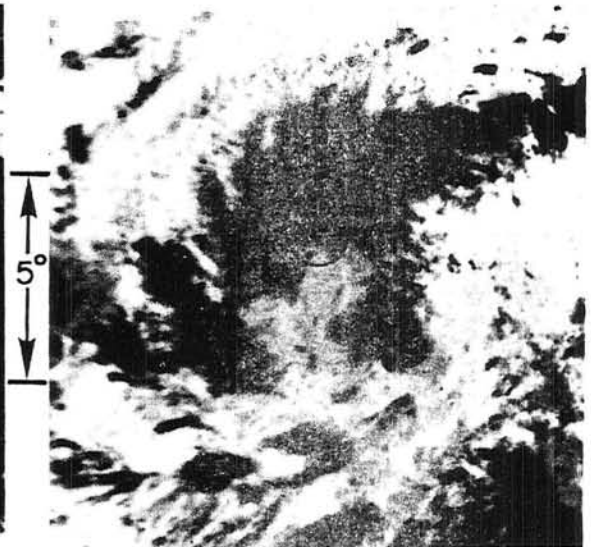
Fig. B20.
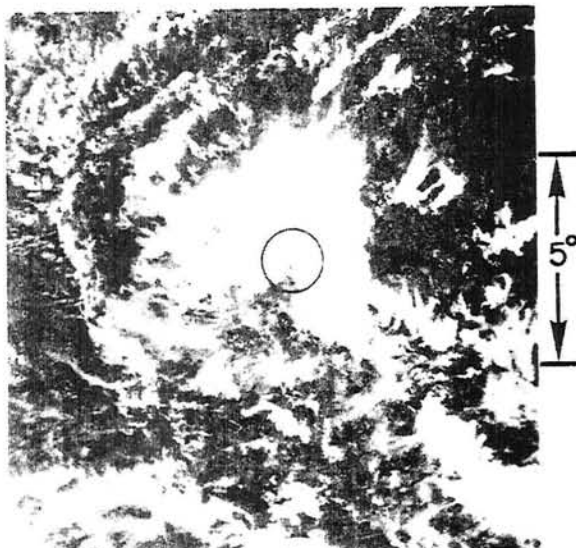
Fig. B21.

Fig. B22.

Fig. B23.
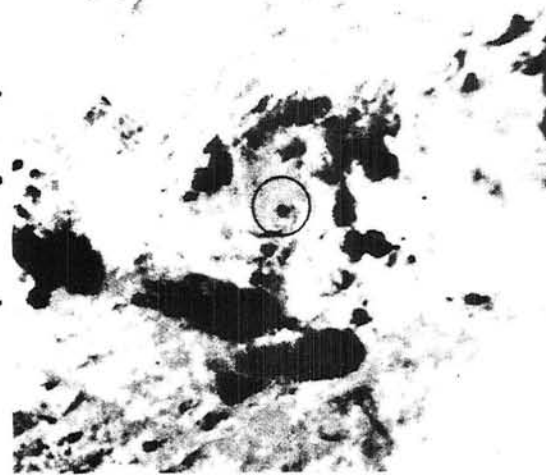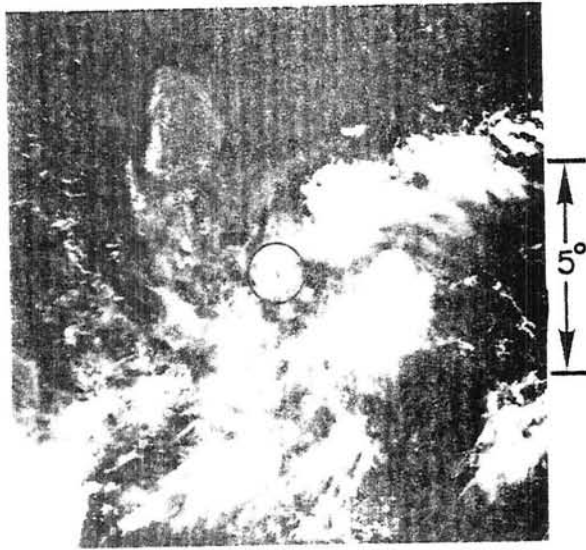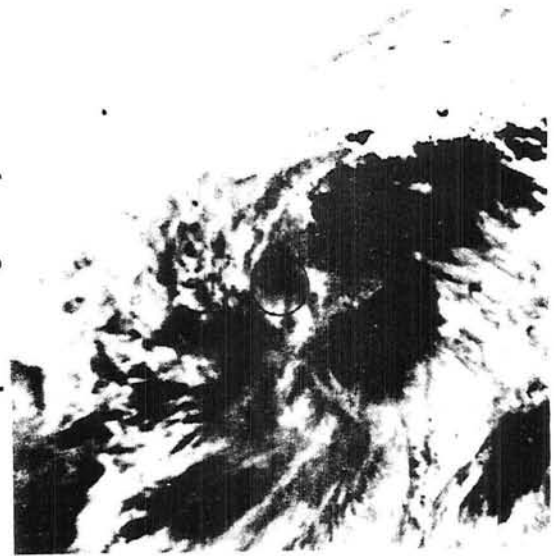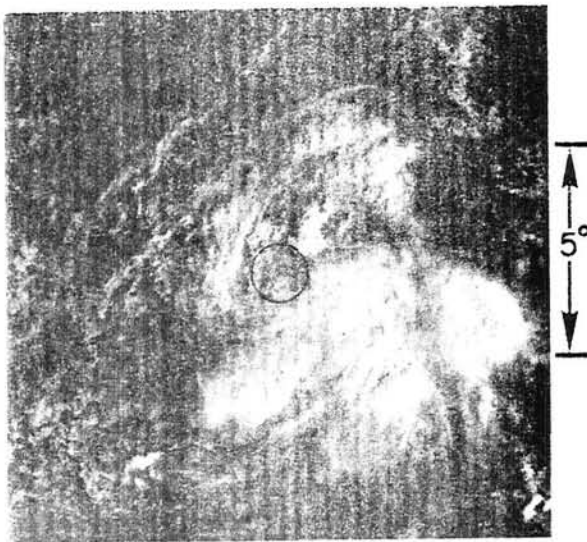

Fig. B24.

Fig. B25.
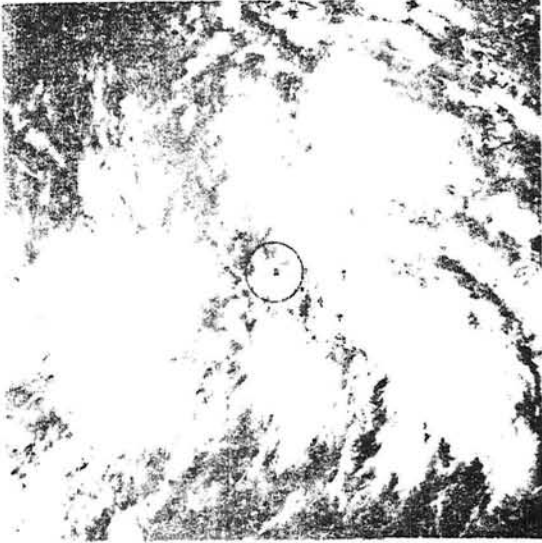
Fig. B26.

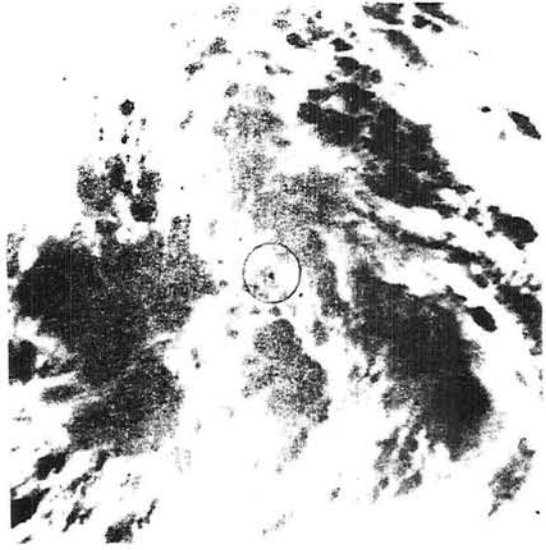

Fig. B27.
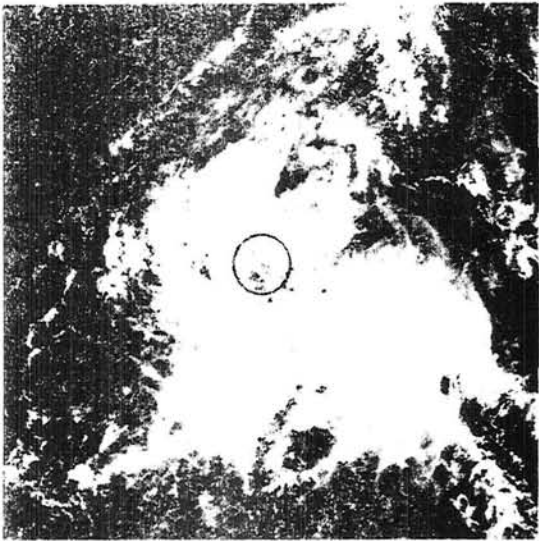
Fig. B28.

Fig. B29.

Fig. B30.

Fig. B31.

Fig. B32.

Fig. 533.

Fig. 534.

Fig. 535.
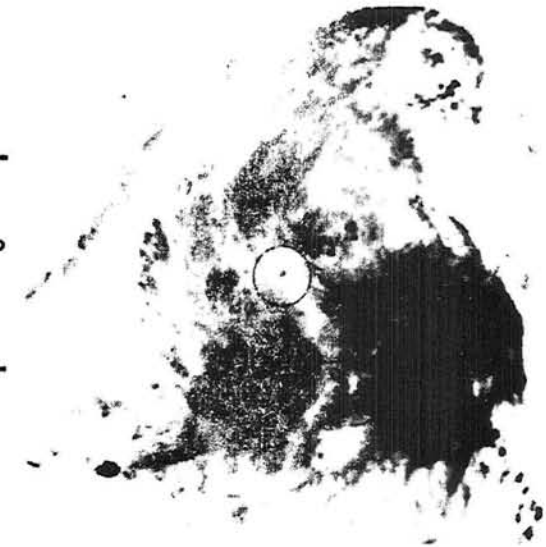

Fig. 536.

Fig. B37.

Fig. B38.

Fig. B39.

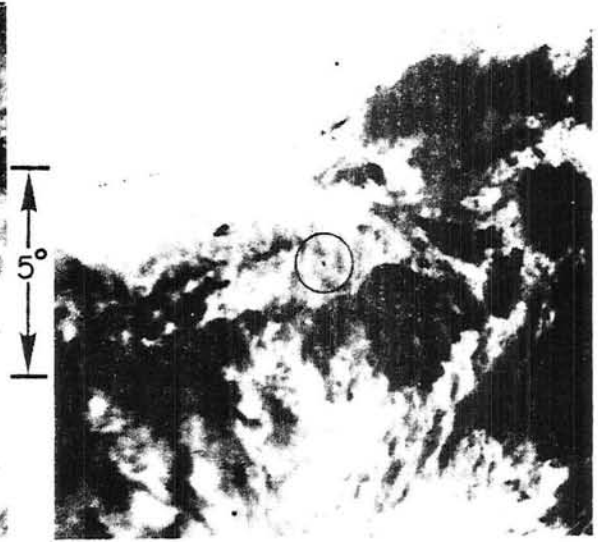

Fig. B40.
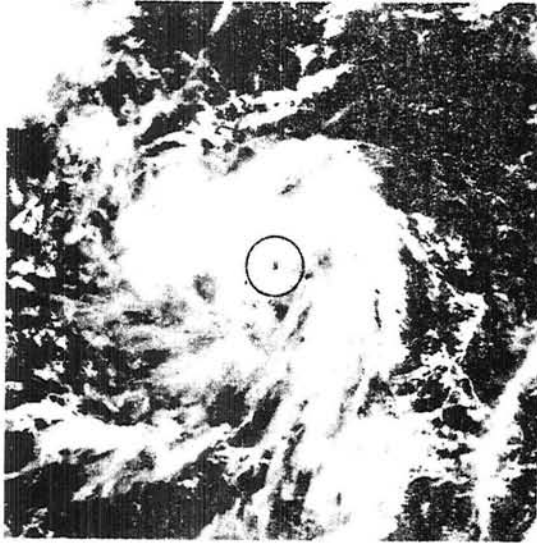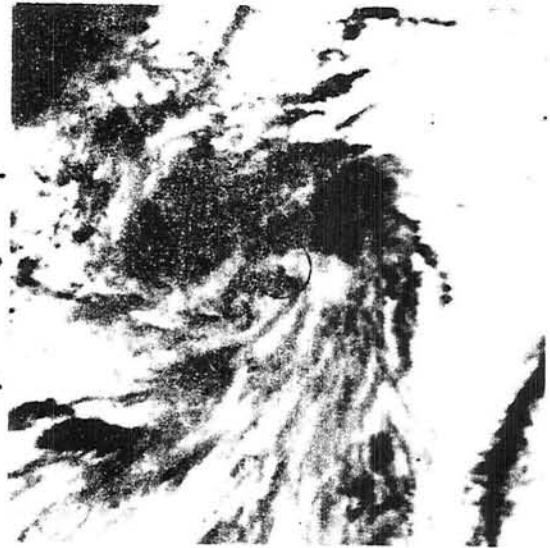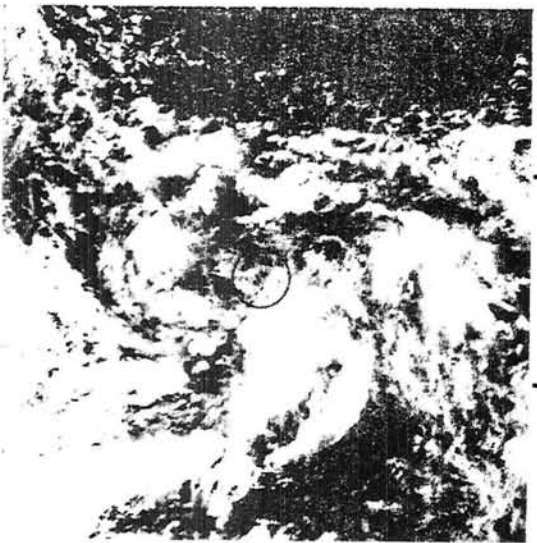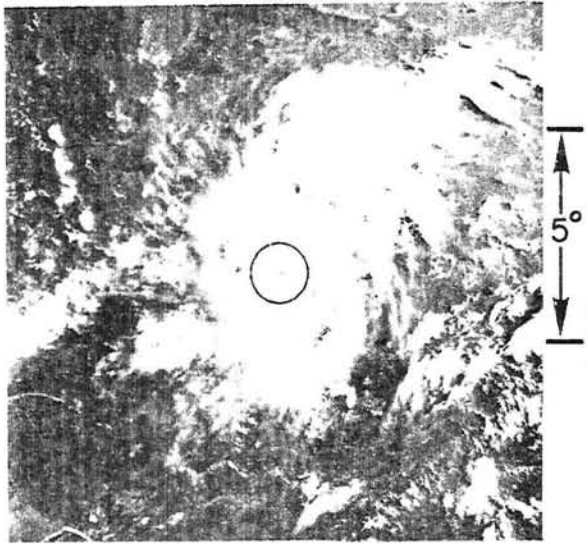
Fig. B41.

Fig. B42.

Fig. B43.

Fig. B44.

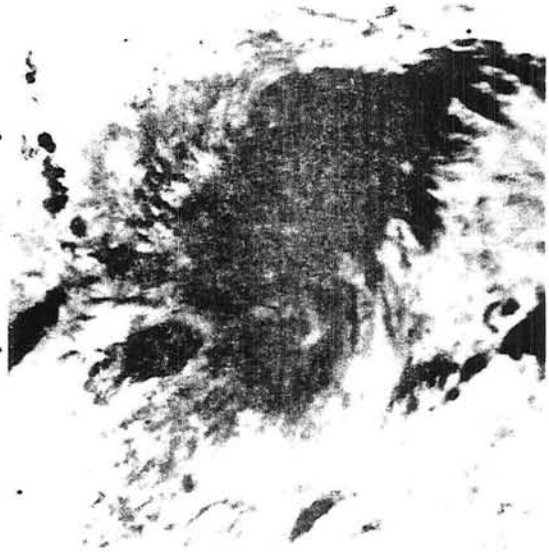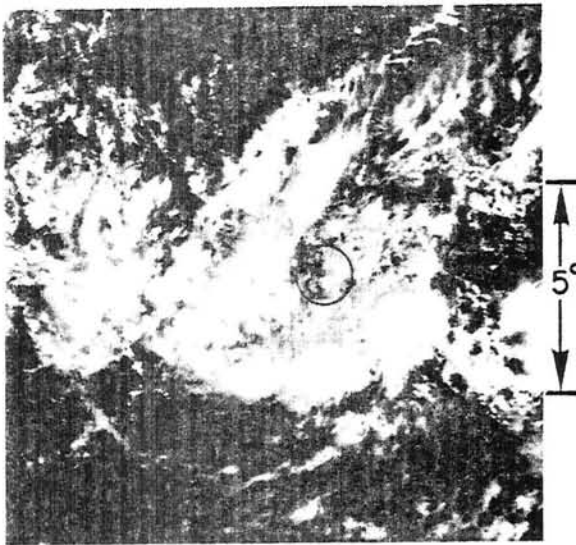Fig. B45.

Fig. B46.

Fig. B47.

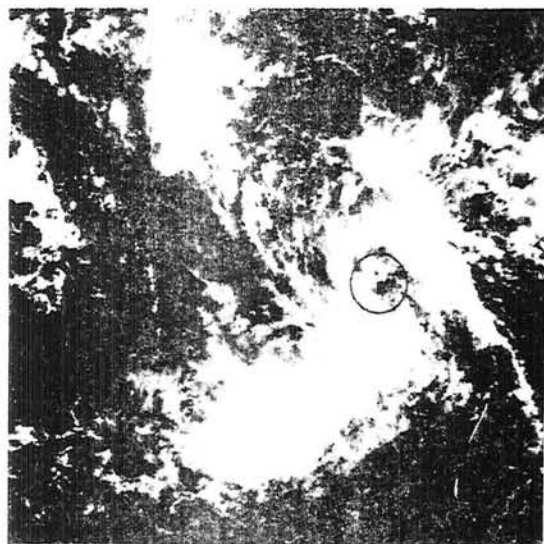Fig. B48.

Fig. B49.

Fig. B50.
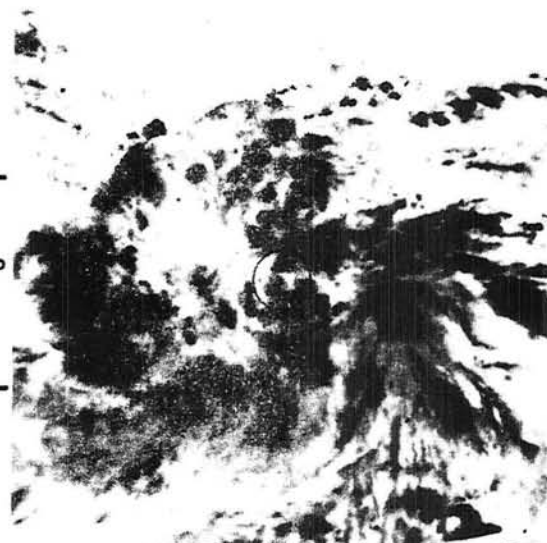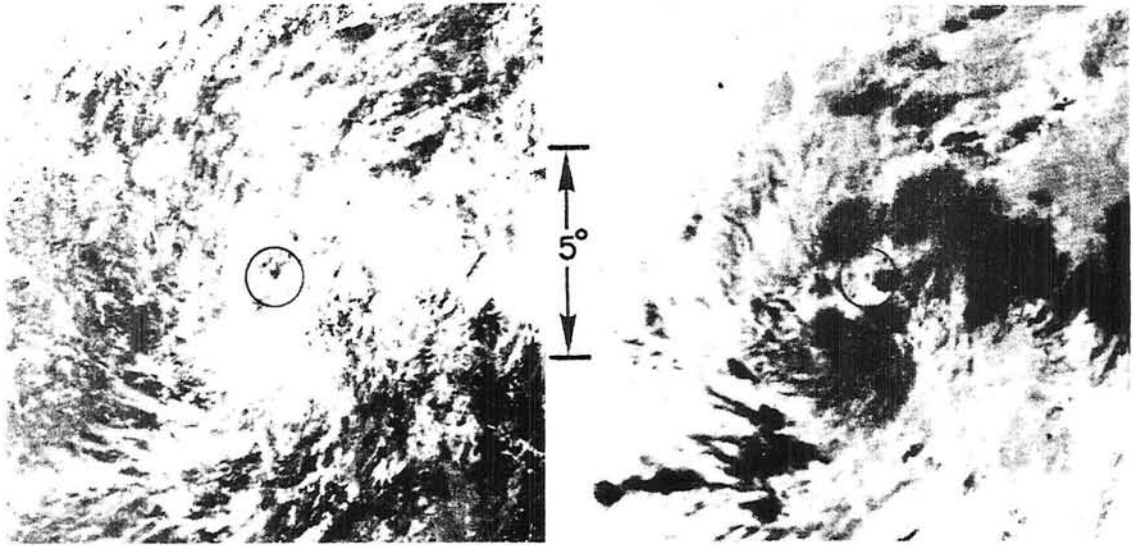

Fig. B51.

Fig. B52.

Fig. B53.   Fig. B54.

APPENDIX C

DATA LISTING OF ALL DMSP FIGURES USED IN THE TEXT

This appendix lists the following additional information for each

DMSP figure used in the text. The scale of all figures in this paper

is 484 km to an inch with the exception of Figs. 24a, b, c, d which

have a scale of 380 km to an inch. All figures were visual data with the

exception of Figs. 27 and 28 which were infrared.

1) Date and time

2) Latitude and longitude of storm center

3) Storm number as reported in the annual typhoon report for the
   year in which the storm was observed

4) Figure number used in the text.

Date	Time(Z)	Latitude(N)	Longitude(E)	Storm Number	Figure
5 JUL 72	0200	7.2	163.0	7	4
15 OCT 72	0109	14.0	172.6	27	13
19 JUN 72	0228	9.4	147.0	6	20a
22 JUN 72	0327	10.8	135.1	6	20b
23 JUN 72	0312	10.6	130.7	6	20c
23 JUN 72	2356	11.3	127.5	6	20d
5 JUL 72	0200	9.5	150.2	8	21a
6 JUL 72	0146	10. 1	147.5	8	21b
7 JUL 72	0313	10.5	144.6	8	21c
10 JUL 72	0230	16.3	136.8	8	21d
7 SEP 71	2107	21.3	160.0	27	24a
8 SEP 71	2040	23.0	159.0	27	24b
7 NOV 72	0012	15.2	112.3	29	24c
7 NOV 72	0404	15.3	112.7	29	24d
22 JUL 72	0118	17.1	161.0	11	25
10 AUG 73	0313	21.1	131.1	10	26
31 OCT 72	0222	14.3	153.7	29	27
21 JUL 72	0133	15.0	165.2	11	28
31 OCT 72	0222	14.3	153.7	29	29
21 JUL 72	0133	15.0	165.2	11	30
26 MAY 72	0128	6.0	169.7	3	33a
29 MAY 72	2151	8.1	159.7	3	33b
30 MAY 72	2124	9.7	158.9	3	33c
1 JUN 72	0143	11.3	157.6	3	33d

APPENDIX C (cont'd)

Date	Time(Z)	Latitude(N)	Longitude(E)	Storm Number	Figure
3 JAN 72	0159	9.3	149.2	1	34a
4 JAN 72	2240	9.8	138.6	1	34b
6 JAN 72	0251	10.0	132.9	1	34c
6 JAN 72	2324	11.7	128.4	1	34d
13 SEP 71	2326	17.5	128.0	29	35a
14 SEP 71	2259	18.2	126.3	29	35b
15 SEP 71	2232	21.5	126.1	29	35c
17 SEP 71	2319	22.8	124.0	29	35d
5 SEP 72	2211	15.4	142.3	18	36a
6 SEP 72	0205	14.4	140.9	18	36b
10 OCT 74	2227	17.8	122.7	27	37a
11 OCT 74	0003	18.4	122.1	27	37b
10 AUG 72	2215	17.0	144.6	14	38a
11 AUG 72	2147	18.4	140.0	14	38b
12 AUG 72	2302	18.8	135.6	14	38c
15 AUG 72	0400	21.2	127.2	14	38d
28 JUL 72	2308	15.8	134.3	12	39a
23 MAY 71	2233	10.5	137.0	8	39b
6 SEP 72	0205	14.4	140.9	18	39c
9 SEP 72	0303	14.7	125.1	20	39d
16 DEC 72	0125	8.9	167.6	33	40a
9 AUG 72	0203	12.2	149.6	14	40b
18 OCT 71	2242	8.2	131.6	36	40c
2 JUN 72	0311	10.0	141.7	99	40d
27 AUG 72	0106	30.9	160.4	15	41a
31 JUL 72	2146	16.0	160.7	13	41b
2 DEC 72	0306	7.3	133.0	32	41c
30 MAY 72	2124	9.7	158.9	3	41d
16 OCT 74	0013	15.8	123.8	28	42a
18 JUL 71	2041	31.2	164.0	17	42b
7 AUG 72	0232	34.5	140.7	13	42c
21 AUG 71	2206	24.9	151.9	23	42d

CSU Dept. of Atmos. Sci. Report No.	Report Title, Author, Date, Agency Support
104	The Mutual Variation of Wind, Shear, and Baroclinicity in the Cumulus Convective Atmosphere of the Hurricane (69pp). W. M. Gray. February 1967. NSF Support.
114	Global View of the Origin of Tropical Disturbances and Storms (105pp). W. M. Gray. October 1967. NSF Support.
116	A Statistical Study of the Frictional Wind Veering in the Planetary Boundary Layer (57pp). B. Mendenhall. December 1967. NSF and ESSA Support.
124	Investigation of the Importance of Cumulus Convection and Ventilation in Early Tropical Storm Development (88pp). R. Lopez. June 1968. ESSA Satellite Lab. Support.
Unnumbered	Role of Angular Momentum Transports in Tropical Storm Dissipation over Tropical Oceans (46pp). R. F. Wachtmann. December 1968. NSF and ESSA Support.
Unnumbered	Monthly Climatological Wind Fields Associated with Tropical Storm Genesis in the West Indies (34pp). J. W. Sartor. December 1968. NSF Support.
140	Characteristics of the Tornado Environment as Deduced from Proximity Soundings (55pp). T. G. Wills. June 1969. NOAA and NSF Support.
161	Statistical Analysis of Trade Wind Cloud Clusters of the Western North Pacific (80pp). K. Williams. June 1970. ESSA Satellite Lab. Support.
---	A Climatology of Tropical Cyclones and Disturbances of the Western Pacific with a Suggested Theory for Their Genesis/ Maintenance. W. M. Gray. NAVWEARSCHFAC Technical Paper No. 19-70 (225pp). November 1970. (Available from U.S. Navy, Monterey, CA). U.S. Navy Support.
179	A Diagnostic Study of the Planetary Boundary Layer over the Oceans (95pp). W. M. Gray. February 1972. Navy and NSF Support.
182	The Structure and Dynamics of the Hurricane's Inner Core Area (105pp). D. J. Shea. April 1972. NOAA and NSF Support.
188	Cumulus Convection and Larger-Scale Circulation, Part I: A Parametric Model of Cumulus Convection (100pp). R. E. Lopez. June 1972. NSF Support.

CSU Dept. of Atmos. Sci. Report No.	Report Title, Author, Date, Agency Support
189	Cumulus Convection and Larger-Scale Circulations, Part II: Cumulus and Meso-Scale Interactions (63pp). R. E. Lopez. June 1972. NSF Support.
190	Cumulus Convection and Larger-Scale Circulations, Part III: Broadscale and Meso-Scale Considerations (80pp). W. M. Gray. July 1972. NOAA-NESS.
195	Characteristics of Carbon Black Dust as a Tropospheric Heat Source for Weather Modification (55pp). W. M. Frank. January 1973. NSF Support.
196	Feasibility of Beneficial Hurricane Modification by Carbon Black Seeding (130pp). W. M. Gray. April 1973. NOAA Support.
199	Variability of Planetary Boundary Layer Winds (157pp). L. R. Hoxit. May 1973. NSF Support.
200	Hurricane Spawned Tornadoes (57pp). D. J. Novlan. May 1973. NOAA and NSF Support.
212	A Study of Tornado Proximity Data and an Observationally Derived Model of Tornado Genesis (101pp). R. Maddox. November 1973. NOAA Support.
219	Analysis of Satellite Observed Tropical Cloud Clusters (91 pp). E. Ruprecht and W. M. Gray. May 1974. NOAA-NESS Support.
224	Precipitation Characteristics in the Northeast Brazil Dry Region (56pp). R. P. L. Ramos. May 1974. NSF Support.
225	Weather Modification through Carbon Dust Absorption of Solar Energy (190pp). W. M. Gray, W. M. Frank, M. L. Corrin, and C. A. Stokes. July 1974.
234	Tropical Cyclone Genesis (121pp). W. M. Gray. March 1975. NSF Support.
---	Tropical Cyclone Genesis in the Western North Pacific (66pp). W. M. Gray. March 1975. U.S. Navy Environmental Prediction Research Facility Report. Technical Paper No. 16-75. (Available from the U.S. Navy, Monterey, CA). Navy Support.
241	Tropical cyclone Motion and Surrounding Parameter Relationships (105pp). J. E. George. December 1975. NOAA Support.

CSU Dept. of Atmos. Sci. Report No.	Report Title, Author, Date, Agency Support
243	Diurnal Variation of Oceanic Deep Cumulus Convection. Paper I: Observational Evidence, Paper II: Physical Hypothesis (106pp). R. W. Jacobson, Jr. and W. M. Gray. February, 1976. NOAA NESS Support.
257	Data Summary of NOAA's Hurricane Inner-Core Radial Leg Flight Penetrations 1957-1967, and 1969 (245pp). W. M. Gray and D. J. Shea. October, 1976. NSF and NOAA Support.
258	The Structure and Energetics of the Tropical Cyclone (180 pp). W. M. Frank. October, 1976. NOAA (NHEML), NOAA (NESS) and NSF Support.
259	Typhoon Genesis and Pre-typhoon Cloud Clusters (79pp). R. M. Zehr. November, 1976.
Unnumbered	Severe Thunderstorm Wind Gusts (81pp). G. W. Walters. December, 1976. NSF Support.
262	Diurnal Variation of the Tropospheric Energy Budget (141 pp). G. S. Foltz. November, 1976. NSF Support.
274	Comparison of Developing vs Non-Developing Tropical Disturbances (81 pp). Steven L. Erickson. July, 1977.

BIBLIOGRAPHIC DATA SHEET	1. Report No. CSU-ATSP-277	2.	3. Recipient's Accession No.

4. Title and Subtitle	5. Report Date
TROPICAL CYCLONE CLOUD AND INTENSITY RELATIONSHIPS	November, 1977
	6.

7. Author(s) Charles P. Arnold (P.I. - William M. Gray)	8. Performing Organization Rept. No. CSU-ATSP-277

9. Performing Organization Name and Address Atmospheric Science Department Colorado State University Fort Collins, Colorado 80523	10. Project/Task/Work Unit No.
	11. Contract/Grant No. DAEA 18-76-C-0050 04-6-022-44036

12. Sponsoring Organization Name and Address	13. Type of Report & Period Covered
United States Army Electronics White Sands Missile Range New Mexico	NOAA National Hurricane and Experimental Meteorology Lab. Coral Gables, FL 33124	Project Report
	14.

15. Supplementary Notes

16. Abstracts

This paper describes an observational study of tropical cyclones based on high resolution visual and infrared Defense Meteorological Satellite Program (DMSP) pictures of western North Pacific storms. It also utilizes composited rawinsonde data about storms in the same geographical region. It discusses the physical characteristics, cloud characteristics and wind and thermodynamic characteristics associated with each of four stages of tropical cyclone development (developing cluster, tropical depression, tropical storm and typhoons). Among the physical characteristics discussed are typical storm sizes, types of banding most often observed, location and type of circulation center, intensification rates, and eye dimensions. Cloud characteristics include the percent of storm area covered by cirrus and convective cloud types and the distribution and characteristics of the basic convective element found in DMSP data. Among the wind and thermodynamic parameters investigated were vertical motion, vorticity, tangential wind, moisture and temperature.

17. Key Words and Document Analysis. 17a. Descriptors

Satellite cloud studies
Tropical storms

17b. Identifiers/Open-Ended Terms

17c. COSATI Field/Group

18. Availability Statement	19. Security Class (This Report) UNCLASSIFIED	21. No. of Pages 154
	20. Security Class (This Page) UNCLASSIFIED	22. Price

FORM NTIS-35 (REV. 3-72)

THIS FORM MAY BE REPRODUCED

USCOMM-DC 14952-P72